SYNTHESIS AND PHOTOPOLYMERIZATION OF NOVEL DIMETHACRYLATES

Nazan Gunduz

Thesis submitted to the faculty of the Virginia Polytechnic Institute and State University in partial fulfillment of the requirements for the degree of

Master of Science

in

Chemistry

James E. McGrath, Chair

Alan R. Shultz

James P. Wightman

June 8, 1998

Blacksburg, Virginia

Keywords: Dimethacrylates, photopolymerization, isothermal photo-DSC, conversion, Trommsdorff effect , steady-state and non steady-state, rate constants

SYNTHESIS and PHOTOPOLYMERIZATIONS of
NOVEL DIMETHACRYLATES

by

Nazan Gunduz

Committee Chairman: Dr. James E. McGrath

Department of Chemistry

(Abstract)

Four potential new monomers were prepared, all of which were structural analogues of BisGMA (*2,2-bis(4-(2-hydroxy-3-methacryloxyprop-1-oxy) phenyl)propane).* The synthesis of these tetrafunctional dimethacrylate monomers was based on structural modifications of Bis-GMA in the core and the side chain and required a two-step reaction. The first step was propoxylation or ethoxylation of the bisphenols and the second step was the methacrylation of the resulting products. The core structures are designated by Bis-A for isopropylidene and 6F for hexafluoropropyl. The side chain structures were designated on the basis of the pendant side chains in the glycidyl moiety as –OH, –H, and $-CH_3$ from the epichlorohydrin, ethyleneoxide, and propyleneoxide reaction products with the bisphenols, respectively. Bis-GMA was commercially obtained and used as a standard for comparison of the experimental monomers. All the monomers were prepared by the following general procedure of propoxylation or ethoxylation of the biphenols followed by methacrylation. They were characterized by NMR, FTIR, DSC and Cone and Plate Viscometry. All the experimental monomers exhibited lower viscosities and glass transition temperatures than the control, which was attributed to the elimination of the hydrogen bonding. The monomers were photopolymerized in a differential scanning calorimetry modified with an optics assembly (DPA 7; Double Beam Photocalorimetric Accessory) to study the photo-induced crosslinking reactions. The influence of monomer

structure, temperature, light intensity, and initiator concentration on the photopolymerization kinetics of ethoxylated and propoxylated dimethacrylates was investigated by isothermal DSC. The DSC curves showed a rapid increase in rate due to the Trommsdorff effect, and then a decline due to the decrease of monomer concentration and the autodeceleration effect. The monomers with lower viscosities and glass transition temperatures exhibited higher conversions of the double bonds. The final extent of conversion increased with curing temperature, light intensity and initiator concentration. The radiation intensity exponent varied from 0.68 (BisGMA) to 0.74 for the ethoxylated 6F system. The initiator exponent were varied from 0.34 (for BisGMA) to 0.44 for the propoxylated BisA system. The ratio of the reaction rate constant (k_t/k_p) was calculated for PropBisAdm from both steady-state and non steady-state conditions.

The effect of dilution on photopolymerization kinetics of BisGMA/triethyleneglycoldimethacrylate (TEGDMA) mixtures was also studied by isothermal photo-DSC. Dilution with TEGDMA significantly reduced the viscosity and glass transition temperatures of the mixtures due to the increase in the flexibility. The extent of polymerization increased with increasing TEGDMA and curing temperature. The calculation of ratio of rate constants (k_t/k_p) was also determined and the significance was discussed herein.

ACKNOWLEDGMENTS

Many people have contributed to my personal and scientific development in the past three years. First of all, I would like to express my sincere thanks to my advisor, Dr. James E. McGrath for giving me the opportunity to work with him. He provides a wealth of knowledge and experience. Thank you, Dr. McGrath, for your support and guidance. I also wish to acknowledge my other committee members. Special thanks go to Dr. Allan R. Shultz for spending countless hours with me from the very beginning, setting up the photo-DSC instrument. It has been always a great treasure to me to have him in my committee for training me and for those valuable discussions and suggestions in every step of my research. I also appreciate Dr. James P. Wightman for his full-of-fun classes and for taking time to read this thesis.

I was also quite fortunate for having the opportunity to interact with the colleagues of our great research group. I deeply appreciate Drs. M. Sankarapandian and H.K. Shobha for their patience, help and good discussions, especially during my transition period when I first started to work in the lab. I truly enjoyed the valuable discussions and wonderful friendship with Drs. Amba Ayambem, Sue Mecham, Qing Ji, Lance Wang, Hong Zhuang, and fellow graduate students Debi Dunson, Isaac Farr, Marvin Graham, William Harrison, Yongning Liu, Jeff Mecham, David Polk, Charles Tchatchoua, and Sheng Wang.

I owe a particular word of thanks to our secretarial staff, Laurie Good, Esther Brann, Millie Ryan, and Joyce Moser for helping me with preprints, manuscripts, faxes, travel arrangements, and for their friendship with always smiling faces.

The early financial support from the Turkish Government gave me the chance to pursue my graduate studies in the USA. Support from the National Science Foundation Science and Technology center, and Chemistry Department at Virginia Tech are sincerely appreciated.

Finally, I would like to extent my special gratitude to my parents, Mr. and Mrs. Kenan Kaptan and Huriye Kaptan for their never-ending love, sacrifice and support. I particularly appreciate my mother, father and sister, Dilek, for taking care of my daughter Erin Ilge Gunduz in Turkey while I finished my master's thesis and prepared for the PhD cumes. My husband, Irfan, has been a great support with his love, understanding, and always believing in me and telling me that I can make it, even after giving birth to my daughter, and starting full time work when she was only 13 days old! Above all, my love goes to my loving daughter Erin Ilge, whose first birthday we missed. I love you and missed you so much.

TABLE OF CONTENTS

LIST OF FIGURES

LIST OF TABLES

LIST OF SCHEMES

LIST OF EQUATIONS

CHAPTER 1. INTRODUCTION

Photo or thermal polymerization of multifunctional monomers form infusible, insoluble three dimensional highly crosslinked networks. These rigid polymer networks have found use in a wide variety of applications such as dental restorative materials, microelectronics, encapsulants, optical lenses and UV-Vis curable adhesives. Acrylates and methacrylates are among the most important examples of the UV-Vis curable materials. This is related to their fast polymerization rates which lead to highly crosslinked polymer structures and their relatively low cost. (1). During polymerization, the formation of a three dimensional network restricts the mobility of the chain segments, resulting in an decrease in free volume and increase in the transition temperature, T_g. These are important factors that influence the reaction kinetics and maximum extent of conversion during polymerization.

Dental composite resins, which essentially consist of a crosslinked polymer matrix, a coupling agent, and inorganic filler particles, utilize aromatic or aliphatic dimethacrylate monomers. Important requirements for dimethacrylate monomers used for this purpose are low water sorption, curing shrinkage and viscosity (2). The improvement of the polymer resin matrix is of great importance to extend the lifetime of the composite restorations. The dimethacrylate (2,2-bis(4-(2-hydroxy-3-methacryloxyprop-1-oxy)phenyl)propane) known as BisGMA and/or derivatives of BisGMA matrix resins are commonly used monomer systems mainly due to its lower volatility and polymerization shrinkage.

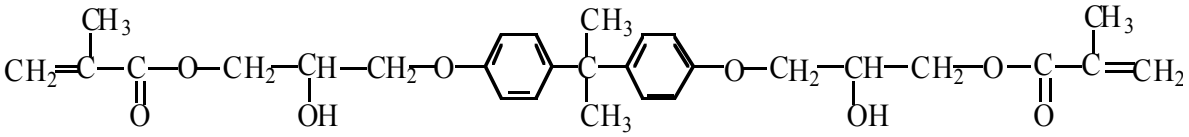

Bis-GMA

However, the long term durability of composite restorations is still not satisfactory.

They can not yet replace mercury amalgams completely for use in posterior restorations (3) due to wear, which may be related to high viscosity of the BisGMA system and considerable residual unsaturation in the polymer matrix.

The first objective of this study was to prepare four difunctional monomers, all of which were structural analogues of BisGMA. These are described as variables in the core and side chain units as illustrated below (Figure 1.1).

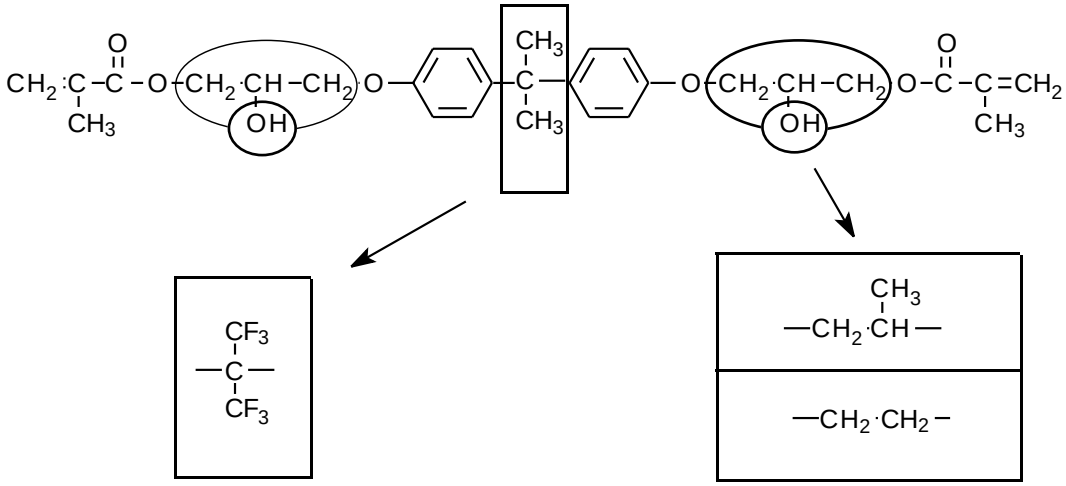

Figure 1.1 The structural modifications of the Bis-GMA in the core and side chain units.

All of the monomers were prepared by the general procedure of propoxylation or ethoxylation of the bisphenols followed by methacrylation. The second objective of the study was to investigate photopolymerization of the experimentally prepared monomers as well as the control BisGMA. A differential scanning calorimeter modified with an optics assembly (DPA 7; Double Beam Photocalorimetric Accessory) was set up and used to study the photo-induced polymerization crosslinking reactions. Although, the thermal polymerization of these monomers were previously studied in detail in our labs, photopolymerizations with respect to various monomers, polymerization temperatures,

initiator concentrations, and light intensities etc., were not known and were the primary objectives for this thesis research.

The most common monomer, BisGMA exhibits a very high viscosity and requires dilution with more flexible, lower viscosity monomers to give filled resin compositions of acceptable consistency. Thus another objective of this research was to study the effect dilution of BisGMA with a low viscosity comonomer (TEGDMA) on the photopolymerization of BisGMA/TEGDMA mixtures. All these photopolymerizations were performed under conditions intended to model dental resin curing conditions, and a camphorquinone/amine initiator system was used at 470 nm.

Chapter 2: LITERATURE REVIEW

2.1 General Aspects and Applications of Multifunctional Monomers

Highly multifunctional monomers are very useful materials and usually form rigid, glassy polymers. These high strength (1) polymer networks are being studied and have found a wide variety applications such as dental restorative materials (2-4), information technology applications (5), optical fiber coatings (5), aspherical lenses (6,7), and lithography (8). For example, such crosslinked polymers can be used in the manufacture of laser video discs or compact discs (5). In these systems, a series of pits arranged in a spiral track contain the information in binary code. A laser lightspot traverses this spiral track and reads the binary coded information which is then converted into an audio/video signal by a photodiode(9). Polymer networks are also used as materials for aspherical lenses which are used to focus the scanning laser lightspot, and in the on-line coating of optical fibers. One of many polymerization processes used in the replication of optical discs and aspherical lenses(10), the monomer-initiator mixture is first spread evenly over the mould that contains the desired information or specific shape, and then irradiated with u.v. light. As the polymer network is formed, it acquires the shape of the mold and thus a replicate is made from a master mold. The kinetic behavior of such polymerizations is important due to the very rapid reaction, and need for exact replication of the master mold with minimum tolerance (10).

The free radical bulk polymerization of diacrylates and dimethacrylates as well as other multifunctional monomers leading to highly cross-linked polymer structures and networks is a complex process and exhibits a number of unexpected behaviors with respect to the reaction kinetics (11). The main parameters of these rather complex systems are autoacceleration and autodeceleration (12,13), which lead to unequal functional group

reactivities (monomeric or pendant double bonds) (14), structural inhomogeneity (15) and volume shrinkage (13).

Figure 2.1.1 shows the normalized polymerization rate as a function of conversion and reveals three distinct regions. Region I indicates a constant normalized rate of classical radical chain polymerization kinetics. Region II, shows a dramatic increase in polymerization rate, autoacceleration, due to the gel effect. Finally Region III indicates a rapid decrease in the polymerization rate as a result of the radical isolation and/or a glass, vitrification effect (7).

Autoacceleration is observed due to the gelation (7) in the initial stage of the network formation as growing chains sharply increase in molecular weight and thus, viscosity. As the viscosity increases during the formation, the mobility of the radical species in the network is restricted. Throughout this stage of the reaction, termination is diffusion controlled and the termination constant is continually decreased. The decreasing termination rate leads to an increase in the number of macromolecular radicals. Because propagation is not as strongly diffusion controlled in this regime, the rate of polymerization increases as the radical concentration increases. Autodeceleration or vitrification, on the other hand, begins in the third region of the reaction as the rate of reaction reaches its maximum. The onset of vitrification occurs when the rapidly advancing T_g of the network becomes equal to the polymerization temperature. This region of the reaction continues until the reaction is essentially stopped. As the rate reaches its maximum, propagation becomes diffusion controlled as well, and begins to decrease dramatically. In this region, autoacceleration becomes balanced by autodeceleration. At later stages, autodeceleration dominates. The autodeceleration causes the rate to decrease much more rapidly than can be accounted for by depletion of reactive groups. This event severely restricts the rate of polymerization.

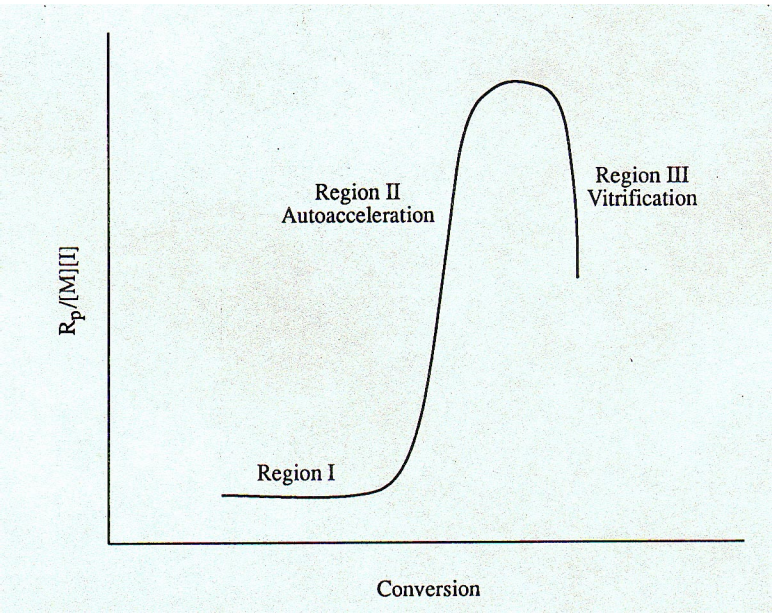

Figure 2.1.1. *Effects of auto-acceleration and vitrification on the normalized rate of polymerization as a function of conversion(84).*

Significant amounts of unreacted functional groups are available in networks cured at low temperatures as a result of vitrification. This is particularly important in the case of radiation curable materials since they are often initially reacted around room temperature which is far below their ultimate T_g.

Various models have been developed to study the effects of autoacceleration and vitrification on radical chain polymerization kinetics. Early models used chain entanglement concepts to describe the gel effect but they did not include vitrification (7). However, more recent models have used free volume concepts to modify the termination and propagation rate constants (16-18).

Several researchers (19,20) have studied the effects of increasing dimethacrylate concentration on the cure behavior of methacrylate and dimethacrylate copolymerization systems. It was found that, as the concentration of dimethacrylate monomer is increased, gelation occurs at lower conversions, severely limiting mobility of polymeric radicals.

Kopecek and co-workers (19) found that increasing the dimethacrylate concentration led to higher double bond conversion for a given polymerization time. Hamielec and co-

workers (20) have also studied copolymerization of methyl methacrylate with ethylene glycol dimethacrylate. Their results show a decrease in conversion where autoacceleration occurs with an increase in the dimethacrylate content of the system. A sudden decrease in the conversion rate was also seen at higher conversions and related to the limited mobility of the monomer molecules (diffusion controlled propagation) and initiator radicals.

2.2 Overview of Dental Composites

The development of dental composites began in the early 1950s at which time silicate cements and unfilled methyl methacrylate (MMA) constituted the esthetic direct filling materials (21). Silicate segments were subject to decay under acidic in vivo conditions and were useful for only about four years on the average (22). While methyl methacrylate materials had the advantages of good esthetic quality and easy polymerization, their limitations included large polymerization shrinkage, lack of sufficient stiffness, and an excessive coefficient of thermal expansion (21). Epoxy resins harden at room temperature with little shrinkage, produce an insoluble polymer, and are adhesive to most solid surfaces. The first dental composites utilized an epoxy resin and aggregates of fused quartz or porcelain particles. The particle size distribution was arranged to maximize the inorganic material by a close packing of the particles (23). The results were encouraging. However, the slow hardening of epoxy resins prevented their use as direct filling materials.

In 1957, Bowen combined the advantages of acrylic resins, epoxies, and bisphenol A glycidyl methacrylate (24). This viscous nonvolatile dimethacrylate (2,2-bis(4-(2-hydroxy-3-methacryloxyprop-1-oxy)phenyl)propane) known as BisGMA (Scheme2.2.1) has much higher molecular weight than methyl methacrylate (MMA), resulting in a corresponding lower polymerization shrinkage and higher viscosity that meets many of the requirements for the resin matrix of dental composites. With the advent of the BisGMA, the composite resins rapidly replaced cements and acrylic resins for esthetic restoration of anterior teeth.

Modern composite resin restorative materials contain a number of components. Resin matrix and inorganic filler particles are major constituents of the composite resins. Beside these two constituents, several others are essential in order to enhance the usability and durability of the material. A coupling agent is required to provide a bond between the inorganic filler particles and the resin matrix, and obviously a system for activating polymerization is necessary. Small amounts of other additives improve color stability(UV absorbers) and prevent premature polymerization (inhibitor such as hydroquinone).

Most composite resins utilize monomers that are aromatic or aliphatic dimethacrylates. Requirements for dimethacrylate monomers used in dental composite matrix resins include low curing shrinkage, water sorption and viscosity (25). The monomer systems of most present-day resin composites are based on BisGMA or derivatives of BisGMA. Due to its large molecular size and chemical structure, BisGMA is superior to MMA by virtue of (2) lower volatility, (3) lower polymerization shrinkage, (4) more rapid hardening, and (5) production of a stronger and higher elastic modulus resin (26). However, the high molecular weight monomers are extremely viscous at room temperatures and use of diluent monomers is essential to attain high filler levels and to produce pastes of clinically usable consistencies.

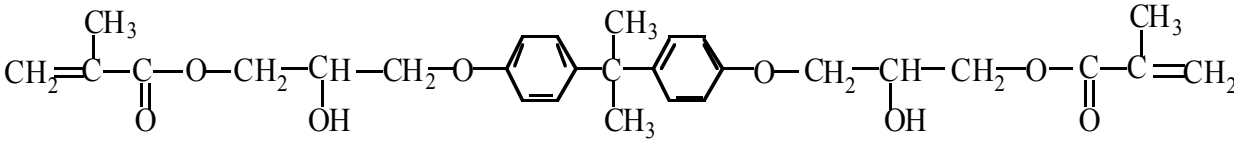

Bis-GMA

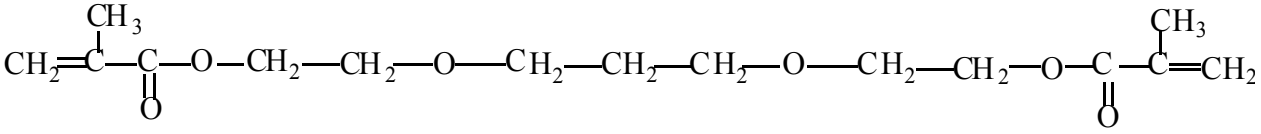

TEGDMA

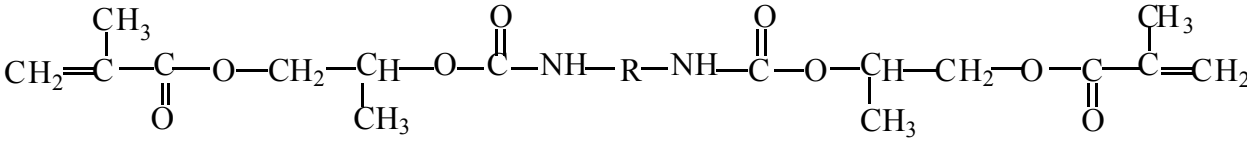

Propyl methacrylate-urethane

(R= 2,2,4-trimethyl hexamethylene)

Scheme 2.2.1. *Structural formulas of Bis-GMA, TEGDMA and Urethane Dimethacrylate (63).*

The most commonly used diluent is triethylene glycol dimethacrylate (TEGDMA) (Scheme 2.2.1). The reduction in viscosity is quite dramatic when TEGDMA is added to BisGMA. A blend of 75:25 v/v BisGMA:TEGDMA has a viscosity of 4300

centipose(cp), whereas the viscosity of a 50:50 blend is 200 cp (27). However TEGDMA has been shown to adversely affect the properties of the matrix resins by increasing the water sorption and curing shrinkage (28). Besides BisGMA, in the remaining resin composites, urethane monomers or oligomers are used as the basis of the monomer system. Compared to BisGMA systems, the composites based on urethane dimethacrylates have lower viscosity, lower water absorption and greater toughness. However, some of these systems may be less color stable. Color stability may also be related to the polymerization system employed (29), e.g., some monomers containing amino groups may be oxidized, resulting in poor color stability.

2.3 Problems and Improvements of Current Dental Composites

Current dental composite resins possess many advantages, such as good mechanical properties, satisfactory esthetic quality, lack of dehydration and low solubility in the mouth. However, as evidenced by their clinical performance, these materials show some problems (30). The primary problems have been polymerization shrinkage and poor wear resistance in restorations of significant bulk under high masticatory forces. The other concerns include a) difficulty of finishing of a smooth surface without causing damage; b) problems in placement; c) post-operative sensitivity associated with leakage; d) color stability. The studies of dental composite resins indicate that the long-term durability is dependent on many variables such as resin formulations, filler particles (type and quantity), processing conditions, crosslinking agents, degree of conversion, applied stress, temperature, and water absorption (31). Among these, water uptake and the structure of the polymer matrix are the most important factors.

The structure of the resin matrix depends upon the structure of the monomers and oligomers used and their extent of conversion. Currently, most of the resins used in commercial composites are either BisGMA or urethane based dimethacrylate systems. The

most commonly used matrix component is 2,2-bis4(2-hydroxy-3-methacryloxy propoxy)phenyl propane (BisGMA) which, due to its chemical structure and large molecular size, is superior to MMA in many aspects, as described previously.

While many commercial BisGMA based composites exhibit satisfactory clinical performance, there are some deficiencies related to the BisGMA resin matrix. First, BisGMA resin-based composites are hydrophilic because of the presence of two hydroxy group (−OH) in the molecule. The hydrophilic character results in relatively high water sorption, which is detrimental to physical and mechanical properties of the composites. Absorbed water molecules can act as a plasticizer to reduce mechanical properties such as tensile and compressive strength, elastic modulus, fracture toughness, and wear resistance. In addition, there is a decrease in the glass transition temperature (T_g) and an increase in the creep potential (32). Water sorption facilitates the chemical degradation of filler-matrix interfaces which lead to adhesion failure, and crack development and propagation in the cured multiphase system (33). All of these deleterious effects can reduce the long-term durability of composite restorations.

Another important factor is that although the methacrylate monomers undergo extensive crosslinking, there remain with the existence of a considerable amount of residual carbon-carbon double bonds (C=C) in the resultant composites. A greater proportion of BisGMA in the resin composites leads to greater residual unsaturation, which can make the polymer matrix particularly susceptible to degradation reaction (34). The extent of cure is dependent on the initiating system and the monomer/oligomer mixture used. Furthermore, the BisGMA system exhibits high viscosity and usually is thinned with some reactive diluent. The high viscosity in the system will restrict the diffusion of the monomers and thus increase the residual unsaturation, which in turn will compromise the properties and clinical performance of the composite resins

To enhance the service performance of dental composite resins, the formulations of composites need to substantially improved. New visible light curing resin systems need to be introduced for composite applications. The improved restorative materials must have

greater moisture resistance, i.e., not to be degraded or plasticized by water, exhibit greater compressive strength and be more resistant to creep failure. During the development of new formulations, one should also aim at achieving better carbon double bond (C=C) conversion. Lower polymerization contraction and good mechanical and biological properties must also be considered.

In order to accomplish the goal of improving current composite restorations, several approaches can be taken. One approach is to prepare some BisGMA analogue which do not contain a hydroxy group in the structure, thus resulting in a monomer with reduced viscosity and reduced water sorption which does not require a diluent (35). New dimethacrylate monomer systems which have moderately low bulk viscosities and improved properties have been reported in the literature (36-39). Synthesis of BisGMA analogues containing some fluorine group or other fluorinated polyfunctional dimethacrylates may be an effective method of increasing the hydrophobicity of the resin matrix, thus contributing to the improvement of the properties of the composites. In addition, some new resin matrix materials consisting of aromatic polyfunctional dimetacrylates can play an important role in the improvement of composites. These new resin matrices would be structurally more rigid, as well as having higher aromaticity, more hydrophobic nature, and higher wet glass transition temperature (T_g) than existing composite resins (27).

In the past decade, many efforts were made to improve the existing BisGMA resin system. The relationships between the structure and properties of composite resins were also evaluated. In order to improve the physical properties of the matrix materials of dental composites, two aromatic dimethacrylate monomers 2,2′-bis(4-methacryloxy ethoxy phenyl) sulfone (MEPS) and 2,2′-bis(4-methacryloxy ethoxy phenyl) propane (MEPP) were synthesized, and the relationships between the chemical structure and physical properties of these materials were investigated (40). It was found that the physical properties of these dimethacrylate copolymers with MMA were increased when the molar ratio of MEPS and MEPP dimethacrylates were increased. The water sorption of MEPS

(35 mole %) copolymers was one-half that of PMMA, and the water sorption of MEPP copolymers showed the same tendency. The physical properties of the MEPS copolymers were superior to those of the MEPP copolymers due to the rigid sulfone groups in the MEPS structure. At high concentrations of MEPS and MEEP, this general tendency was clearly shown. Generally, monomers containing the hydrophobic methylene chain have lower water sorption than those containing the ethylene oxide (CH_2CH_2O) chain (41,42). It was shown that these dimethacrylates were useful for improving the physical properties of resin matrix materials. However, MEPS dimethacrylate has a high melting point and showed relatively low solubility with MMA or other conventional dental methacrylate monomers.

For the purpose of determining the structure-property relationships of dental composite materials, Kawaguchi et.al. (43) synthesized several aromatic dimethacrylates with different chemical backbones. They found that the mechanical properties (e.g. compressive strength, modulus of elasticity) of dimethacrylate and MMA copolymers increased when the concentration of the dimethacrylate was increased. The introduction of the Bisphenol A and Bisphenol S backbones is useful for improving the physical properties of dental composites. Inclusion of alkyl groups in the backbone reduce the melting point and improve the solubility of aromatic dimethacrylates. It was observed that dimethacrylates containing $(CH_2)_n$ groups in the backbone yield generally more desirable physical properties than those containing $(CH_2CH_2O)_n$ groups (43).

To develop new dimethacrylate monomers which produces matrices with mechanical and physical properties superior to those of matrices produced from the dimethacrylate monomers currently employed, five types of BisMPEPP monomers with different side chain lengths were prepared from a commercial Bis MEPP monomer mixture, and their structure-property relationships were assessed (44). The results indicated that the mechanical properties (elastic modulus, compressive strength) decreased with increasing the side chain lengths of Bis MPEPP monomers, along with water sorption increase. BisGMA polymers showed higher values for elastic modulus (in dry condition)

than did the BisMPEPP polymers. Under wet conditions, however, the decrease of mechanical and physical properties of the BisGMA polymers was larger than for the BisMPEPP polymers, which could be explained by the higher water sorption of BisGMA polymers (45). The properties of the BisMPEPP polymers largely depend on their structural nature , especially the segmental mobility of their side chains. An increase of the segmental mobility of the monomers may increase the creep of the polymers. Therefore, BisMPEPP-based restorative composite resins should be avoided in molar resorations which are subjected to considerable stress by the force of occlusion.

To improve the physical and mechanical properties of the dental resin matrix in the wet condition, some polyfunctional dimethacrylates were prepared to modify the hydrophilic nature of BisGMA resin (46). It was found that the mechanical properties of the visible light cured (VLC) unfilled resins prepared from these polyfunctional dimethacrylates were very dependent on the monomer structure. There was a correlation between the water sorption of the unfilled resins and the reduction in their mechanical properties under wet conditions. The VLC resins based on hydrophobic dimethacrylates showed relatively lower water absorption than the BisGMA resin. With respect to the BisGMA-F monomer, the fluoro-group containing dimethacrylate has some advantages for use as a dental resin system. Fluoro-containing dimethacrylates were effective in reducing the refractive index of the monomers and increasing the hydrophobicity of their polymers. Under wet conditions, the BisGMA-F resin showed higher mechanical properties than the BisGMA resin, but the creep performance of BisGMA-F resin was not studied. Further studies on the properties of the composites based on these dimethacrylate monomers suggested that BisGMA-F based composites had mechanical properties superior to BisGMA based materials (47).

Based on the results of previous studies (48) one can hypothesize that the current dental composites are structurally capable of creep deformation in an oral environment (27). A correlation between creep and homologous temperature (T/T_g) for these composite resins appears to exist. The improvement of the moisture resistance, degree of cure, and the

retention of the glass transition temperature(T_g) under wet conditions could improve the creep resistance and other physico-mechanical properties of the existing dental composite resins as well. Liu (27) prepared new polyfunctional aromatic dimethacrylate resins, yielding new visible light-cured materials which have a more hydrophobic and rigid structure, have less water sorption and higher wet (water saturated) glass transition temperature (T_g) than the commonly used Bis-GMA based matrix resins (27).

Shobha et al.(49) synthesized novel dimethacrylate monomers of propoxylated bisphenols to establish a correlation between their structure and some important properties such as viscosity, curing shrinkage and wetting behavior. These dimethacrylates, designed to possess linear and flexible structures, exhibited much lower viscosities compared to the conventionally used Bis-GMA. They exhibited a good correlation with the viscosity and curing shrinkage behavior with the varied monomer structures.

Potential substitute monomers which are structural analogues of Bis-GMA, namely CH_3 Bis-GMA (A) and 3F Bis-GMA, were synthesized.

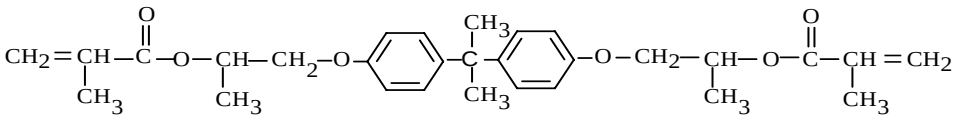

(A)

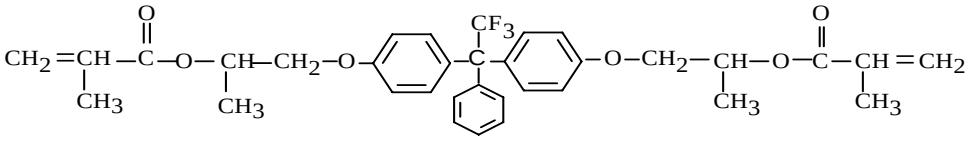

(B)

The effects of dilution of these monomers as well as the control Bis-GMA with dimethacrylate monomer TEGDMA were evaluated (50).

To improve the properties of composite materials, organic or composite fillers prepared from several polyfunctional dimethacrylate monomers were copolymerized with a dimethacrylate resin matrix to prepare new dental crown and bridge resins (51). It was found that mechanical and physical properties of the resultant composites were greatly

enhanced by the composite fillers. The improved properties were due to the resultant highly crosslinked structure resulting from the reaction between the composite filler and matrix monomer. It was observed that the concentration of the double bonds in the matrix was dependent on the length of the crosslinking chain, with short crosslink chains between monomers leading to higher residualdouble bond concentration.

It is claimed in the literature that polyfunctional acrylates were considered to be superior over polyfunctional methacylates in regard to the improvement dental restorative materials. This was due to the better polymerization characteristics e.g., higher reaction activity and degree of polymerization, of polyfunctional acrylates than the corresponding dimethacrylates (52). Investigation (28) of the relationship between the polymerization characteristics and the chemical structures of polyfunctional acrylates and methacrylates by using differential scanning calorimetry (DSC) and high performance liquid chromatography (HPLC) indicated that the extent of polymerization (E_p %) and the efficiency of crosslinking (E_c) values of various monomers increased with an increase in the number of chain members between the functional groups, while the amount of residual monomer (R_m) and the amount of pendent double bond (D_p) decreased. The dimethacrylates consisting of aliphatic chains polymerized more readily than those containing aromatic units. The diacrylates showed a high rate of polymerization in comparison with the corresponding dimethacrylates. It was observed that there was a strong correlation between the polymerization characteristics (E_p, R_m, D_p, and E_c) and the monomer structure, chain length, and framework between two functional groups. This conclusion was in quite good agreement with that previously claimed (53). The high extent of polymerization of the matrix resin is required for improved dental composites.

2.4 Fundamental Considerations of Photopolymerization

Photo curing is the polymerization (in a three-dimensional network) of a chemical system which is initiated by an incident light. The curing, that is to say the transformation from a liquid into a non-tacky solid (54), is very fast.

The raw materials for photocuring make up one of the fastest growing segments of the specialty chemical industry. To initiate the polymerization of the chemical formulation an incident radiation is necessary. The radiation can be ionising (e.g. electron beam) or electromagnetic. The electromagnetic spectrum from lower to higher energy and frequency is given below:

	Radiowaves	
	Microwaves	*longer wavelength*
	IR	
	Visible light	
	UV	
higher energy	X-ray	
	γ-rays	

Radiowaves and microwaves are not powerful enough to initiate polymerization. Curing with IR is used principally as a heat source for thermal curing. Visible light can initiate polymerization when using the right photoinitiator system and is generally used in dental fillings for safety reasons. UV light is most commonly used in non-dental situations and needs a photoinitiator system which is converted by the absorbed light into initiating radicals or cations. X-rays and γ-rays require strong shielding to protect the operators and therefore are only used in very special cases.

Prior to 1970s the power of UV lamps did not exceed 40 W/cm and therefore was not sufficient to overcome oxygen inhibition effectively. Then, in order to overcome oxygen inhibition, the lamp manufacturers increased the power of the UV lamps (Table 2.4.1)

Pulsed Xenon lamps offer very high output in short bursts or pulses, which are useful for certain applications. Most commercial UV-curing lines use medium-pressure mercury vapor lamps with outputs of 80 Watts (54).

Table 2.4.1 *Increase in Power of UV-Vis Lamps*

Increase in power of UV-Vis lamps

Year	Power (Watts)
1960	40
1970	80
1980	120
1987	160
1989	200
1990	240

Most monomers do not produce initiating species with sufficiently high yields when they are exposed to light, so a photoinitiator must be added to the formulation. Once initiated, the chain reaction will develop very much as in a conventional thermal polymerization, except for the much larger rates of initiation that can be reached by intense illumination. The overall process can be presented schematically as follows:

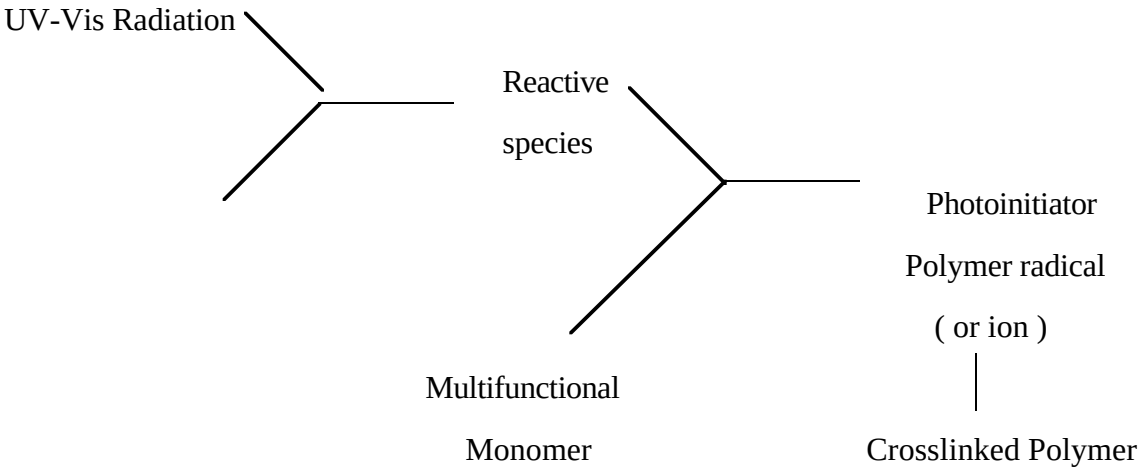

Scheme 2.4.2. *Schematic Presentation of Light Induced Polymerization*

For free radical polymerizations, the evolution of heat from the photoinduced polymerization can be described by consideration of the reaction sequence in Scheme 2.4.3. The below scheme is true for single homolytic cleavage of an initiator and addition of the radicals to monomer.

A photon of light ($h\nu$) is absorbed by the photoinitiator (PI) to yield an excited species (PI*) that readily decomposes to radicals (R·). The radicals then initiate polymerization by reaction with monomer M in the initiation step.

Light absorption $\quad PI \xrightarrow{h\nu} PI^* \quad (1)$

Radical generation $\quad PI^* \longrightarrow R^{\cdot} \quad (2)$

Initiation $\quad R^{\cdot} + M \xrightarrow{k_i} RM^{\cdot} \quad (3)$

Propagation $RM_n^{\cdot} + M \xrightarrow{k_p} RM_{n+1}^{\cdot}$ (4)

Termination by coupling or disproportionation $RM_n^{\cdot} + RM_n^{\cdot} \xrightarrow{k_t}$ Polymer (5)

Termination by trapping of polymer radical $RM^{\cdot} \xrightarrow{k_t'}$ Polymer trapped (6)

$$R_p = k_p / k_t^{1/2} \cdot \phi_{int}^{1/2} \cdot I_{abs}^{1/2} [M] \quad (7)$$

$$R_p = k \cdot [M] \quad (8)$$

$$k = (k_p / k_t^{1/2}) \cdot (\phi_{int}^{1/2} \cdot I_{abs}^{1/2}) \quad (9)$$

$$R_t = 2 k_t \cdot RM^{\cdot} \quad (10)$$

where terms are defined as below:

k_i = initiation rate constant

k_p = propagation rate constant

k_t = termination rate constant

k_t' = termination by isolation of polymer chain

ϕ_{int} = quantum yield for radical initiation via Eq. (2)

[M] = monomer concentration

I_{abs} = light intensity absorbed by photoinitiator

k = composite rate constant for polymerization as defined by Eq. (9)

R_p = polymerization rate = $-$ d[M]/dt

R_t = termination rate

Scheme 2.4.3. *Reaction Sequences in Light Induced Polymerization (55).*

This process is followed by successive addition of monomer units (M) to the growing polymer chain ($RM^{\cdot}$) in the propagation step. The repetition of this propagation process results in the evolution of a large amount of heat. Termination can take place by the interaction of two polymer radicals either by coupling or disproportionation [Eq.(5)]

UV-vis curing is based on photoinitiated polymerization which is mediated by photoinitiators. Photoinitiators (PI) are required to absorb light in the ultraviolet-visible spectral range, generally 250-550 nm, and convert this light energy into chemical energy in the form of reactive intermediates, such as free radicals, which subsequently initiate polymerization. Light absorption by the PI requires that an emission line from the light source overlap with an absorption band of the PI. In this event, The PI is raised to an electronically excited state PI*, as shown in Eq. (11), by promotion of an electron to a higher energy orbital.

$$PI + light \rightarrow PI^* \qquad (11)$$

The lifetime of PI* is short, generally less than 10^{-6} s. During this time, PI* can undergo several processes including (1) decay back to PI with emission of light and/or heat, (2) excited-state quenching back by O_2, monomer or other quenching agent (Q), and (3) a chemical reaction yielding the initiator species, such as $I^{\cdot}$ or I^{+}, as shown in Scheme 2.4.4 below.

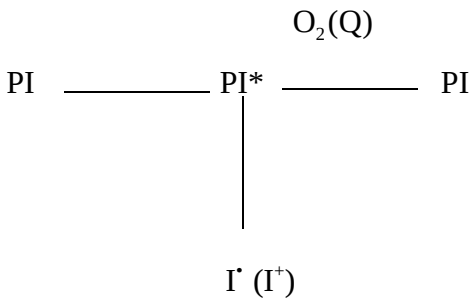

Scheme 2.4.4 *General representation of photoinitiated radical polymerization (55)*

The rate of initiation (R_i) is expressed as the rate of formation of PI*, which corresponding to the number of photons absorbed by the PI per unit time and volume (I_a), times the fraction (F) of PI* that yields initiator species:

$$R_i = I_{abs} \text{ x } \phi_{int} \qquad (12)$$

The term ϕ_{int} indicates the initiation quantum yield and I_{abs} corresponding to the intensity of light absorbed by the PI and is related to the incident light intensity (I_o), the number of photons incident to the system per unit time and area, and the absorbency of the PI. Equation is given below (Eq. 13) in which d is the pathlength of light (or thickness of a film):

$$I_{abs} = I_o(1\text{-}10^{-A}) / d \qquad (13)$$

The absorbance (A) is proportional to the PI concentration and pathlength as shown in Eq. (14), where ε is the molar decadic absorptivity of the PI :

$$A = \varepsilon \text{ x } d \text{ x } c \qquad (14)$$

Equation 14. *Beer - Lambert equation.*

Equations (12)-(14) show that the rate of initiation (R_i) increases proportionally with I_o, but not with photoinitiator concentration (c). As photoinitator concentration and absorbance increase, the proportion of absorbed incident light decreases exponentially per unit thickness. It can also be noted from the Equation 14 that PI concentration is proportional to film thickness (55).

Visible photoinitiator systems have a number of advantages over uv photoinitiator compositions. Visible sources requiring 110 volts (56) produce no ozone, and have none

of the dangers associated with ultraviolet wavelengths which the eye cannot detect (7). Visible light initiators are mostly used at much lower concentrations than are the uv ketonic systems due to their higher absorption coefficients. In addition, visible systems can be designed to either bleach as they initiate polymerization, or not do so. Thus it is possible to add a dimension of flexibility in depth of cure in the visible light that is impossible to attain in the uv (56).

Extensive efforts have been directed towards the development of very efficient photoinitiators (57,58), oligomers (59-60) and monomers (61,62). 1,2-Diketones, such as camphorquinone in combination with a suitable co-initiator have been long known initiators. These diketones exhibit low intensity $n\pi^*$ transitions in the range between 400 and 500 nm with extinction coefficients around 20-50 litres/mol.cm (54) It is indicated that since triplet energies of 1,2-diketones are in the range of 50-70 kcal/mol (210-239 kJ/mol), no homolytic fragmentation takes place from the lowest triplet states. In fact, these diketones abstract hydrogen from the co-initiator to give ketyl radicals.

Amines are mostly used as co-initiators in these systems. The α-amino-alkylradicals initiate the polymerization reaction, while the ketyl radical mainly dimerizes or disproportionates. As the diketone is destroyed by photochemical reduction (Figure 2.4.5), these initiators can undergo bleaching and allow the curing of thick layers, up to 20 mm in dental restoring materials (54).

However the efficiency of hydrogen abstraction in 1,2-diketone/amine initiator systems is low and the initiators formed are less reactive compared to other types of photoinitiators for pigmented systems (54). While the 1,2-diketone/amine initiator systems have been replaced by more efficient photoinitiators in most industrial applications, they are mostly used in dental compositions. Visible light is used in this application since UV radiation is harmful to the oral mucosa. The fact that the most frequently used 1,2-diketone, camphorquinone, is not physiologically hazardous outweighs its having some drawbacks such as low curing speed.

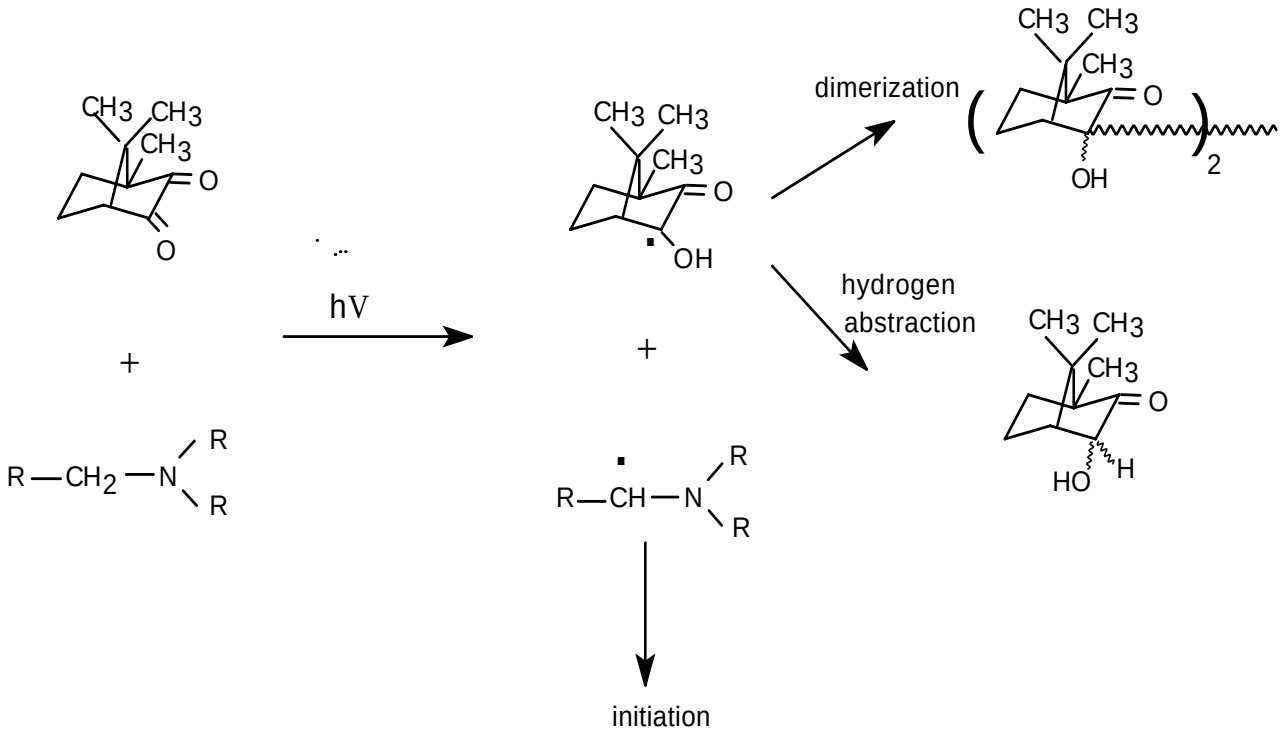

Scheme 2.4.5 *Camphorquinone/Amine Initiation Reaction Scheme(63)*

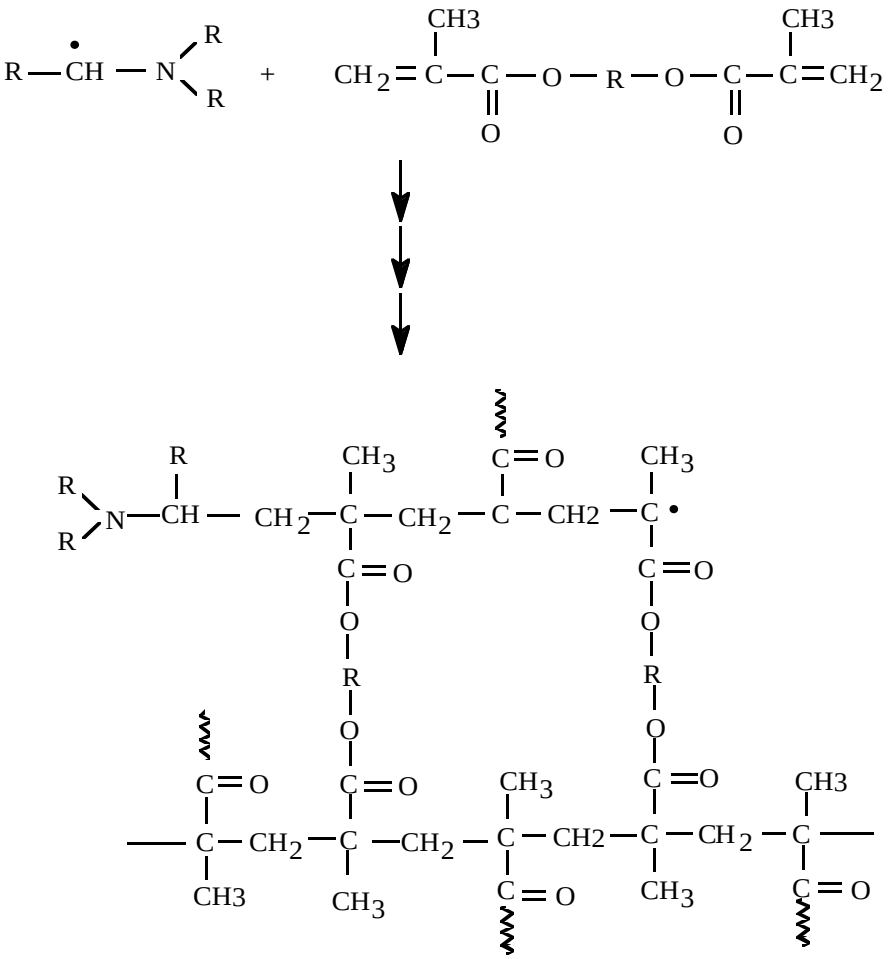

Scheme 2.4.6. *Photoinitiated Crosslinking Polymerization of a Dimethacrylate Monomer*

2.5. Basic Features of Exotherm Curves

Exotherm curves can be plotted as the rate of heat evolution (in mcal/s or cal/s) versus photolysis time as depicted in Figure 2.5.1 below. Alternatively, the exotherm curve may be represented as a plot of percent conversion per second (% s^{-1}) versus time: the percent conversion per second at a particular time is obtained by dividing the value of rate at that time by the total enthalpy of polymerization calculated for 100% conversion

In most of the photopolymerization exotherms, there is an induction period (T_{ind}) prior to the onset of polymerization. This induction period may be due to residual oxygen and/or inhibitors that have been added to prevent premature (thermal) polymerization. (55).

Following the onset of polymerization exotherm, a maximum rate of polymerization (H_{max}), which is the fastest rate of polymerization achieved during polymerization, is reached in a given time (T_{max}). As the rate of polymerization decreases, due to the decrease of monomer and the formation of a highly viscous cross-linked network, the rate of heat evolution drops so that at such a low level it can not be distinguished from the noise of the baseline. However, this does not necessarily mean that the polymerization has completely stopped; it represents the limit of the exotherm unit in recording the heat evolved.

Ultimate percent conversion of the reactive functional group/groups involved in the polymerization process can also be obtained from the basic exotherm curve. By integrating of the area under the entire exotherm curve (in calories) and dividing by the expected enthalpy of polymerization corresponding to the size of sample, the ultimate percent of conversion can be deduced.

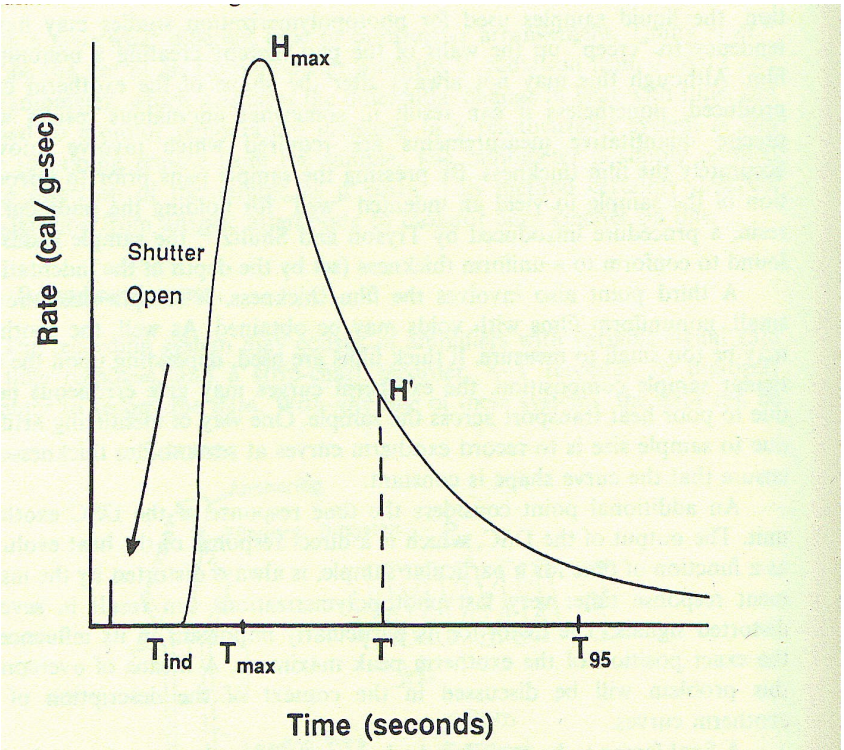

Figure 2.5.1 *Typical exotherm generated from photopolymerization at a constant temperature. The rate on the y-axis is given in terms of dH/dt, with H in terms of cal/g.(55)*

The percent conversion per second can be calculated at any point during the polymerization. In addition, by comparing the integrated exotherm curve from time zero (time at which the sample is first exposed to the light source) to a given time, T', with the total heat expected for 100 % conversion, the cumulative percent conversion is obtained. By measuring the corresponding height, H', of the exotherm curve, both percent conversion and the corresponding polymerization rate at time (T') can be obtained. All of the parameters defined above are illustrated in Figure 2.5.1

Additionally, the composite rate constant, k, as shown in Equation (8), can be calculated at any time, T', by dividing the curve height, H', of the exotherm curve, corresponding to the selected time (or percent conversion), by the total "expected heat" if all of the unconverted monomer units still present were to be converted (64).

In a practical manner, recording and evaluating exotherm curves involves assessing the background heat due to the radiation absorbed by both the sample and the sample pan

and converted directly into heat. Bair and Blyler reported that an empty aluminum pan in a DSC sample cavity exposed to a tungsten-halogen lamp with 95% of the radiation above 375 nm resulted in a signal of 13 cal/s versus 23 cal/s when a carbon disk absorbing all of the light is placed in the sample cavity (65). Thus, the empty aluminum pan absorbs 57% while reflecting 43% of the light. In order to ensure the absorption of light by the sample band is balanced, both the sample and reference pans must receive equal doses of radiation from the source.

2.6 Exotherm Literature Review

Photocalorimetry has been widely used to obtain kinetic and rate data on each component that impacts on the mechanism and efficiency of photopolymerization, e.g., monomer structure, light intensity, inhibitor concentration, oxygen inhibition. Important data dealing with maximum polymerization rate, ultimate conversion, postcuring (after light removal), inhibition time have also been extracted by many researchers. In some cases, actual rate constants for propagation (k_p) and termination (k_t) have been measured. This section of the thesis gives a detailed review of the literature on exotherm analysis of photopolymerization.

2.6.1. Photoinitiator Type and Concentration

One of the key components in any photocurable resin system is the photoinitiator. Since the photoinitiator governs the type and number of radical species generated upon absorption of light, it is evident that the exotherm curve will reflect the effect of photoinitiator structure on the polymerization process. And also, the concentration of a particular photoinitiator will determine the kinetics and rate of polymerization.

The overall efficiencies of many photoinitiators in generating a cross-linked network have been studied in terms of the actual percentage of light absorbed, the maximum rate achieved as well as the ultimate conversion efficiency (55,66,67). Results by Bush et al., showed the effect of an optimum concentration when attempting to maximize the relative

curing rate in a photopolymerization process (68). The data presented for photocuring of a thiol-ene resin using benzophenone as a photoinitiator show that, as the thickness of the film being cured increases, the percent of photoinitiator required for maximum polymerization rate decreases. For thick films it was found that as the concentration was increased beyond an optimum value, the polymerization rate (taken as H_{max})dropped to essentially zero due to high absorption of light at the surface. In general, similar results are found for the free radical polymerization of all mono- and multifunctional monomers, i.e., H_{max} increases and then decreases with increasing photoinitiator concentration.

In addition to general comparisons of the efficiency of a series of photoinitiators, exotherm curves can also be analyzed to provide a relationship between the polymerization rate and such factors as the light absorbed, I_{abs}. As can be seen from Eqs. (8) and (9) k, the composite polymerization rate constant, is related to I_{abs} in a manner identical to that of the polymerization rate. Ikeda and co-workers recorded exotherm curves for lauryl acrylate at several benzoin methyl ether photoinitiator concentrations. They plotted the results in the form of conversion fraction (x) versus photolysis time (Figure 2.6.1.1). By differentiating the conversion fraction versus time plots at a series of times, values for dx/dt were obtained as a function of the conversion fraction x. Extrapolation of the dx/dt versus x plot in (Fig. 2.6.1.1-B) to zero conversion (i.e., $x = 0$) yields the value for k at the beginning of the reaction, i.e., at time zero. The resulting "zero time" k values, for a given conversion fraction x, were plotted versus the square root of the photoinitiator concentration ($c^{1/2}$) (Figure 2.6.1.2).

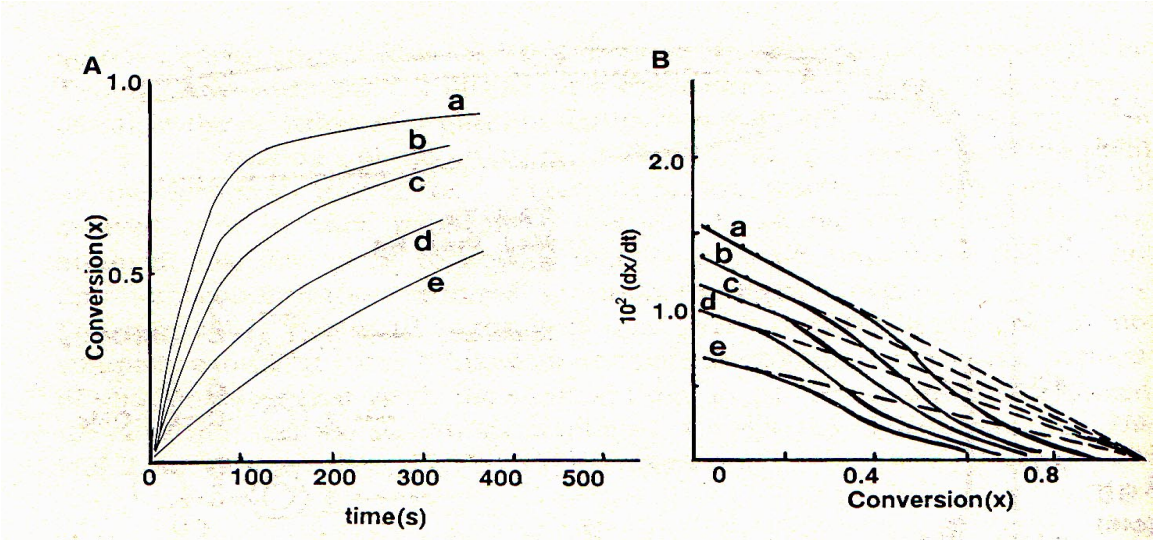

Figure 2.6.1.1 *Polymer conversion vs. time (A) and dx/dt vs. conversion (B) for photo-polymerization of lauryl acrylate with varying initiator concentration(mol initiator/ mol monomer): (a) 0.01; (b) 0.08 ; (c) 0.06 ; (d) 0.04 ; (e) 0.02. All measurments were carried out under light irradiation of 838 μW/cm^{-2} and a wavelength of 365± 15 nm. (55)*

The straight line obtained from the data confirms the relationship in Eqs. (8) and (9), under conditions where I_{abs} is proportional to *c*. Moore *et al.* 69,70) has also used a similar procedure for making plots of *k* versus photoinitiator concentration. They calculated *k* values at the peak polymerization rate by dividing the peak height (H′), of the exotherm curve, corresponding to the monomer concentration, in terms of heat (kcal/mole) remaining at time T′.

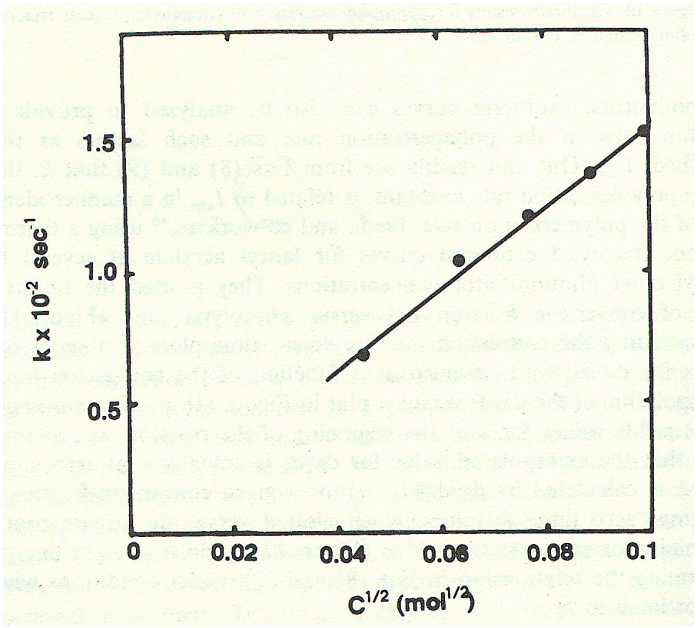

Figure 2.6.1.2 *Plot of limiting rate constant k versus the square root of benzoin methyl ether photoinitiator concentration (55).*

2.6.2. Effect of Inhibitors

Inhibitors, either available in a mixture as impurities or added to prevent prepolymerization, can change the kinetics of a photoinitiated polymerization in several ways such as; (1) a delay in the onset of heat evolution, (2) an increase in the time (T_{max}) required to reach the maximum polymerization rate (H_{max}), (3) a decrease in H_{max}, (4) a decrease in the overall percent conversion measured (total area under the exotherm curve), and (5) a change in the exotherm curve shape (55).

Kloosterboer and Lippits (10) conducted a study of the photopolymerization of HDDA and the inhibiting effect of p-benzoquinone. They found that, in a nitrogen atmosphere under low incident light intensity, H_{max} value significantly decreased and T_{max}

value increased. They also found that the effect of benzoquinone was diminished by increasing the intensity of the light source. Apparently the higher intensity lamp source reduces the inhibitor effect on the polymerization rate, but does not completely eliminate it.

2.6.3. Kinetics and Temperature

In the first calorimetric analysis of photopolymeization processes, Benough and Melville (71,72) calculated the ratio $k_p/k_t^{1/2}$ for several neat monomers. They found half order dependencies of the rate on light intensity suggesting bimolecular termination of polymer radicals in the early stages of polymerization for all monomers studied. They reported individual rate constants (both termination and propagation) as a function of percent conversion and temperature, as well as individual activation energies for propagation (E_p) and termination (E_t). The results reflected the much faster decrease in the rate of termination (k_t) relative to propagation (k_p) with increasing conversion, which corresponds to autoacceleration.

The 1979 report by Tryson and Shultz on the determination of the kinetics of the photoinitiated polymerization of lauryl acrylate (LA), 1,6-hexanediol diacrylate (HDDA), and pentaerylthritol tetraacrylate (PET_4A) system is a landmark paper (73) establishing a basis for development of the field. They pioneered measuring the photopolymerization kinetics of a rapidly crosslinking system by using a DSC-based photocalorimeter. They made direct calculations of the propagation and termination rate constants. Also the dependence of the polymerization rate on factors such as light intensity, initiator concentration, and temperature was determined. Both steady-state and non-steady-state conditions were utilized to study the effects of chemical and physical parameters on photopolymerization of crosslinking multifunctional monomer systems. Tryson and Shultz (73) recorded exotherms at several temperatures and obtained rate data for Arhenius plots as a function of percent conversion. They also made calculations of propagation and termination rate constants (k_p and k_t) by evaluating the polymerization exotherms under both steady-state and non-steady-state conditions. Subsequently, pseudo-activation

energies, $E_a = E_p^{1/2} - E_t$, were obtained from Arrhenius plots (74). The substantial decreases in the calculated values for k_p and k_t with increasing percent conversion shows the effect of the cross-linked network in reducing all rate processes involved in the polymerization.

Cook studied the photopolymerization kinetics of several bisphenol-A dimethacrylate resins by isothermal differential scanning calorimetry over a wide range of temperatures (-40 to 160 ^{o}C). It was found that the limiting conversion was low at low temperatures near the glass transition temperature (T_g) of the monomer but increased rapidly as the curing temperature was raised. At higher cure temperatures, the polymerization rate reached a plateau and then tended to decrease, which was explained as due to the effect of depolymerization of the chains (12).

A dependence of conversion on curing temperature in free radical polymerization has been observed for methyl methacrylate (MMA)/ethylene glycol dimethacrylate (EGDMA)(87), in the photocuring of polyester urethane diacrylates (75) and related resins (76), with photopolymerization of dimethacrylates and diacrylates with bisphenol-A backbones (77). It is commonly accepted that polymerization practically ceases when the Tg of the developing network approaches the curing temperature. However, Levin, et al.(78) presented their unexpected results in which the rate of polymerization of a uv-cured acrylate system is decreased as the polymerization temperature is raised. This was explained by the increase of $k_t^{1/2}$ which is much faster with temperature than k_p.

The final properties of the cured polymer can be significantly affected by the polymerization temperature. In the case of polymers whose glass transition temperatures are close to the cure temperature, the loss in mobility caused by vitrification during polymerization causes large effects in the final properties of the material (92). Overton and co-workers attributed the change in properties at high curing temperatures to an increased rate of termination relative to propagation together with an increase in the degree of termination by disproportionation (80).

2.6.4. Light Intensity Effect

Tryson and Shultz provided a detailed study of the rate dependence on incident light intensity I_0 (73). Using neutral density filters with various attenuating efficiencies, they recorded exotherms for three monomers, while maintaining an identical initiator concentration and temperature, changing only the light intensity. They found that the dependence of rate on I_0 for LA and PET_4A gave exponents of about 0.6 (independent of percent conversion), results for HDDA showed an increasing dependence of rate on light intensity ranging from 0.65 at 15.3 % conversion to 0.97 at 53.5 % conversion. In the case of HDDA, the dependence of rate on I_0 at 53.5 % conversion was suggested to be primarily due to termination by immobilization of radicals in the cross-linked network.

Wight showed that lowering the light intensity by about 70 % resulted in a significant decrease in the exotherm peak maximum (H_{max}) and an increase in T_{max} for mono/multi functional monomers studied (81). Morgan et al. found a linear dependence of log ($H_{max)}$ on the log of the light intensity with a slope of 0.5 indicating a radical-radical coupling process for termination of a trifunctional monomer polymerization (82).

The effect of light intensity on the rate of photopolymerization as a function of conversion was illustrated by Anseth et al. in Figure2.6.4.1 below. They found that the maximum double-bond conversion that is reached increases from 0.48 for the polymerization initiated by 0.6 mW/cm^2 to 0.56 for the polymerization initiated by 4.7 mW/cm^2. They attributed the increased maximum double-bond conversion at increased polymerization rates to greater free volume availability at later stages of the conversion.

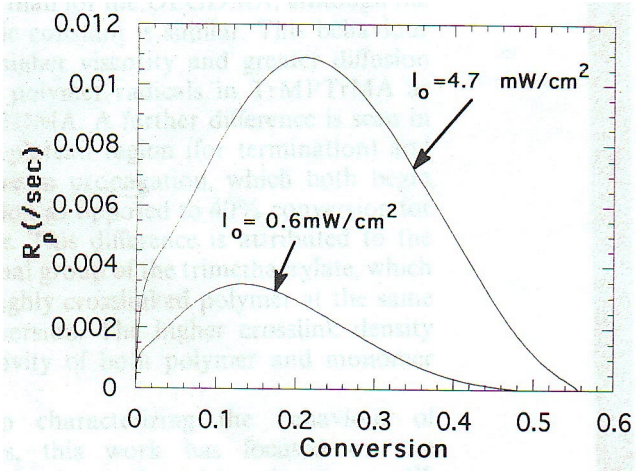

Figure 2.6.4.1 *Rate of polymerization as a function of double-bond conversion forDEGDMA polymerized at two different light intensities* (11).

2.6.5. Effect of Oxygen on Photopolymerization

Oxygen is a well-known strong inhibitor of radical-induced polymerizations due to its high reactivity towards radicals. By scavenging the initiator radicals, oxygen reduces the rate of polymerization, thus longer exposure time is required (83).

The kinetic curves obtained in the presence of air usually have a sigmoid shape, with an initial induction period due to the inhibition effect of atmospheric oxygen (83,84). One of the first examples of the effects of oxygen on photocuring was described by Wight (81). The DSC results in Figure (2.6.5.1) below for photopolymerization of a blend of mono, di and oligomeric acrylates in air and nitrogen atmosphere clearly show both an inhibiting and retarding effect on the polymerization process. For the three samples cured in air (curves C-E), the induction time decreased with an increase in the relative light intensity (I_{rel}). In addition to long induction times in the presence of oxygen, the integrated areas of the exotherm curves indicate a significant decrease in the ultimate conversion compared to the N_2 cured samples.

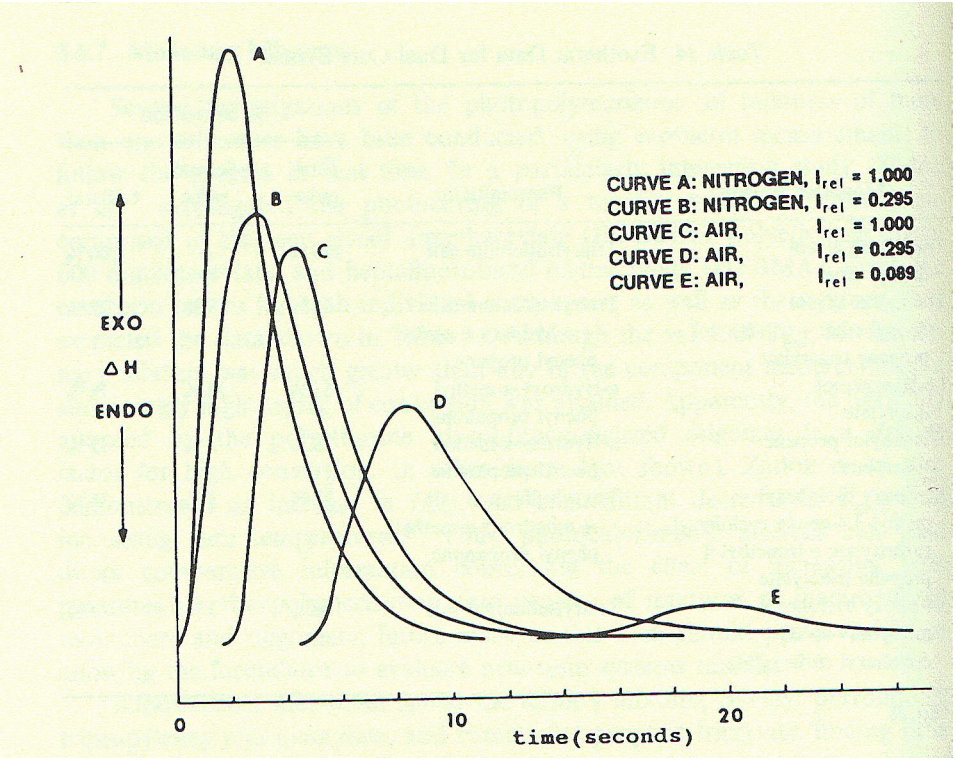

Figure 2.6.5.1 *Photopolymerization of an acrylate blend in nitrogen (A,B) and air(C-E) atmosphere* (83).

This effect disappears if the irradiation is performed under nitrogen (81). The significant disappearance of oxygen inhibition on photopolymerization is illustrated in Figure 2.6.5.1 by Decker (82). It was proved by Decker et al. (83, 84) that in thin films, the reaction is strongly inhibited, as oxygen easily diffuses into them and interferes with the polymerization by scavenging both the initiating ($R^{\cdot}$) and polymeric ($P^{\cdot}$) radicals. The extent of photopolymerization has been found to decrease sharply with the decrease of thickness of monomer films irradiated in contact with air. In these systems, the light intensity has to be increased to allow the monomer to compete with oxygen for the scavenging of the initiator radicals (84).

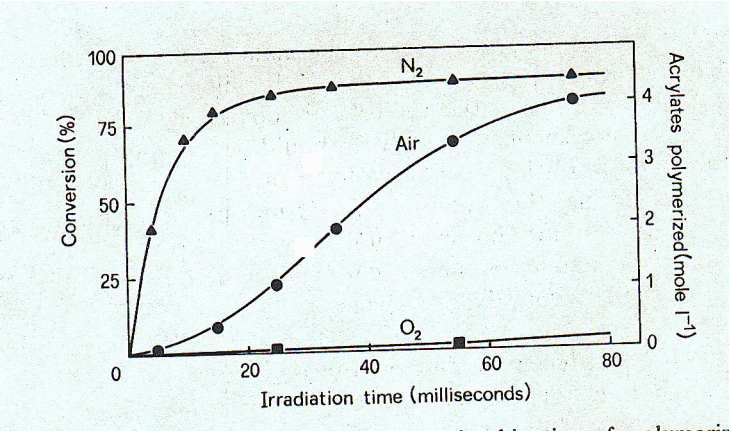

Figure 2.6.5.2 *Influence of atmospheric oxygen on the kinetics of polymerization of a polyurethane-diacrylate resin (82)*

Upon irradiation, the photoinitiator molecules are excited to singlet and triplet states which are highly unstable and cleave into radical fragments. It is indicated that these excited states are usually not quenched by oxygen during their very short lifetime($<10^{-9}$ s) however, the initiator radicals, $R^{\cdot}$, are scavenged by the dissolved oxygen molecules. The free radicals that escape from oxygen scavenging initiate the polymerization. The relative concentration of oxygen and monomer and also the respective rate constants determine the efficiency of the two competitive processes (85).

In the presence of air, the following series of events is postulated in the overall reaction scheme of photopolymerization (86).

$$R^{\cdot} + O_2 \xrightarrow{k_o} RO_2^{\cdot} \quad (15)$$

$$RO_2^{\cdot} + DH \longrightarrow RO_2H + D^{\cdot} \quad (16)$$

$$D^{\cdot} + O_2 \longrightarrow DO_2^{\cdot} \quad (17)$$

$$DO_2^{\cdot} + DH \longrightarrow DO_2H + D^{\cdot} \quad (18)$$

$$P^{\cdot} + O_2 \longrightarrow PO_2^{\cdot} \quad (19)$$

$$PO_2^{\cdot} + DH \longrightarrow PO_2H + D^{\cdot} \quad (20)$$

$$DO_2^{\cdot} + DO_2^{\cdot} \longrightarrow \text{termination} \quad (21)$$

Scheme 2.6.5.1. *Overall Effect of Oxygen in Photopolymerization(86)*

DH represents a donor molecule which is the monomer itself or an added tertiary amine. The peroxide radicals have been considered ineffective to initiate the polymerization and finally they disappear by hydrogen abstraction or bimolecular termination. Decker, et al. reported that highly oxidizable compounds, such as tertiary amines, reduce the induction period by generating α-amino radicals, D ˙, that consume oxygen by the chain process. Tertiary amines with an optimum concentration also allow the system to reach a maximum polymerization rate. Moreover, if amine concentration is high enough to reduce the oxygen content, through Eqs. (17) and (18), polymerization may proceed without inhibition (86).

Oxygen also affects post-photopolymerization. During vitrification, radicals are extensively trapped, and upon exposure to air, these radicals are oxidized and form hydroperoxides (87). Decker, et al. observed additional polymerization upon heating the samples in the presence of air. The increase of conversion was larger in the presence of than in the absence of oxygen with multifunctional acrylic monomers. This is due to the presence of peroxide groups, formed by oxygen scavenging of the initiator radicals. Upon heating, hydroperoxide groups will generate alkoxy and hydroxy radicals which can induce additional polymerization.

2.7. Techniques for analysis of network structure

The effective use of these materials and tailoring them for any particular application requires a good understanding of the relationship between the structure and properties of the polymers. Since the structure and properties of these materials are determined predominantly by the polymerization conditions, following the structure and property evolution during the reaction is critical. In the case of crosslinked polymers, this reaction characterization is even more important. This is because the structure and properties are fixed following polymerization and further processing such as melting and annealing (1) is impossible.

The use of conventional initiators to polymerize these networks leaves radicals entrapped in highly crosslinked regions (5,88-89). The presence of these trapped radicals makes it unable to heat the network system without further polymerization. Therefore, it is very difficult to evaluate their structural heterogeneity by measuring mechanical and dielectric properties as a function of temperature and frequency. Kannurpatti et.al. (1) utilized a novel technique employing "iniferters," i.e., controlled "living" radical polymerization to photopolymerize the networks and prevent trapping of free radicals in these networks. It was shown that crosslinked polymers made in this manner can be studied for their properties to evaluate their heterogeneous structures. By using iniferters in these free radical polymerizations (90) it has been found that the reaction mechanism is such that radicals do not become trapped, even in highly crosslinked polymer networks. This hypothesis was also supported by calorimetric evidence in which no further reaction took place upon heating the polymer network.

a) Conventional Polymerization.
upon heating the crosslinking
density of the network increases

b) Living Radical Polymerization.
no further increase of conversion
upon heating

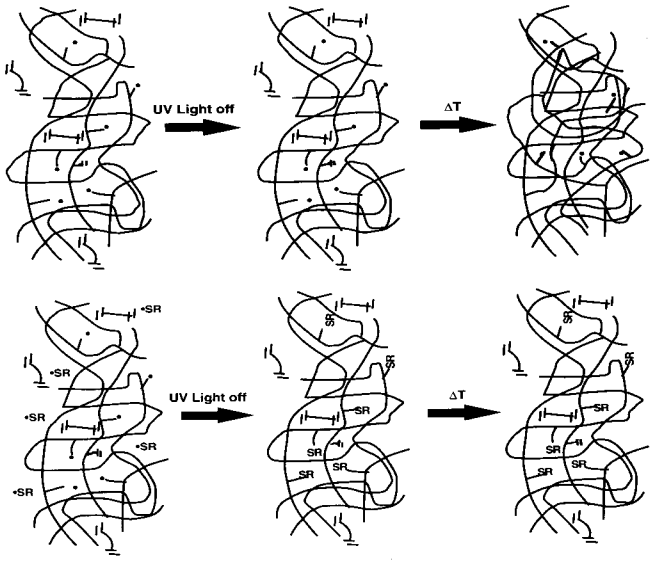

Figure 2.7.1 *Comparison of Conventional and Controlled "Living" Radical Polymerization Schemes (1)*

Dynamic mechanical measurements provides a good understanding regarding the heterogeneous nature of the distribution of relaxation times of the segments of these network polymers. Such analyses on copolymers yield correlation between the structural inhomogeneity (heterogeneity in the mobilities of the segments) and the comonomer composition. Dynamic mechanical analyses and dielectric analyses have been employed by several researchers to make inferences regarding the structural heterogeneity of polymer networks formed by free radical polymerizations (91-93). Polydimethacrylates, for instance, have been characterized in terms of crosslinks and pendant double bonds, on the assumption that crosslinking is random (94). Turner, et.al. (94) reported some mechanical properties of dimethacrylate networks. A Bis-GMA copolymer exhibited a very broad transition, more than 100 ^{o}C, from the glassy to the rubbery state. Following a convention used in DMA, a value of T_g = 48 ^{o}C was assigned by reference to the maximal value of mechanical loss, i.e., of tan δ.

While other techniques (95-97) such as neutron scattering and small-angle X-ray scattering(SAXS) may be employed to study directly the inhomogeneity of the polymer structure, the effectiveness of these techniques has been demonstrated mainly in networks

formed by step (condensation) polymerizations and less densely crosslinked polymers. It has been reported by researchers (91-93) that directly observing structural inhomogeneities is especially difficult in multi(meth)acrylate systems because of the very low gel point conversion (typically less than 1%) and complexities of the free radical polymerizations.

Solid-state NMR spectroscopy (98,99) and swelling techniques (100) have been extensively used to gather evidence regarding the heterogeneity of these multi(meth)acrylate network systems. In addition, the presence of a very inhomogeneous structure was confirmed by researchers using photochromic probes (101,102) and transmission electron microscopy (103).

The degree of cure of these network systems may be also expressed as the weight fraction of gel. Chemical analysis of extracts, obtained with a suitable solvent, can give useful information about the sol content and about its chemical composition. The use of High Performance Liquid Chromatography (HPLC) enables the quantitative determination of mobile, extractable compounds. These compounds can either have not reacted or have been formed during the curing process. Kloosterboer et al. (88) reported the monomer and temperature dependence of the solvent extraction/HPLC analysis of a model compound, namely 1,6-hexanediol.

Miyazaki and Horibe (115) also investigated the relationship between the polymerization characteristics and chemical structure of the cross-linked dimethacrylates. The amount of pendant double bonds and the efficiency of cross-linking were calculated from both extent of polymerization (from DSC) and the amount of residual monomer (from HPLC).

Chapter 3. Experimental

3.1 Synthesis

3.1.1 Solvents and Chemicals Used

3.1.1.1 Solvents

Tetrahydrofuran (THF)

Supplier: EM Science

Molecular weight (g/mol): 72.11

Density (g/cc): 0.87

Boiling Point (^{0}C/mmHg): 66/760

Purification: Used as received

Structure:

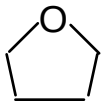

Ethyl Ether [$(C_2H_5)_2O$]

Supplier: Mallinckrodt

Molecular Weight(g/mol): 74.12

Density(g/cc): 0.708

Boiling Point (^{0}C/mmHg): 34.6

Purification: Used as received

Structure: $C_2H_5-O-C_2H_5$

1,2 Dichloromethane (CH_2Cl_2)

Supplier: EM Science

Molecular Weight(g/mol): 86.95

Density(g/cc): 1.362

Boiling Point (^{0}C/mmHg): 40

Purification: Used from a newly opened bottle or fractionally distilled from CaH_2.

Structure: CH_2 Cl_2

3.1.1.2 Monomers

2,2-bis(4-(2-hydroxy-3-methacryloxyprop-1-oxy)phenyl)propane (BisGMA)

Supplier: Polysciences Inc.(Warrington, Pa, USA)

Molecular Weight(g/mol): 510.6

Viscosity(Pa s):1200

Purification: Used as received.

Structure:

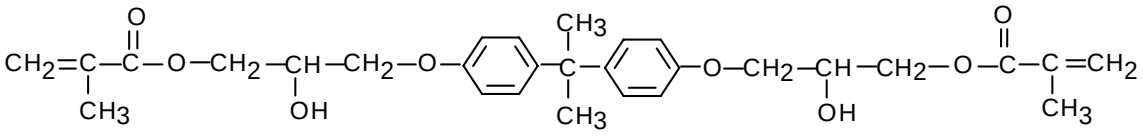

Triethyleneglycoldimethacrylate (TEGDMA)

Supplier: Polysciences Inc.(Warrington, Pa, USA)

Molecular Weight(g/mol): 286.33

Viscosity(Pa s):

Density(g/cc): 1.092

Purification: Used as received.

Structure:

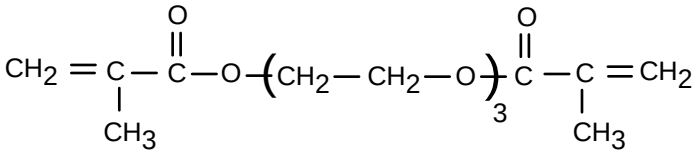

Propoxylated BisA dimethacrylate (2,2-bis(4-(2-methacryloxyprop-1-oxy)phenyl)propane

Supplier: Synthesized in high purity according to the procedure in section 3.1.2.9

Molecular Weight(g/mol): 480.545

Viscosity(Pa s): 0.3

Purification: Purified by column chromatography(silica gel) using ethyl ether/hexane mixture as eluent.

Structure:

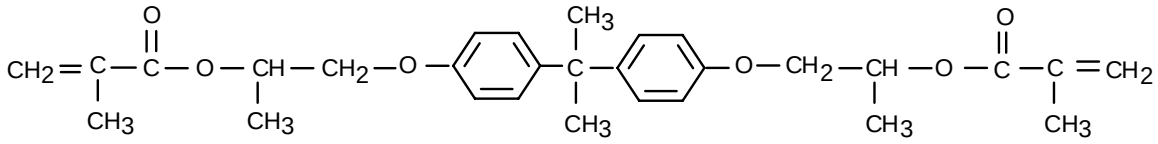

Ethoxylated BisA dimethacrylate (2,2-bis(4-(2-methacryloxyethyl-1-oxy)phenyl)propane)

Supplier: Synthesized in high purity according to the procedure in section 3.12.12

Molecular Weight(g/mol): 452.53

Viscosity(Pa s): 3.0

Purification: Purified by column chromatography(silica gel) using ethyl ether/hexane mixture as eluent.

Structure:

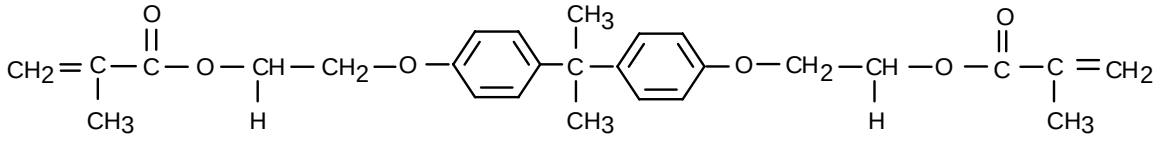

Propoxylated 6F dimethacrylate (1,1,1,3,3,3-hexafluoro-2,2-bis (4-(2-methacryloxyprop-1-oxy)phenyl)propane

Supplier: Synthesized in high purity according to the procedure in section 3.1.2.11

Molecular Weight(g/mol): 588.53

Viscosity(Pa s): 0.8

Purification: Purified by column chromatography(silica gel) using ethyl ether/hexane mixture as eluent.

Structure:

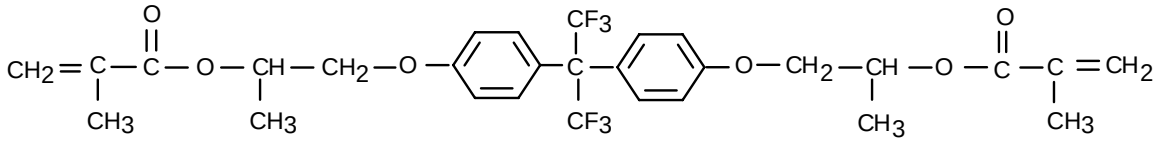

Ethoxylated 6F dimethacrylate (1,1,1,3,3,3-hexafluoro-2,2-bis (4-(2-methacryloxyethyl-1-oxy)phenyl)propane)

Supplier: Synthesized in high purity according to the procedure in section 3.1.2.13

Molecular Weight(g/mol): 560.18

Viscosity(Pa s): 1.5

Purification: Purified by column chromatography(silica gel) using ethyl ether/hexane mixture as eluent.

Structure:

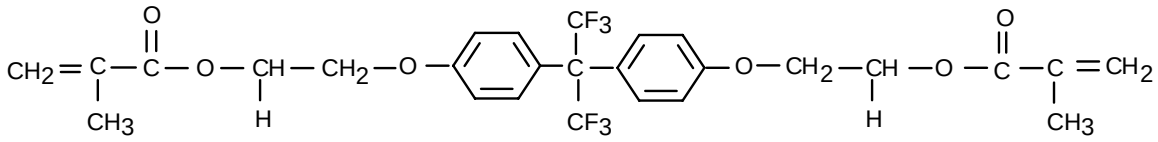

3.1.1.3 Other Chemicals

Bisphenol A [4,4'(isopropylidene)diphenol]

Supplier: Dow Chemical

Molecular Weight(g/mol): 228.29

Melting Point(^{0}C): 158-159

Purification: Used as received.

Structure:

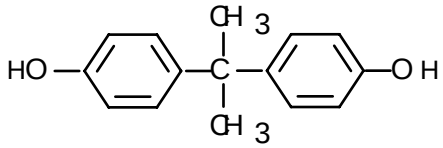

Hexafluoro Bisphenol A , 6F [4,4' (hexafluoraisopropylidene)diphenol]

Supplier: Riedel-de Haen

Molecular Weight(g/mol): 336.23

Melting Point(^{0}C) : 161-163

Purification: Used as received.

Structure:

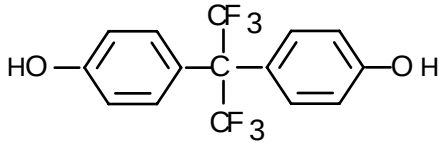

Propylene oxide (1,2-epoxypropane)

Supplier: Aldrich

Molecular Weight(g/mol): 58.08

Boiling Point(^{0}C/mmHg): 35

Density(g/cc): 0.830

Purification: Fractionally distilled from CaH_2 under nitrogen blanket

Structure:

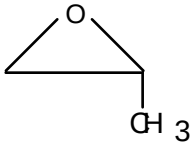

Tetra ethylamonium iodide [$\mathbf{N(C_2H_5)_4^+ I^-}$]

Supplier: Aldrich

Molecular Weight(g/mol): 257.16

Melting Point(^{0}C): > 300

Purification: Used as received

Triethylamine [$N(C_2H_5)_3$]

Supplier: Fisher

Molecular Weight(g/mol): 101.19

Boiling Point(^{0}C/mmHg): 88.8

Density(g/cc): 0.726

Purification: Used as received

Sodium Hydroxide (NaOH)

Supplier: Mallinckrodt Inc.

Molecular Weight(g/mol): 40.0

Purification: Used as received.

Hydrochloric acid (HCl)

Supplier: EM Science

Molecular Weight(g/mol): 36.46

Density(g/cc): 1.2

Purification: Used as received.

Sodium bicarbonate ($NaHCO_3$)

Supplier: EM Science

Molecular Weight(g/mol): 84.01

Purification: Used as received.

Sodium sulfate (Na_2SO_4)

Supplier: Aldrich

Molecular Weight(g/mol): 142.04

Melting Point(^{0}C): 88.4

Purification: Used as received.

Ethylene carbonate

Supplier: Aldrich

Molecular Weight(g/mol): 88.06

Melting Point(^{0}C): 37-39

Purification: Used as received.

Structure:

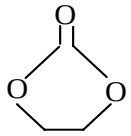

Methacryloyl chloride

Supplier: Aldrich

Molecular Weight(g/mol): 104.54

Boiling Point(^{0}C/mmHg): 95-96

Density(g/cc): 1.07

Purification: Fractionally distilled from CaH_2 under nitrogen and stored at 3-4 ^{0}C.

Structure:

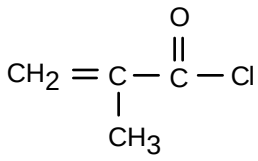

Camphorquinone, [2,3-bornanedione], (CQ)

Supplier: Aldrich

Molecular Weight(g/mol): 166.22

Melting Point(^{0}C): 198-200

Purification: Sublimed at 96 ^{o}C under reduced pressure.

Structure:

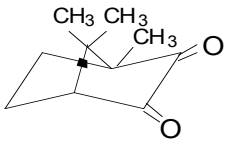

N,N-Dimethyl-p-toluidine (DMpT)

Supplier: Aldrich

Molecular Weight(g/mol): 135.21

Boiling Point(^{0}C/mmHg): 211

Density(g/cc): 0.937

Purification: Fractionally distilled from CaH_2.

Structure:

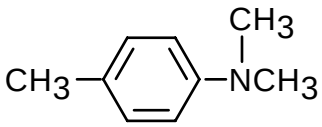

4-Dimethylaminopyridine (DMAP)

Supplier: Aldrich

Molecular Weight(g/mol): 122.17

Melting Point(^{0}C): 112-114

Purification: Used as received

Structure:

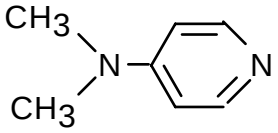

3.1.2 Preparation of Monomers

3.1.2.1 Synthesis of propoxylated bisphenol-A [(2,2-bis(4-(2-hydroxyprop-1-oxy)phenyl) propane) (Prop-BisA)]

The synthesis of propoxylated-bisA, via aliphatic nucleophilic substitution of propylene oxide on bisphenol-A has been reported (97).

The propoxylated-bisA was synthesized by the reaction of bisphenol-A (2,2-bis(4-(2-hydroxyprop-1-oxy)phenyl)propane (114.5 g, 0.5 mole) with propylene oxide (140.23 ml, 116.39 g, 2 mole) in the presence of sodium hydroxide(8 g, 0.2 mole) (Scheme 1). To a clean, dry one-necked 2 liter round-bottomed flask equipped with a magnetic stir bar, 600 ml of THF and 150 ml of deionized water was added. Bisphenol-A was then added and followed by addition of sodium hydroxide. A septum was placed on the flask and the slurry was stirred until the contents of the reaction vessel become homogeneous. Then, propylene oxide was introduced to the flask, and the reaction vessel was immersed in an ice bath for an hour and then in a water bath maintained at 40 ^{o}C and stirred for 48 hours. The propoxylation reaction scheme is shown below.

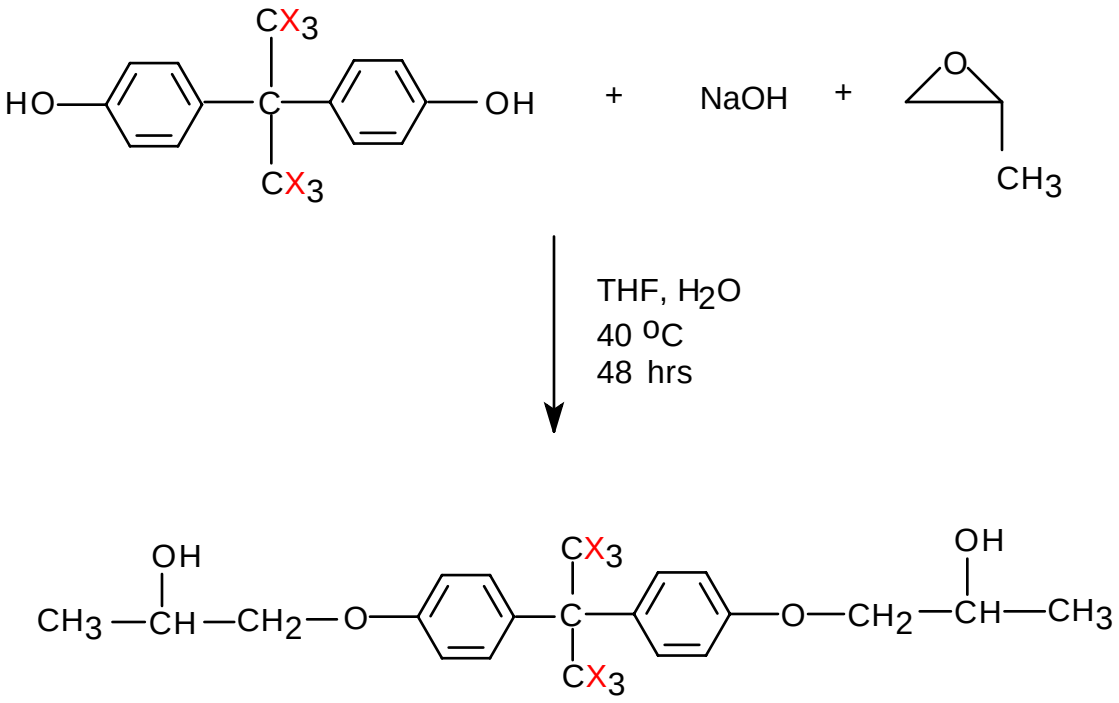

X = H : BisA

X = F : 6F

Scheme 3.1.1 Reaction Scheme of Propoxylation of BisA/6F

A sample calculation of the mol ratios of the reactants is shown below :

Mole ratio of reactants: BisA : NaOH : Propylene oxide = 1 : 0.4 : 4

MW(BisA) = 228.3 g/mole

m(BisA) = 114 g

n(BisA) = (114.5 / 228.3) = 0.501 mole

n(NaOH) = 0.4 x n(BisA)

n(NaOH) = 0.4 x 0.501 = 0.20 mole

MW(NaOH) = 40 g/mole

m(NaOH) = (40 x 0.2) = 8 g.

n(PrOx) = 4 x n(BisA)

n(PrOx) = 4 x 0.501 = 2.00 mole

MW(PrOx) = 58.08 g/mole ; d(PrOx) = 0.83 g/cm^3

m(PrOx) = (58.08 x 2.00) = 116.39 g.

V = m / d = 116.39(g)/ 0.83 (g/cm^3) =140.23 cm^3

Equations 1. A sample calculation of the mole ratios of the reactants for the synthesis of Propoxylated BisA

Quantitative conversion was evidenced by the complete disappearance of the aromatic resonances centered at 6.79 and 7.05 ppm and the appearance of the shifted resonances at 6.70 and 7.12 ppm in ^{1}H NMR.

3.1.2.2 Purification of Propoxylated BisA

The reaction mixture was neutralized with concentrated HCl (24 ml, 0.24 mol). Upon neutralization, the contents of the vessel were separated into two homogeneous

layers. The solvent was removed from the organic layer by rotary evaporation under reduced pressure and the crude product was dissolved in diethyl ether.

The aqueous layer was separated and extracted twice with ether. The combined ether layers were then extracted three times with water to remove unreacted or one side reacted phenols, three times with aqueous, saturated NaCl solution to remove excess water. The mixture was then dried over MgSO4 and the solvent stripped by rotary evaporation. The major side-product of the reaction, propylene glycol was removed in a Kugelrohr apparatus at 130 °C and ~27 Pa pressure. The product was crystallized (m.p. 99-100 °C) over a 2 week period and isolated in a 97 % yield.

3.1.2.3 Synthesis of Propoxylated 6F-bisphenol [(1,1,1,3,3,3-hexafluoro-2,2-bis(4-(2-hydroxyprop-1-oxy)phenyl)propane (Prop6F)]

Propoxylated-6F was synthesized in a manner virtually identical to the synthesis of propoxylated-bisA detailed in section 3.1.2.1 (Scheme3.1.1). First, 500 ml of THF and 125 ml deionized water were added into a clean, dry one-necked 2 liter flask equipped with a magnetic stir bar. 6F (91 g, 0.27 mol) was then added followed by the addition of sodium hydroxide (4.3 g, 0.11 mol). A septum was placed on the flask and the slurry was stirred until the contents of the reaction vessel were homogenous. Propylene oxide (75.6 ml, 62.73 g, 1.08 mol) was added to the flask and the reaction vessel was immersed in an ice bath for an hour and then in a water bath maintained at 40 °C and stirred for 48 hours. The shift of the aromatic proton resonances in ^{1}H n.m.r. was again used to indicate reaction completion.

3.1.2.4 Purification of Propoxylated 6F

After neutralization of the reaction mixture with concentrated HCl (13 ml, 0.132 mol), the contents of the vessel separated into two homogenous layers. The solvent was

removed from the organic layer by rotary evaporation under reduced pressure and the crude product was dissolved in diethyl ether. The aqueous layers was separated and extracted twice with ether. The combined ether layers were then extracted three times with water to remove unreacted or one side reacted phenols, and finally three times with aqueous, saturated NaCl solution to remove excess water. The mixture was then dried over Na_2SO_4 and the solvent stripped by rotary evaporation. The major side-product of the reaction, propylene glycol was removed in a Kugelrohr apparatus at 130 ^oC and ~27 Pa pressure. The solid, amorphous product was isolated in a 93 % yield.

3.1.2.5 Synthesis of ethoxylated bisphenol-A [(2,2-bis(4-(ethoxy)phenyl)propane) (Et-BisA)]

The ethoxylated-BisA was synthesized by the bulk reaction of bisphenol-A(2,2-bis(4-(2-hydroxyprop-1-oxy)phenyl) propane(100.5 g, 0.351 mol) with ethylene carbonate (68 g, 0.772 mol) in the presence of tetraethyl ammonium iodide $\{N(C_2H_4)_4^+I^-\}$

3.53 g, (0.0176 mol) (Scheme 3.1.2). Bisphenol A and $N(C_2H_4)_4^+I^-$ were charged to a clean, dry three-necked 250 ml round-bottomed flask equipped with a condensing arm and a magnetic stir bar. The flask was then placed in a temperature controlled oil bath set to 160 ^oC and nitrogen was bubbled. Ethylene carbonate was then added to the reaction vessel. After melting of the contents of the flask, nitrogen flow rate was increased and the reaction was allowed to continue about 4 hours. Completion of reaction was confirmed by TLC and infrared spectroscopy.

Reaction scheme of ethoxylation of BisA/6F is shown in Scheme 3.1.2 below.

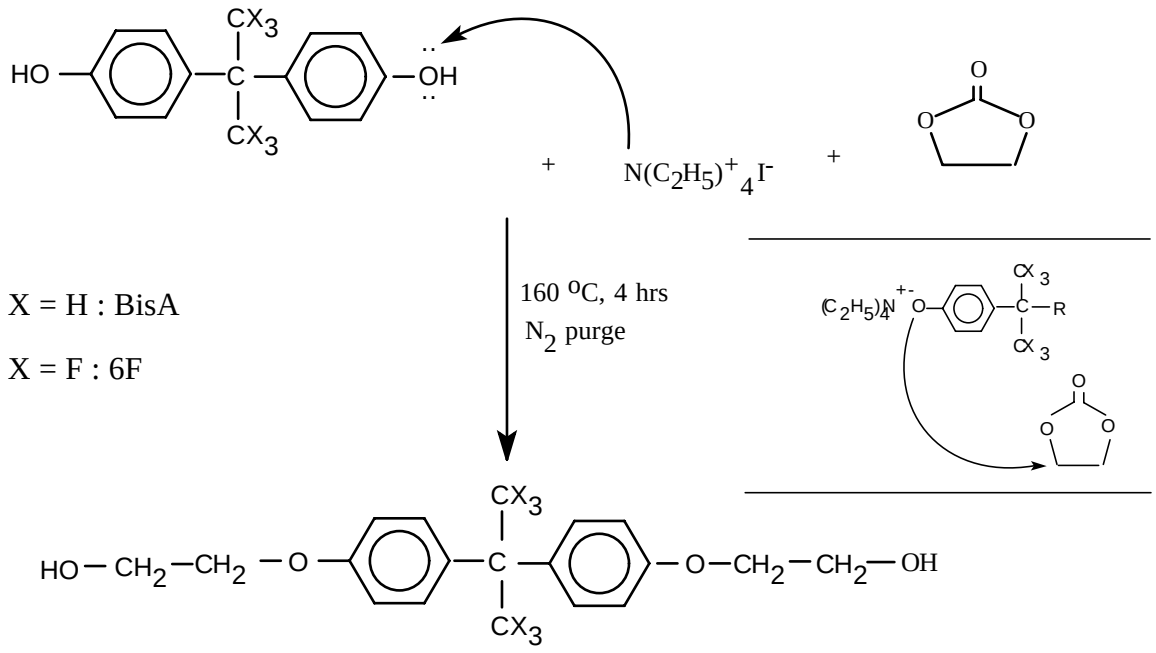

Scheme 3.1.2. Reaction Scheme of Ethoxylation of BisA/6F

A sample calculation of the mole ratios of the reactants is shown below:

Mole ratio of reactants : BisA : TEA : $C_2H_2CO_3$ = 1 : 0.05 : 2.2

MW(BisA) = 228.3 g/mole

m(BisA) = 100.5 g

n(BisA) = (100.5 / 228.3) = 0.44 mole

n(TEA) = 0.05 x n(BisA)

n(TEA) = 0.05 x 0.44 = 0.022 mole

MW(TEA) = 257.16 g/mole

m(TEA) = (201.05 x 0.022) = 5.657 g.

$n(C_2H_2CO_3)$ = 2.2 x n(BisA)

$$n(C_2H_2CO_3) = 2.2 \times 0.44 = 0.968 \text{ mole}$$

$$MW(C_2H_2CO_3) = 88.06 \text{ g/mole}$$

$$m(C_2H_2CO_3) = (88.06 \times 0.968) = 85.24 \text{ g.}$$

Equations 2. A sample calculation of the mole ratios of the reactants for the synthesis of Ethoxylated BisA.

3.1.2.6 Purification of Ethoxylated BisA

A flaky solid product was obtained by filtration. The product was purified by washing with hot water and methanol and dried in a vacuum oven at 90 °C. The product was obtained in high yield (86 %). Proton NMR and TLC was used to confirm the purity and structure of EtBisA.

3.1.2.7 Synthesis of Ethoxylated 6F [(1,1,1,3,3,3-hexa fluoro-bis(4-(ethoxy)phenyl) propane) (Et-6F)]

The ethoxylated-6F was synthesized by the bulk reaction of 6F (93.7 g, 0.278 mol) with ethylene carbonate (5.892 g, 0.612 mol) in the presence of tetraethylammonium iodide $\{N(C_2H_5)_4^+I^-\}$(3.58 g, 0.014 mol). 6F and $N(C_2H_5)_4^+ I^-$ were charged to a clean, dry three-necked 250 ml round-bottomed flask equipped with a condensing arm, a temperature controlled oil bath set to 160 °C, and a magnetic stir bar. Nitrogen was bubbled through the hot mixture after melting. Ethylene carbonate was then added to the reaction vessel. After melting of the contents of the flask, nitrogen flow was started at a rate of ~200/min, and the reaction was allowed to continue about 4 hours. TLC and FTIR were used to confirm the completion of reaction.

3.1.2.8 Purification of Ethoxylated 6F

It was difficult to dissolve the crude product for purification. The product was melted by a heat gun, transferred to an extraction funnel and then dissolved in chloroform. The solution of the crude product was first extracted with dilute (5 w/v %) NaOH, next with deionized water, and finally with saturated NaCl solution. All the extractions were repeated at least three times. After the chloroform solution was dried over Na_2SO_4, the solvent was stripped by rotary evaporation, and the product was kept in a vacuum oven overnight at 80 ^{0}C.

3.1.2.9 Synthesis of propoxylated-BisA dimethacrylate [2,2-bis(4-(2-methacryloxy prop-1-oxy)phenyl)propane (Prop-BisAdimet)]

The Prop-BisA dimethacrylate was synthesized by the esterification reaction of prop-BisA with methacryloyl chloride in the presence of triethylamine as acid scavenger and 4-dimethylaminopyridine as a catalyst in a mole ratio of 1 : 2.1 : 2.2 : 0.05 respectively. To a clean, flame dried, three-necked two liter round bottomed flask fitted with an overhead stirring, a water condenser, a pressure equilibrated addition funnel, thermometer, and nitrogen inlet, was added 1000 ml of dichloromethane (CH_2Cl_2). Propoxylated bisphenol-A (109.7 g, 0.319 mole) was then dissolved in the CH_2Cl_2. Triethylamine (70.99 g, 82.36 ml 0.701 mol) was charged to the flask through the addition funnel. A water/ice bath was placed around the reaction vessel and stirring was begun. The mixture was kept stirring for ~ 30 min and then distilled methacryloyl chloride (70.03 g, 65.44 ml, 0.67 mole) was added dropwise to the flask through the addition funnel at a rate such that the temperature of the reaction mixture was maintained at less than 30 ^{o}C. It was realized by the author that the addition rate of the acid chloride is very important for reducing the impurity of unreacted acid chloride. Therefore, methacryloyl chloride was

added very very slowly. After addition of all the acid chloride, 4-dimethylaminopyridine (0.016 mole, 1.955 g) used as a co-catalyst to hasten the completion of the reaction was added and the water/ice bath was removed. The contents of the reaction vessel were then stirred for an additional 4 hours. During this time, the triethylamine hydrochloride salts formed. The completion of reaction was checked by TLC and FTIR.

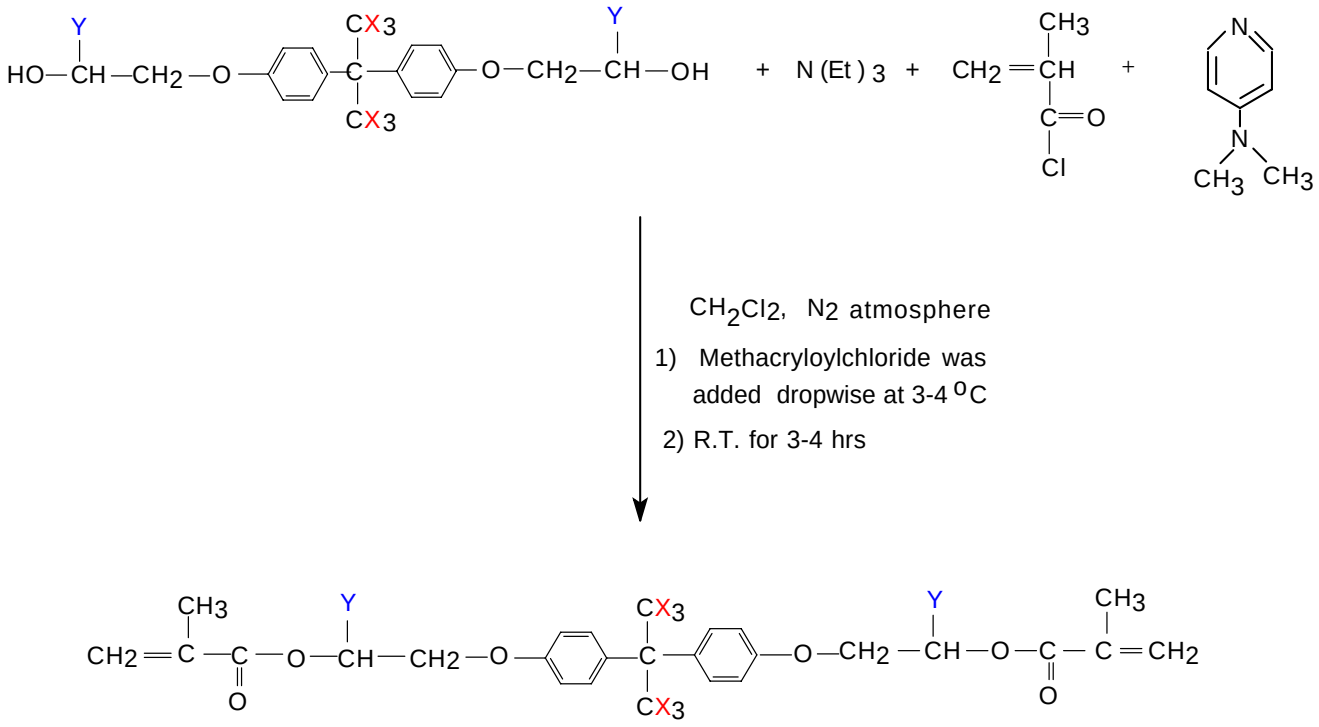

X = H ; Y = CH_3 : PropBisA

X = H ; Y = H : EtBisA

X = F ; Y = CH_3 : Prop6F

X = F ; Y = H : Et6F

Scheme 3.2.3 Methacrylation of propoxylated BisA/6F and/or ethoxylated BisA/6F

A sample calculation of the reactants is shown in Equations (3) below.

Mole ratio of reactants:

PropBisA : $N(Et)_3$: Methacryloyl chloride : DMAP= 1 : 2.2 : 2.1 : 0.05

MW(propBisA) = 344 g/mol

m(propBisA) = 109.7 g

n(propBisA) = (109.7 / 344) = 0.319 mole

$n(NEt_3)$ = 2.2 x n(propBisA)

$n(NEt_3)$ = 2.2 x 0.319 = 0.701 mole

$MW(NEt_3)$ = 101.2 g/mole ; d = 0.8618 g/cm^3

$m(NEt_3)$ = (101.2 x 0.701) = 70.99 g

$V(NEt_3)$ = m/d = 70.99 (g) / 0.862 (g/cm^3) = 82.36 cm^3

n(methacryloyl chloride) = 2.1 x n(propBisA)

n(methacryloyl chloride) = 2.1 x 0.319 = 0.67 mole

MW(methacryloyl chloride) = 104.54 g/mole

d(methacryloyl chloride) = 1.07 g/cm^3

m(methacryloyl chloride) = (104.54 x 0.67) = 70.03 g.

V(methacryloyl chloride) = m/d = 70.03 (g) / 1.07 (g/cm^3) = 65.44 cm^3

n(DMAP) = 0.05 x n(propBisA)

n(DMAP) = 0.05 x 0.319 = 0.016 mole

MW(DMAP) = 122.17 g/mole

m(DMAP) = 122.17 x 0.016 =1.955 g.

Equations 3. A sample calculation of the mole ratios of the reactants for the synthesis of Propoxylated BisA dimethacrylate.

3.1.2.10 Purification of Propoxylated BisA dimethacrylate (PropBisAdimet)

After the completion of the above reaction, more solvent (CH_2Cl_2) was added to the flask and the contents of the vessel were washed twice with ice cold water in an extraction funnel to remove triethylamine hydrochloride salts. The water layer was removed and the organic layer was then extracted with ice cold, dilute (5 % v/v) HCl, saturated NaCl solution, and dilute (5 % w/v) $NaHCO_3$ solution. All the extractions were repeated at least three times. The combined CH_2Cl_2 layers were then dried over Na_2SO_4 and the solvent was removed from the organic layer by rotary evaporation under reduced pressure. Before removing the solvent 0.2 mol % hydroquinone(HQ) was added as an inhibitor to prevent polymerization during the removing process and the subsequent storage.

The most important impurity of this esterification reaction is unreacted acid chloride. Extraction of the product with H_2O, HCl, NaCl, and $NaHCO_3$ solutions was not enough for complete purification. Therefore, the product was further purified by column chromatography (silica-gel) using chloroform/ether as eluent. Before removing the solvent by Rotavap® again 0.2 mole% HQ was added as an inhibitor. The purity of the propoxylated BisA dimethacrylate was confirmed by TLC and NMR.

3.1.2.11 Synthesis of propoxylated-6F dimethacrylate (Prop-6Fdimet)

The Prop-6F dimethacrylate was synthesized by the esterification reaction of prop-6F with methacryloyl chloride in the presence of triethylamine as an acid scavenger and 4-dimethylaminopyrdine as a catalyst in a mole ratio of 1 : 2.1 : 2.2 : 0.05 respectively.

To a clean, flame dried, three-necked two liter round bottomed flask fitted with overhead stirring, a water condenser, a pressure equilibrated addition funnel, thermometer, and nitrogen inlet, was added 1000 ml of dichloromethane (CH_2Cl_2). Propoxylated 6F

(98.7 g, 0.218 mole) was then dissolved in CH_2Cl_2. Triethylamine (48.53 g, 56.31 ml 0.4796 mol) was charged to the flask through the addition funnel. A water/ice bath was placed around the reaction vessel and stirring was begun. The mixture was kept stirring for ~ 30 min and then distilled methacryloyl chloride (47.85 g, 44.73 ml, 0.4578 mole) was added dropwise to the flask through the addition funnel at a rate such that the temperature of the reaction mixture was maintained at less than 30 ^{o}C. After addition of all the acid chloride, 4-dimethylaminopyridine (0.011 mole, 1.33 g) used a catalyst to fasten the completion of the reaction was added and the water/ice bath was removed and contents of the reaction vessel were stirred for an additional 4 hours. At this time, the triethylamine hydrochloride salts formed. The completion of reaction was checked by TLC and FTIR.

3.1.2.12 Synthesis of Ethoxylated BisA dimethacrylate [(2,2-bis(4-(2-methacryloxy ethyl-1-oxy)phenyl)propane(H-BisGMA)]

Ethoxylated BisA dimethacrylates was synthesized by a similar procedure to propoxylated BisA dimethacrylateas as detailed in section 3.1.7.

Ethoxylated BisA (70.4 g, 0.222 mole) was dissolved in 800 ml dicholoromethane (CH_2Cl_2) in a previously flame-dried, clean, three-necked round bottomed flask fitted with overhead stirring, a water condenser, a pressure equilibrated addition funnel, thermometer and nitrogen atmosphere. Triethylamine (49.52 g, 68.21 ml, 0.49 mole) was charged to the flask through the addition funnel. A water/ice bath was placed around the reaction vessel and stirring was begun. The mixture was kept stirring for ~ 30 min and then distilled methacryloyl chloride (48.74 g, 45.55 ml, 0.466 mole) was added dropwise to the flask through the addition funnel at a rate such that the temperature of the reaction mixture was maintained at less than 30 ^{o}C. After addition of all the acid chloride, 4-dimethylaminopyridine (0.011 mole, 1.356 g) was added, the water/ice bath was removed and the contents of the reaction vessel were stirred for an additional 4 hours. During this

time, the triethylamine hydrochloride salts formed. The completion of reaction was checked by TLC and FTIR.

3.1.2.13 Synthesis of Ethoxylated 6F dimethacrylate [(1,1,1,3,3,3-hexafluoro-2,2-bis(4-(2-methacryloxyethyl-1-oxy)phenyl)propane(H-6F)]

Ethoxylated 6F dimethacrylate was synthesized by a procedure similar to that of propoxylated BisA dimethacrylates as detailed in section 3.1.2.9

Ethoxylated 6F (79.4 g, 0.1872 mole) was dissolved in 800 ml dicholoromethane (CH_2Cl_2) in a previously flame-dried, clean, three-necked round bottomed flask fitted with overhead stirring, a water condenser, a pressure equilibrated addition funnel, thermometer and nitrogen atmosphere. Triethylamine (41.68 g, 57.41 ml, 0.412 mole) was charged to the flask through the addition funnel. A water/ice bath was placed around the reaction vessel and stirring was begun. The mixture was kept stirring for ~ 30 min and then distilled methacryloyl chloride (41.11 g, 38.42 ml, 0.393 mole) was added dropwise to the flask through the addition funnel at a rate such that the temperature of the reaction mixture was maintained at less than 30 ^{o}C. After addition of all the acid chloride, 4-dimethylaminopyridine (0.0094 mole, 1.144 g) was added and the water/ice bath was removed. The contents of the reaction vessel were then stirred for an additional 4 hours. The completion of the reaction was checked by TLC and FTIR.

3.2 Characterization

3.2.1 Spectroscopy

3.2.1.1 Proton NMR Spectroscopy

NMR (Nuclear Magnetic Resonance) spectroscopy was used to confirm the structure and purity of reaction products. Proton NMR spectra were taken on a Varian Unity 400 (400 MHz) spectrometer. Deuterochloroform was used as a solvent (~ 5 % w/v) and a 7.24 ppm chloroform chemical shift was used as the internal reference.

3.2.1.2 Infrared Spectroscopy

FTIR (Fourier Transform Infrared Spectroscopy) spectra on a Nicolet 2000 spectrometer was used to establish the completion of reaction in the monomer syntheses. Spectral analysis revealed the presence of carbonyl and vinyl groups, as shown by absorption bands at stretching frequencies of 1728 cm^{-1} and 1638 cm^{-1}, respectively. The degree of cure (or conversion) of the dimethacrylate matrix resins was also determined by FTIR spectroscopy from the absorbance ratio of the C=C stretch of the methacrylate group (at 1638 cm^{-1}) to the reference aromatic ring peak (at 1607 cm^{-1}) in the cured and uncured samples**.**

3.2.2 Melting Point Measurements

Melting points were determined on a Lab Devices Melt-Temp II.

3.2.3 Thermal Analysis

3.2.3.1 Photo DSC-DPA 7

A Dupont-DSC 7 instrument was used to determine the glass transition temperatures of the monomers and a Perkin Elmer DSC-DPA 7 (Differential Scanning Calorimetry-Double Beam Photocalorimetric Accessory) apparatus was used to study polymerization exotherms.

3.2.3.2 DPA-7 Apparatus and Sample Preparation

A Perkin-Elmer DSC-7 was modified with an optics assembly, DPA 7 (Double Beam Photocalorimetric Accessory) to study the photo-induced polymerizations by measuring the exotherm rates of irradiated samples. The optical accessory DPA 7 for the DSC 7 consists of the following components: (see Figure 3.2.1 DPA-7 light path).

- Optical bench with shutter control,
- Transfer optics / monochromator, shutter, beam splitter, and deflecting mirror,
- A lamp housing,
- A power supply for operating various short-arc lamps.

The optical part of the calorimeter includes the following elements:

(a) A short-arc Xenon (Xe) lamp 450 W was used as the light source;

(b) A monochromator without the water heat filter;

(c) Neutral density filters to modulate the light intensity;

(d) Manual shutter to control the irradiation time.

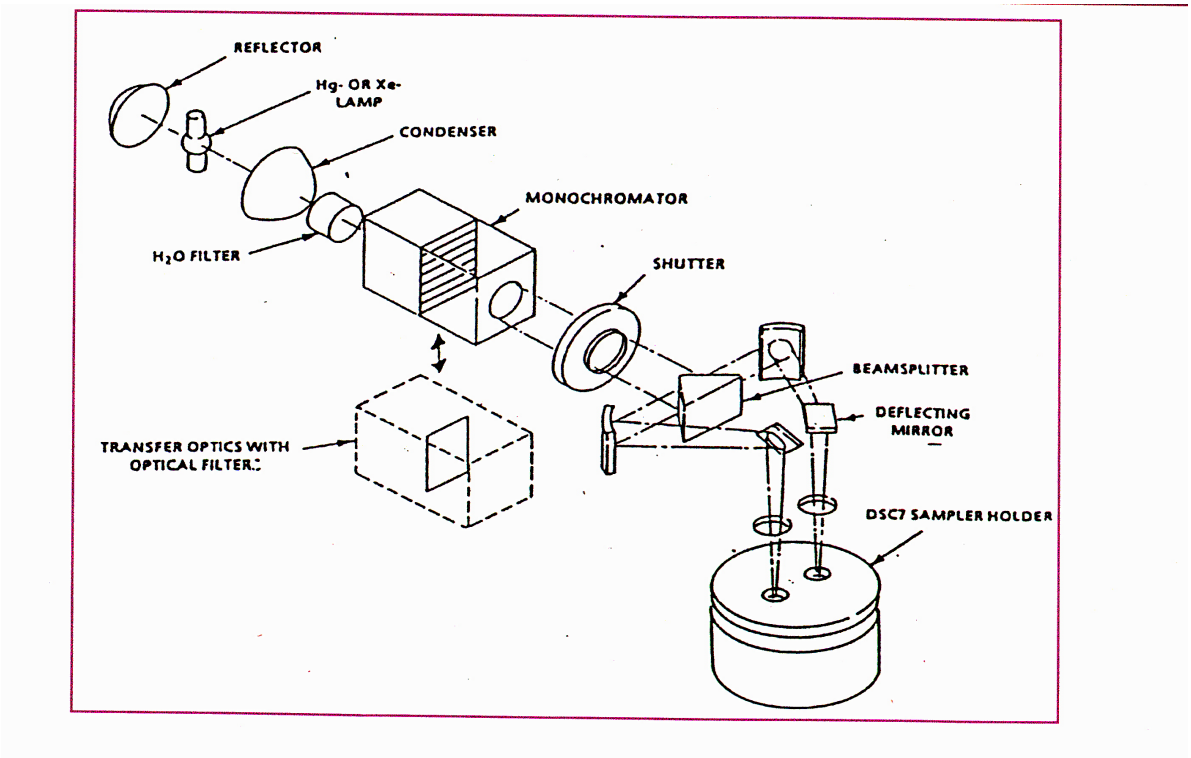

Figure 3.2.1 Photopolymerization apparatus: DSC-DPA 7 Light Path

The rate of heat evolution was followed under isothermal conditions for photopolymerizations of monomers initiated with 470 nm wavelength visible light at various initiator concentrations (0.25, 0.5, 1.0 mole%), light intensities (0.13, 0.393, 1.43, 4.51 mW/cm^2) and reaction temperatures (30, 40, 50, 60 ^oC). Propoxylated BisA dimethacrylate, Ethoxylated BisA dimethacrylate, Propoxylated 6F dimethacrylate, Ethoxylated BisA dimethacrylate monomers were synthesized and studied for photoinitated polymerization. BisGMA(2,2-bis(4-(2-hydroxy-3-methacryloxyprop-1-oxy)phenyl)propane) was used as a control. Camphorquinone (CQ) and N,N-Dimethyl-p-toluidine (DMpT) initiator system were used as a initiator/reducer pair.

The polymerizations were performed in a modified aluminum pan. In order to maintain uniform sample thickness with 7-8 mg sample sizes used it was necessary to use modified aluminum sample pans. Standard aluminum sample cups were pressed into the shape shown in cross section in Figure 3.2.2 below. With this modification, meniscus

formation is prevented or minimized due to the step configuration. The depth d of the sample cups used was 0.63 mm for holding sample volume of 10 µl.

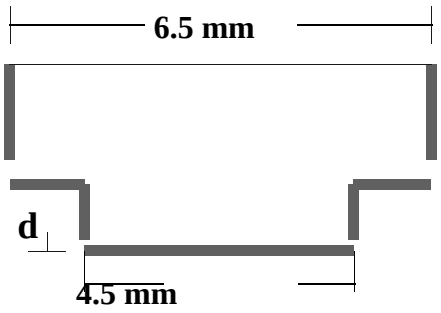

Figure 3.2.2 Cross section of aluminum DSC sample pan used for photopolymerization studies.

3.2.3.3 Measurement of Light Intensity

Since the DSC 7 measures differential energy delivery rate (differential power), it can be used directly for measuring the light intensity. For such measurements, graphite discs were inserted into the measuring cells to absorb the light irradiation. During irradiation, sample cell and reference cell were covered alternately without touching the sample cover. Figure 3.2.3 shows the progress of such a measurement, where a is a measure of the light intensity of sample cells that was not covered. The values for a was calculated by taking the difference of heat flow(mW) when the light is on and when the light is off. These electrical power (mW), was divided by the area, and gave the value of the light intensity at the sample surface (Equation 4).

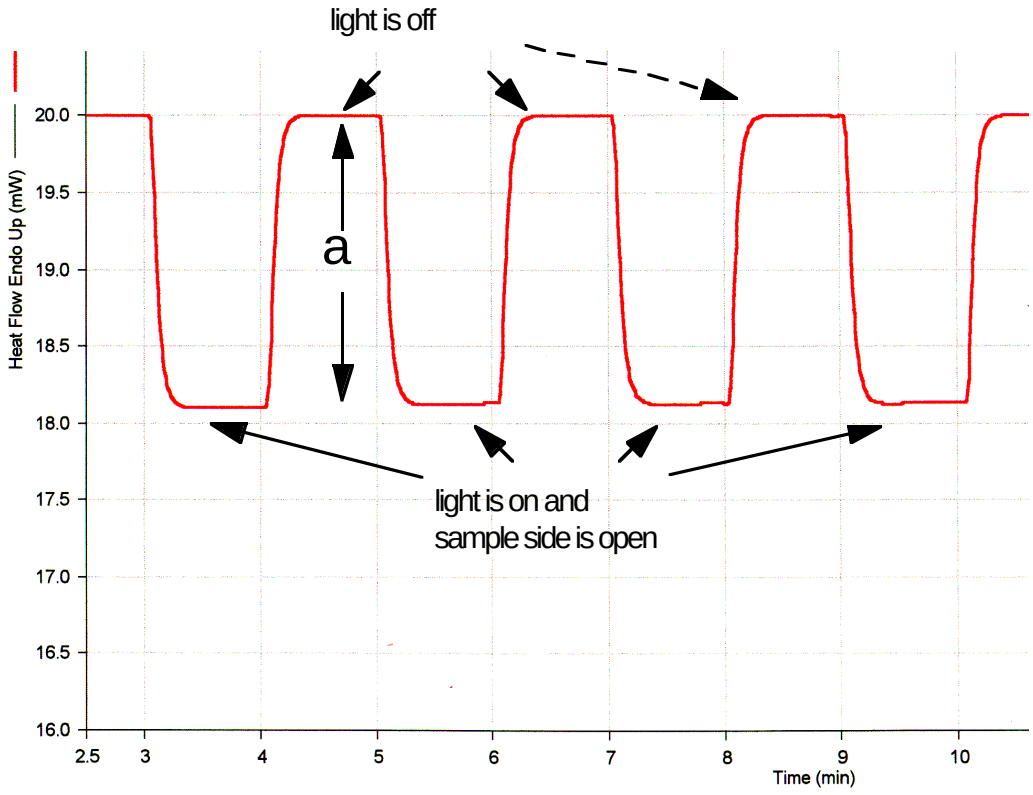

Figure 3.2.3 Measurement of Light Intensity

$$\text{Light Intensity} = \frac{mW_{(\text{light on})} - mW_{(\text{light off})}}{\text{light area } (cm^2) \text{ at sample position}}$$

Equation 4. Calculation of light intensity by DSC-DPA 7.

The difference in heat flow between sample and reference cells corresponds to the baseline shift with and without irradiation. In order to correct for any shift of the

baseline due to differential light absorption between sample and reference, an irradiation was performed at four different intensities with well-cured samples of the same mass in the sample and reference cells . Figure 3.2.4 shows the shift of baseline due to the differential absorption between sample and reference at 4.51 mW/cm^2 light intensity.

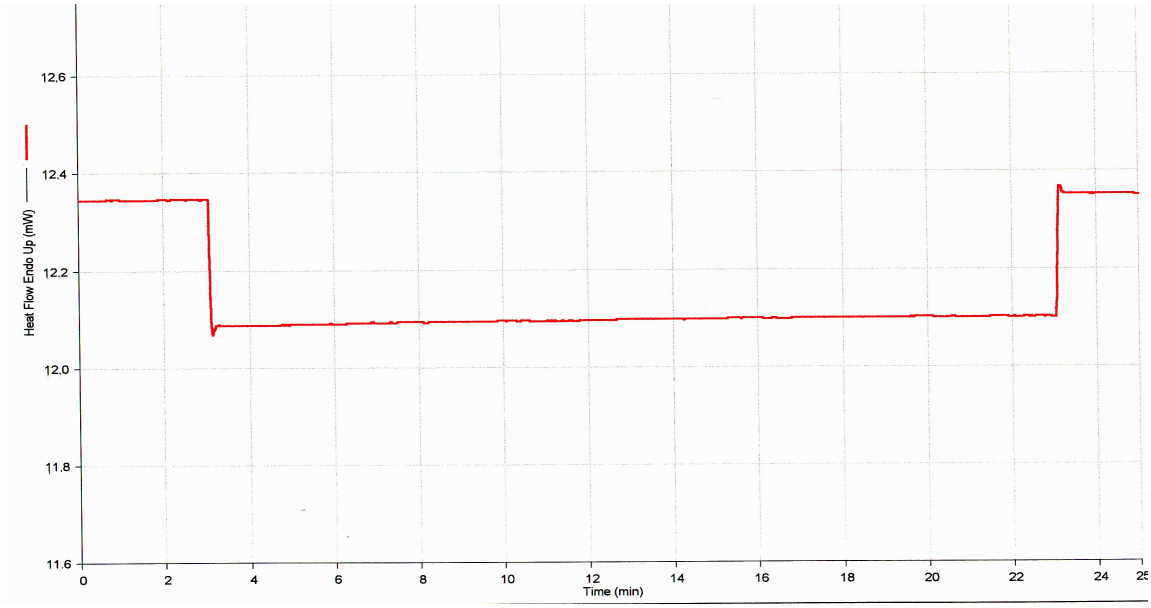

Figure 3.2.4 Baseline shift due to the differential absorption between polymerized sample and polymerized reference sample both illuminated at 4.51 mW/cm^2 light intensity.

The final thermograms (Figure 3.2.5) were obtained by subtracting curve of baseline shift at appropriate wavelength from the thermograms of photoinitiation polymerization**.**

Sample preparation : The monomer (7-8 mg) was placed in the DSC aluminum pan, carefully weighed and quickly transferred to the sample holder in the DSC apparatus in a dark room. For a reference, the corresponding monomer of almost the same weight was

previously polymerized by irradiation in isothermal mode under nitrogen atmosphere and then placed in the reference holder. Before irradiation, each sample was kept in the DSC furnace for 5 min to allow temperature stabilization and during this period a stream of nitrogen (20 ml/min) was passed through the instrument to remove residual oxygen trapped in the sample during mixing and weighing. After keeping each sample at the polymerization temperature under nitrogen for 5 min, the DSC run was started, the light was manually switched on at the 3 min mark and maintained at the selected intensity for 20 min., and the run was completed at 25th min. A typical thermogram of photoinitiated polymerization is shown in Figure 3.2.5 below. Exotherm rates as a function of time were also observed under isothermal conditions for the dark reaction. Experiments of the dark reaction were carried out by switching off the light source at varying stages of the polymerization and recording heat release rate profiles.

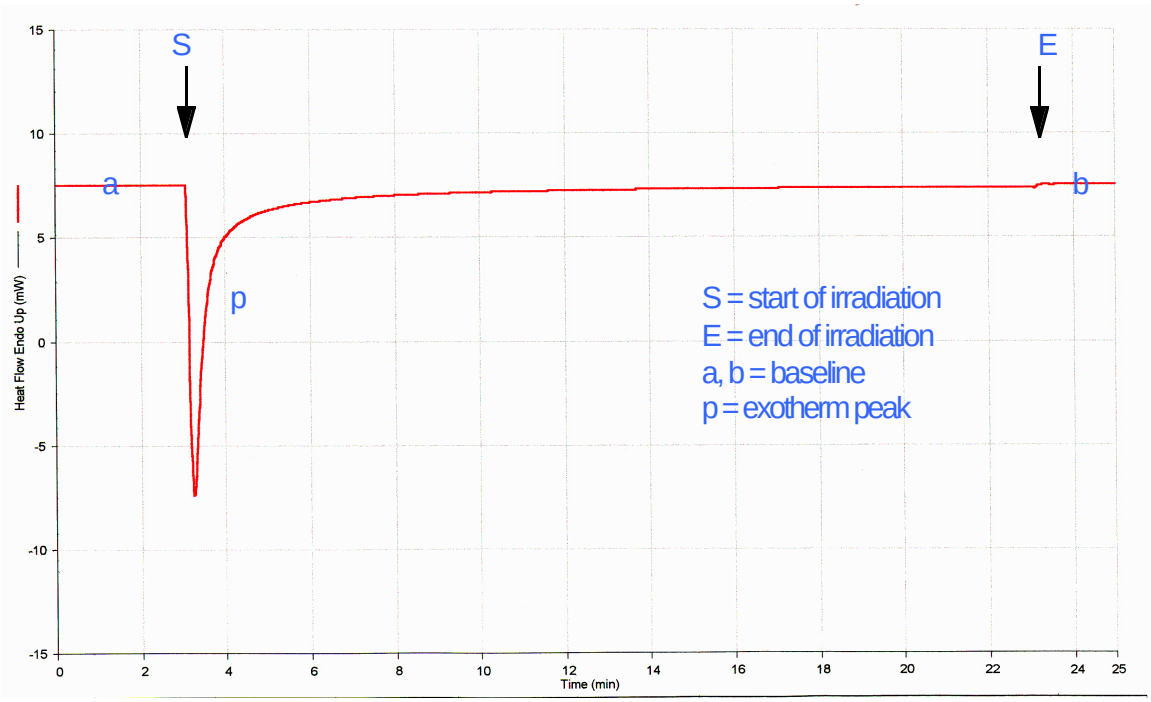

Figure 3.2.5 Typical thermogram of photoinitiated polymerization after baseline correction. a and b: baseline without radiation; p: polymerization exothermic peak; S: start of irradiation; E: end of irradiation.

The heat of polymerization (ΔH_p) was calculated from the area between exotherm curve and the baseline (Figure 3.2.5). The extent of polymerization (Ep %) was defined by the following equation (115) where ΔH_p, is the measured heat of polymerization per gram of sample per mole of monomer and H_m is the heat of polymerization of methyl methacrylate (13.1 kcal/mol). (122).

$$Ep\ (\%) = \frac{\Delta H_p}{H_m \times 2} \times 100$$

Equation 5. Calculation of ultimate extent of polymerization (Ep %)

In the second part of the following chapter, effect of dilution on the photopolymerization kinetics of BisGMA-TEGDMA mixtures was studied. For this purpose five different monomer mixtures were prepared with various BisGMA and TEGDMA ratios (BisGMA (wt %)/ TEGDMA (wt%): 100/0 ; 90/10 ; 50/50 ; 15/85 ; 0/100). The mixtures were stirred at room temperature in dark until we make sure the

viscous liquid (BisGMA) and flexible diluent (TEGDMA) give a homogenous mixture. The monomer mixtures were photopolymerized using 1.0 mol % CQ an 0.3 wt% DMpT. Calculation of extent of polymerization and photopolymerization results are discussed in detail in chapter 4 section 4.2.

CHAPTER 4. RESULTS and DISCUSSIONS

4.1 Synthesis and Photopolymerization of Bis-GMA Analogous Dimethacrylates

4.1.1 Preparation of the Monomers

In this study, four potential new monomers were prepared, all of which were structural analogues of Bis-GMA (*2,2-bis(4-(2-hydroxy-3-methacryloxyprop-1-oxy) phenyl)propane*). Synthesis of these dimethacrylate monomers, based on structural modifications of Bis-GMA in the core and the side chain, require a two-step reaction. The first step is propoxylation or ethoxylation of the bisphenols and the second step is the methacrylation of the resulting products. The core structures are designated by Bis-A and 6F, and the side chain structures are designated on the basis of the pendant side chains in the glycidyl moiety as −OH from Bis-GMA to −H, and $-CH_3$. Bis-GMA was commercially obtained and used as a standard for comparison of the experimental monomers. Figure 4.1.1 shows the structural modifications of the Bis-GMA in the core and side chain units. All the monomers were prepared by the following general procedures of propoxylation or ethoxylation of the bisphenols followed by methacrylation. General structures of the all experimental monomers are given in Figure 4.1.2

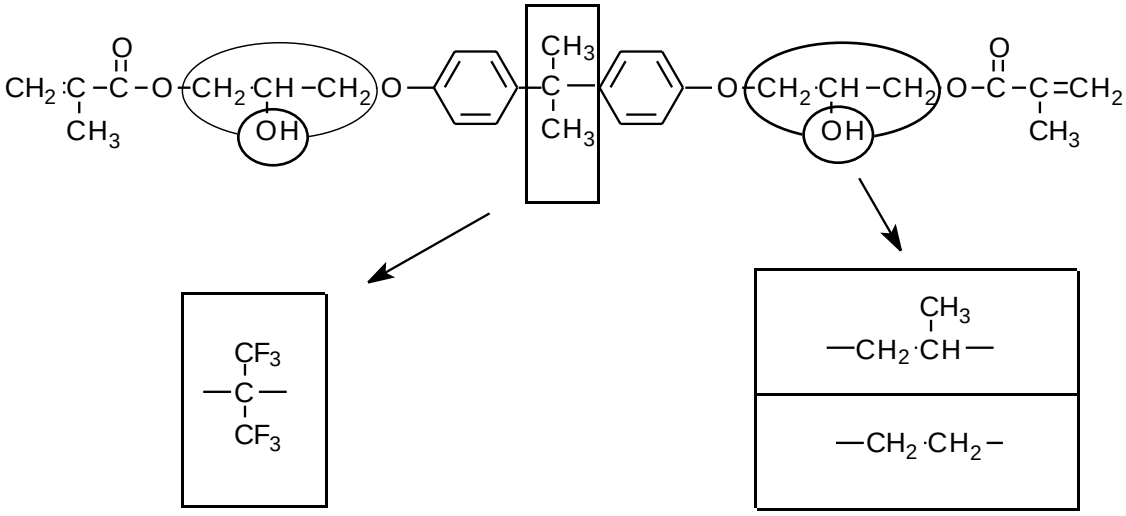

Figure 4.1.1 *The structural modifications of the Bis-GMA in the core and side chain units.*

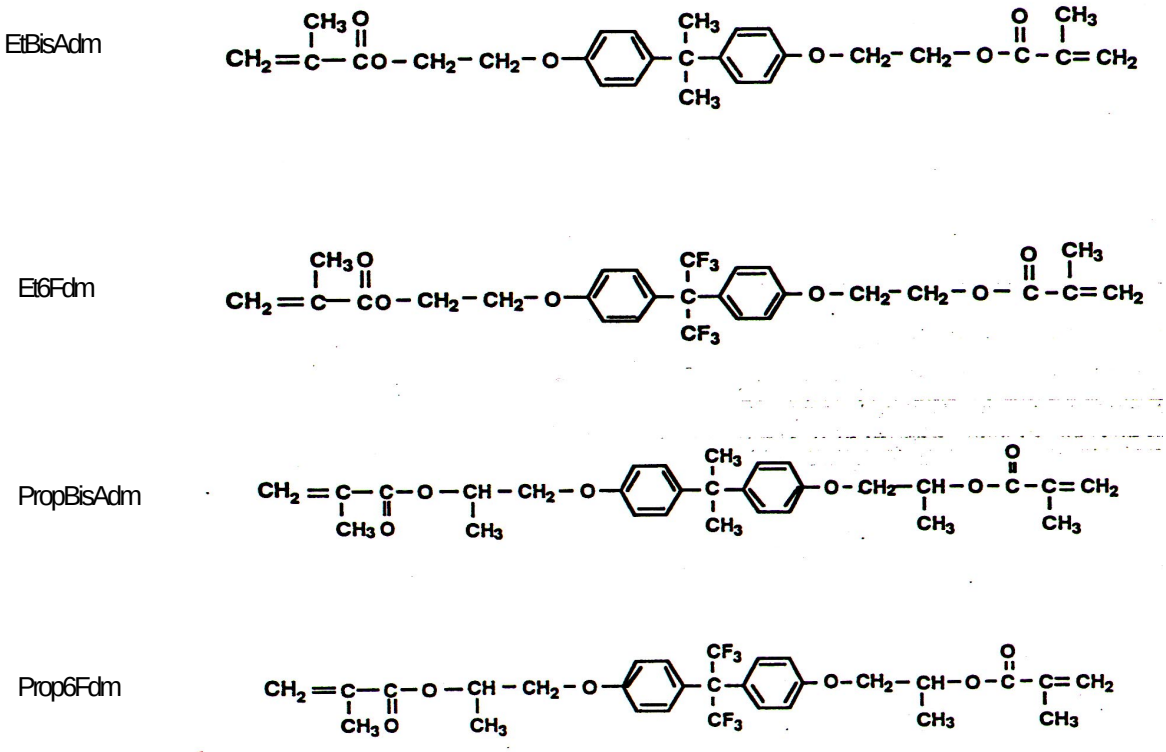

Figure 4.1.2 *General presentation of experimentally prepared monomers*

4.1.1.1 Synthesis and Characterization of Propoxylated-Bisphenol A (PropBisA) and Propoxylated 6F (Prop6F)

Propoxylated-BisA was synthesized by the reaction of bisphenol-A [(2,2-bis(4-(2-hydroxyprop-1-oxy)phenyl) propane] with propylene oxide in the presence of sodium hydroxide (Scheme 3.1.1). The major side-product of the reaction, propylene glycol was removed by distillation under reduced pressure (~26.7 Pa.) in a Kugelrohr apparatus at around 130 ^{o}C. The purity of the resulting yellowish-white, solid product was confirmed by TLC (thin layer chromatography in a mixture (35/65 by volume) of ethyl acetate and hexane) and NMR. Quantitative conversion was also evidenced by the complete disappearance of the aromatic resonances centered at 6.79 and 7.05 ppm and the appearance of the shifted pattern at 6.70 and 7.12 ppm in ^{1}H n.m.r (Figure 4.1.3). The melting point of the product was obtained at 97-100 ^{o}C and the overall yield in monomer grade was about 97 %.

Propoxylated-6F was synthesized (Section 3.1.4) by a similar method to that of propoxylated bisA. The purification of the product was done by several extractions followed by distillation in a Kugelrohr apparatus at 130 ^{o}C and ~27 Pa pressure. The shift of aromatic protons in ^{1}H n.m.r. (Figure 4.1.3) was again used to indicate completion of the reaction. The solid, amorphous product was isolated in a 93 % yield.

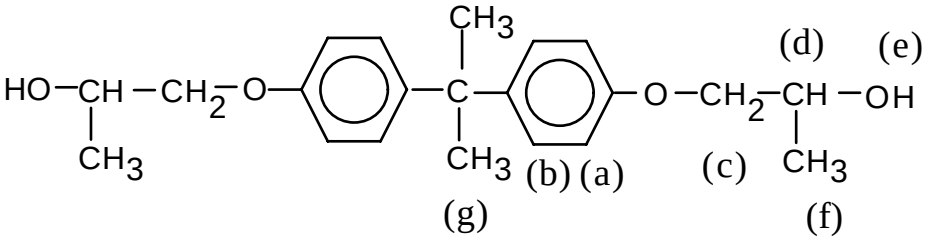

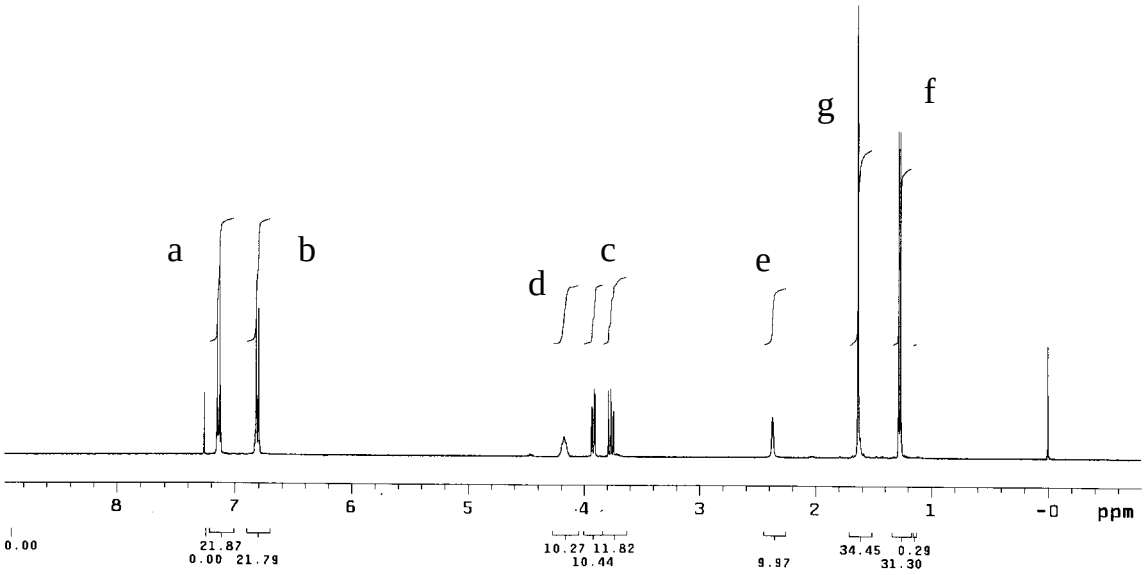

Figure 4.1.3 *Proton NMR spectrum of Propoxylated-Bis A*

4.1.1.2 Synthesis and Characterization of Ethoxylated-Bisphenol A (EtBisA) and Ethoxylated 6F (Et6F)

The monomers with ethoxyl side chain groups were prepared (Schme 3.1.2) by the bulk reaction of bisphenols with ethylene carbonate in the presence of tetraethyl ammonium iodide $\{N(C_2H_5)_4^+I^-\}$. The ethoxylation reaction of bisphenols was previously discussed in detail in the previous chapter.

4.1.1.3 Methacrylation of the Propoxylated and Ethoxylated Bisphenols

The second step in the preparation of dimethacrylate monomers with isopropyl or ethane units was the esterification of the propoxylated and ethoxylated bisphenols. The propoxylated and ethoxylated bisphenols were reacted with methacryloyl chloride in the presence of triethyl amine as acid scavenger, dimethylaminopyridine as catalyst and methylene chloride as solvent. Each reaction product was dissolved in more solvent and washed several times with H_20, ice-cold dilute HCl, dilute sodium bicarbonate solution and then with saturated sodium chloride solutions. Finally, the organic layer was separated and dried over anhydrous Na_2SO_4. Pure products were obtained after applying column chromatography to all the viscous liquids. The methacrylation reaction of propoxylated and/or ethoxylated bisphenols was previously discussed in detail in the previous chapter.

The yields were found to be between 78-86 %. The products were analyzed by ^1H nuclear magnetic resonance (NMR) (Figure 4.1.4), and Fourier transform infrared (FTIR) spectroscopy.

The proton NMR (in d-$CDCl_3$ solvent) of these dimethacrylates exhibited simple patterns in the aromatic region (6.8-7.4 ppm). The dimethacrylates exhibited the following peaks:

6.2 ppm (2H, s, vinyl proton *trans* to ester),

5.6 ppm (2H, s, vinyl proton *cis* to ester),

5.2-5.4 ppm (2H, multiplet, methine proton),

3.9-4.1 ppm (4H, multiplet, methylene protons),

1.85ppm (6H, s, methyl protons of methacrylate group) and

1.4 ppm (6H,d, methyl protons of the propoxyl group).

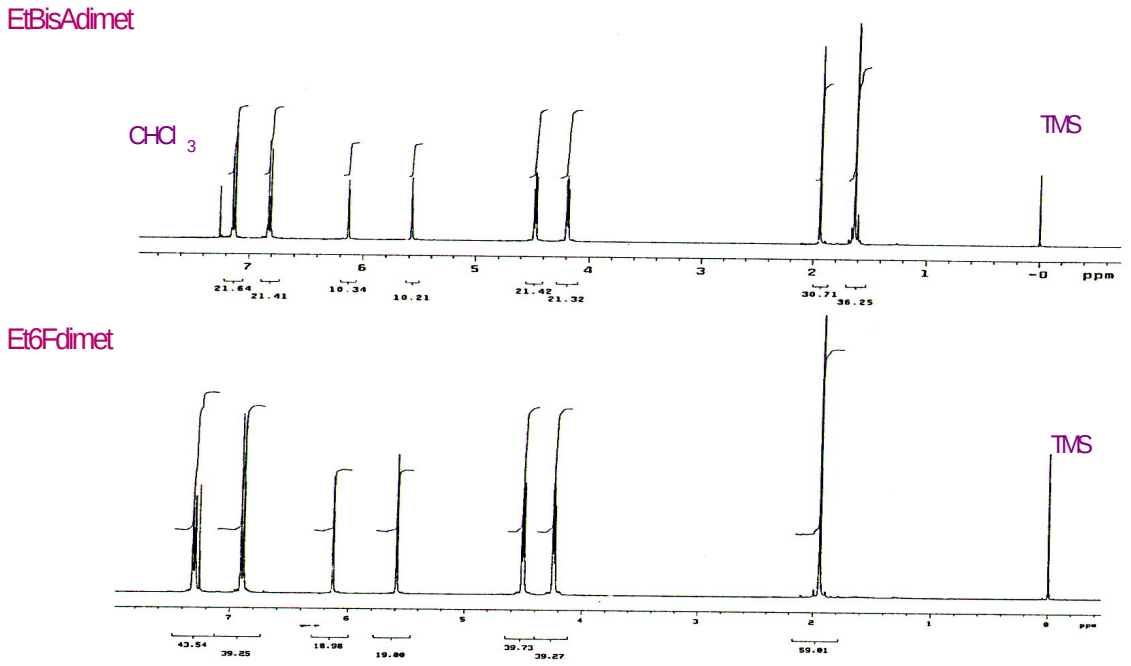

Figure 4.1.4 (a) *Proton NMR spectra of synthesized monomers*

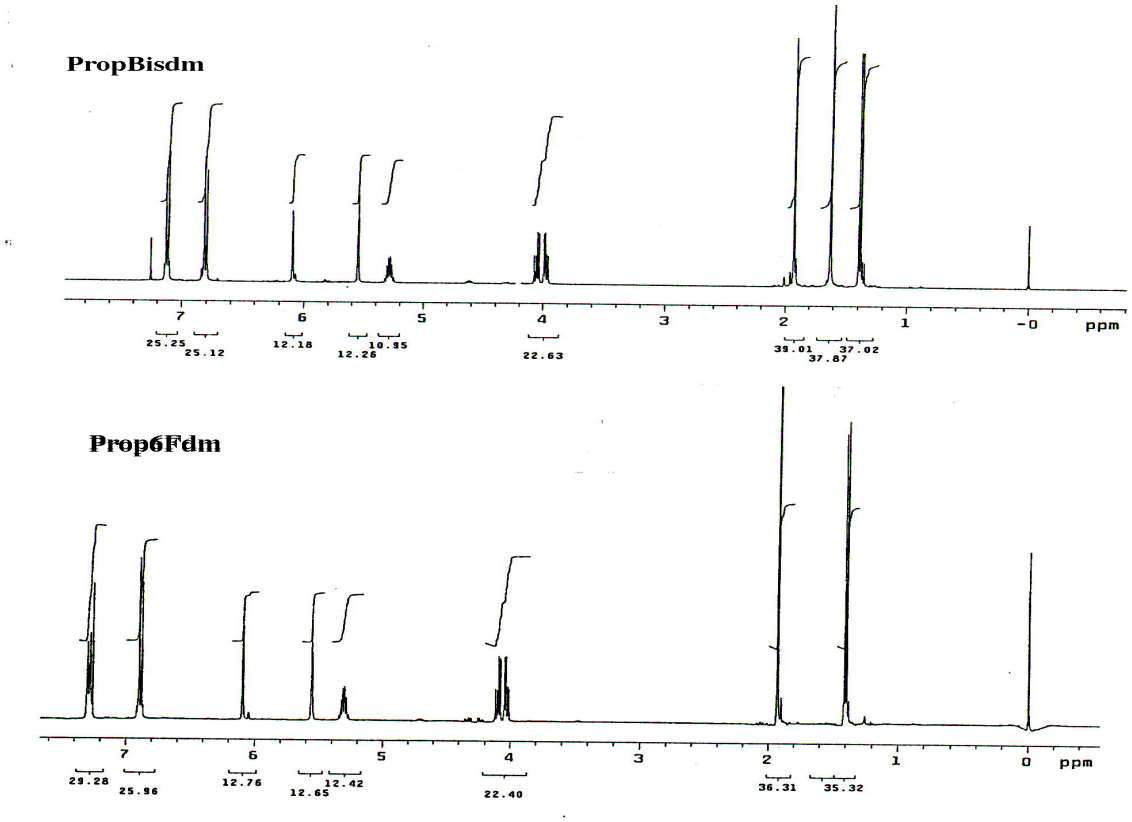

Figure 4.1.4 (b) *Proton NMR spectra of synthesized monomers*

The IR spectra of these dimethacrylates exhibited peaks at 1700-1730 cm^{-1} (carbonyl stretching) and 1630-1640 cm^{-1} (C=C stretching). A typical FTIR spectrum for propoxylated BisA dimethacrylate is shown in Figure 4.1.5.

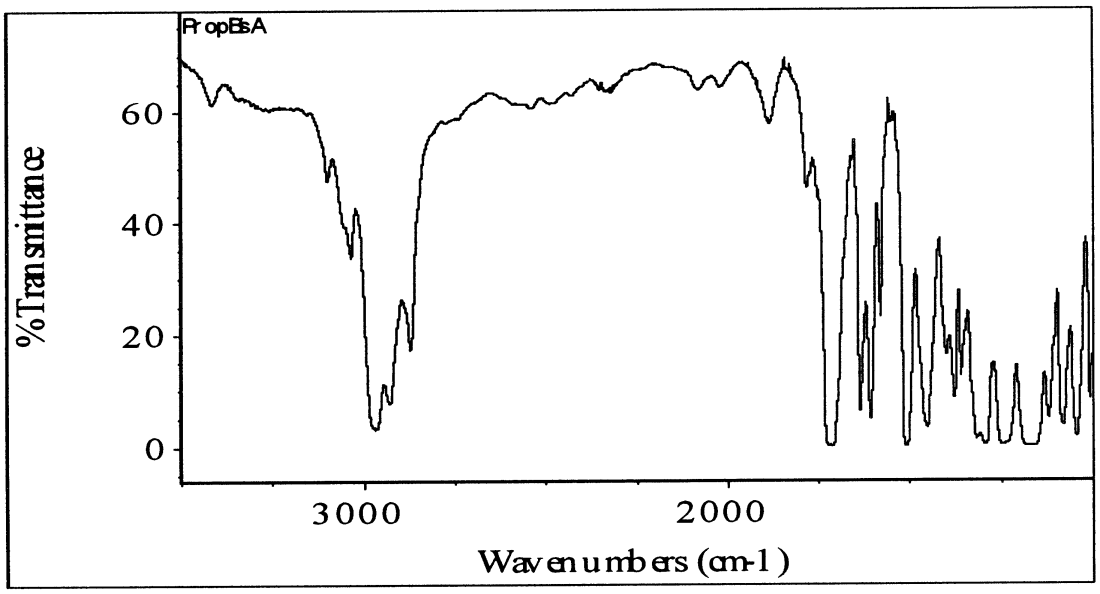

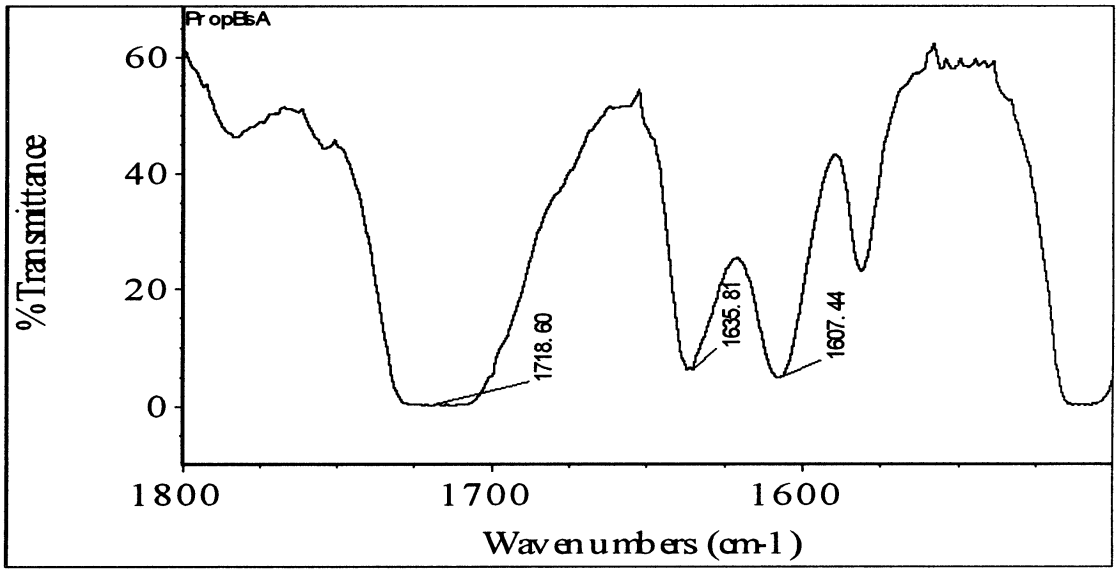

Figure 4.1.5 *FTIR spectrum of Propoxylated BisA dimethacrylate*

4.1.1.4 Viscosity Behavior and Glass Transition Temperatures of the Dimethacrylate Monomers

Glass transition temperatures (T_g) and bulk viscosities of the neat monomers have been measured (37). These data, as well as the T_g and bulk viscosity of BisGMA are presented in Table 4.1.1.

Compared to the viscosities of the experimental monomers, the viscosity of BisGMA is very high. The very high viscosity of BisGMA is due to intermolecular hydrogen bonding. All the experimental monomers investigated exhibited much lower viscosities due to the absence of hydrogen bonding. The FTIR spectrum of BisGMA in Figure 4.1.6 shows the presence of the hydroxyl group at a stretching frequency of 3458.3 cm^{-1}. Comparison of the viscosities among these monomers reveals that the structural variation of these side chains structures profoundly affects their viscosity behaviour. Incorporation of the $-CH_3$ side group increases the flexibility of the structure and reduces the viscosity. A slightly opposite effect on free volume is suggested by the T_g values of the 6F monomers.

Table 4.1.1 *Glass Transition Temperatures (T_g) and Viscosities of Neat Monomers*

Monomer	T_g (°C) [a]	Viscosity [b] (Pa.s)
PropBisAdm	-26.6	0.3
EtBisAdm	-23.3	3.0
Et6Fdm	-17.5	1.5
Prop6Fdm	-15.6	0.8
BisGMA	-6	>100

a) Differential Scanning Calorimetry (DSC)

b) Brookfield Cone and Plate Viscometer at R.T.

The determination of the T_g of the monomers is a critical issue as it has been demonstrated previously (106) that the aromatic dimethacrylates with lower T_g values exhibited higher conversions compared to the ones with higher T_gs. All the experimental monomers exhibited lower T_gs than that of BisGMA. In a comparison of the ethoxylated

and propoxylated analogues of BisA and 6F monomers, the latter systems exhibited higher T_gs due to the increased rigidity introduced by the relatively bulky fluorine groups. Since all the experimental monomers exhibit lower T_gs than the control BisGMA, one can expect higher conversions from these monomers.

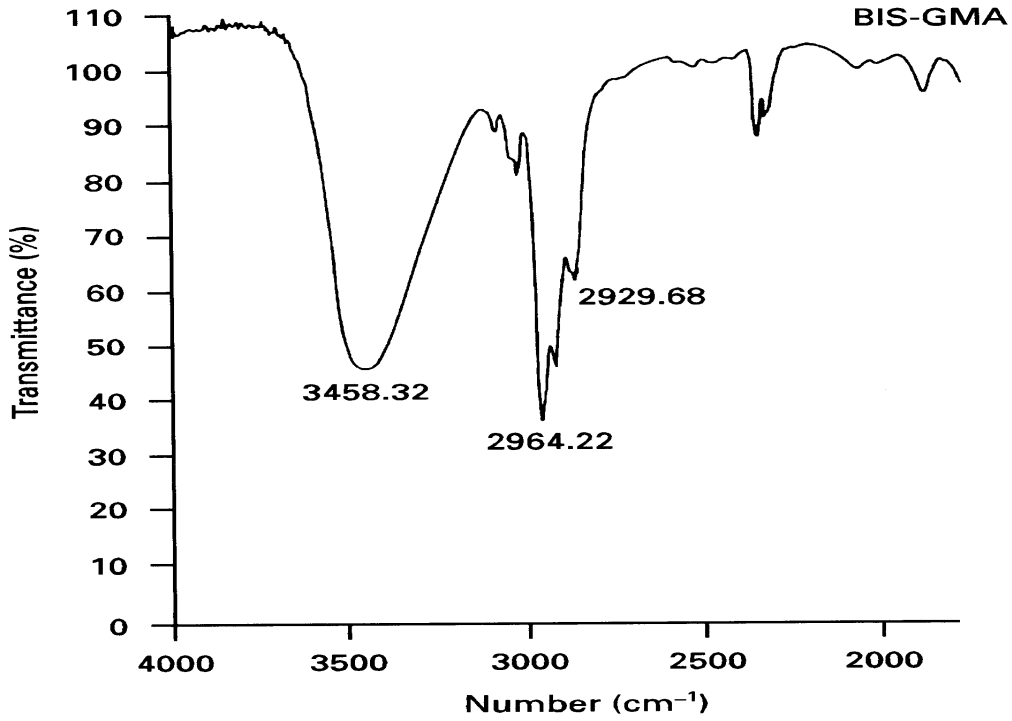

Figure 4.1.6 *FTIR spectrum showing the presence of the hydroxyl group at 3458 cm^{-1} in BisGMA*

4.1.2 Photopolymerization of the BisGMA Analogue Monomers

The monomers were polymerized in a differential scanning calorimeter modified with an optics assembly (DPA 7; Double Beam Photocalorimetric Accessory) to determine photo-induced crosslinking reactions. Polymerization reaction rate profiles of these dimethacrylate monomers exhibited several typical features. In this section of the thesis many of these features will be illustrated and discussed.

4.1.2.1 Effect of Monomer Structure

Monomers were mixed with 1.0 mol % camphorquinone (CQ) and 0.3 wt % N,N-dimethyl-para-toluidine (DMpT) and polymerized at 40 °C by 4.51 mW/cm^2 light intensity from a 470 nm monochromatic source. PhotoDSC thermograms of the experimental monomers as well as the control, BisGMA, are given in Figure 4.1.7.

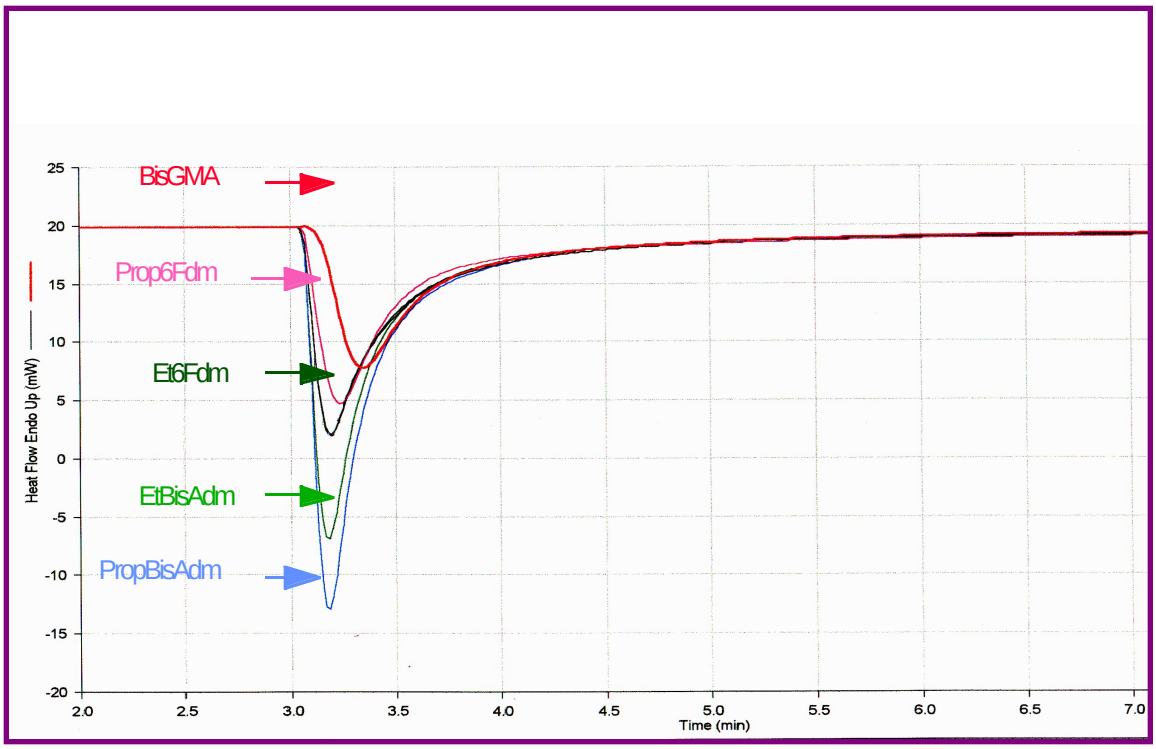

Figure 4.1.7 *Heat flow, dQ/dt (mW), versus time for the photopolymerization at 40 °C of 7-8 mg samples of various monomers (+20 mW position of initial dQ/dt is arbitrary). The shutterwas opened at 3.00 min.*

In this figure, all the experimental monomers show very similar rate curves in which a sharp increase in rate is seen as soon as the light is turned on. Compared to the experimental monomers, this increase is slower in BisGMA which may be due to the very high viscosity of this monomer. The one common feature in the thermograms is that two distinct regions can be identified for all five monomers. The initial portion of the curves involves a rapid increase in the polymerization rate due to the "Trommsdorff " or "gel" effect. During this portion of the polymerization, as the viscosity increases a network forms, the mobility of the radicals decreases dramatically. As a result of this reduction in the radical mobility, the termination rate decreases. The decreased rate of termination results in a large build-up in the radical concentration, thus increasing the polymerization rate. This phenomenon has been discussed by others (11,79). At some point in this autoacceleration region, the termination mechanism becomes reaction-diffusion controlled. Instead of termination occurring by radicals diffusing to each other, the less mobile radicals primarily attack unreacted double bonds available in the system and reach each other by "reaction diffusion". The polymerization rate reaches a maximum value and then begins to decrease. In this second phase, the polymerization rate decrease is caused by continuing double bond depletion and a process referred to as autodeceleration, due to the approach of vitrification of the system. In this region propagation also becomes diffusion controlled, and ultimately both propagation and termination steps depend on "reaction diffusion" and spatial accessibility.

The data in Figure 4.1.7 show a similar trend in polymerization rate behavior for the experimental monomers and BisGMA However, BisGMA exhibits a much slower rise to the maximum rate. This variation can be explained by the very high viscosity of the monomer. The maximum rate can be written in a decreasing order of
PropBisAdm > EtBisAdm > Et6Fdm > Prop6Fdm > BisGMA.

The ultimate conversion for each monomer was calculated from the area bounded by the baseline and the rate vs. time curve using the equation $E_p\ (\%) = [\Delta h_p / (h_m \times 2)] \times 100$. Here Δh_p (J/g) is the polymerization heat per gram obtained from the area, and h_m (J/g) is

the heat per gram of the specific monomer representing complete reaction of one of its two double bonds. As mentioned in section 3.2.3, the basis for h_m is a heat of polymerization of 13.1 kcal/mole for methylmethacrylate (122).

The heats of polymerization (J/g) and percent conversions from the DSC-DPA results for the dimethacrylate resins subjected to the visible light curing for a total of 20 min. are presented in Table 4.1.2.

Table 4.1.2 *Glass transition temperatures, viscosities(at R.T), heats of polymerization, and ultimate percent conversions of the various monomers (cf. Figure 4.1.7 for polymerization conditions).*

Monomer	T_g (^oC)	Viscosity (Pa.s)	$-\Delta h_p$(J/g)	E_p (%)
PropBisAdm	-26.6	0.3	175.7	77
EtBisAdm	-23.3	3.0	167.3	69
Et6Fdm	-17.5	1.5	117.5	60
Prop6Fdm	-15.6	0.8	100.6	54
BisGMA	-6	>100	68.7	32

The values of bulk viscosities and glass transition temperatures (T_g) (37) are also provided again in Table 4.1.2 for the convenience of the reader. . All the experimental

monomers, which exhibit much lower viscosities than that of BisGMA, give higher extents of polymerization. The E_p values range from 32 % (in BisGMA) to 77 % (in PropBisAdm). The difference in the E_p's of the experimental monomers is probably due to the difference in their initial viscosities and to their different vitrification/conversion relations. The monomer with a lower viscosity may allow for an enhanced diffusion of reactive groups during the initial stage of polymerization. The resin with a lower monomer T_g also reaches vitrification at a higher extent of conversion.

Monomers with lower viscosities also showed lower glass transition temperatures (a slight exception in order of EtBisAdm and Et6Fdm). Variation of ultimate conversions with monomer T_g gives a linear relationship in which decreasing of T_g from -6 °C (BisGMA) to -26 °C (PropBisAdm) results in an increase of E_p (%) by more than a factor of two (Figure 4.1.8).

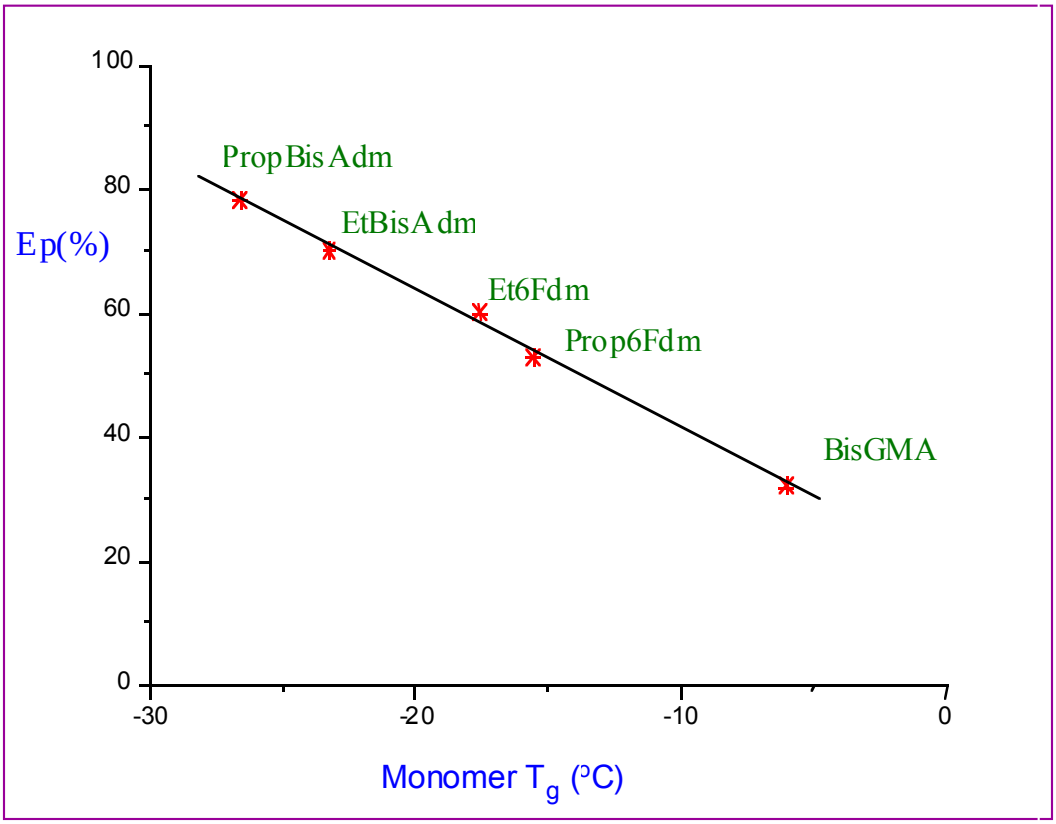

Figure 4.1.8 *Variation of E_p (%) (at 40 °C) with Monomer T_g (°C)*

Fractional monomer conversions as functions of irradiation time were obtained from the integrated exotherm curves by means of a partial areas software program as shown in Figure 4.1.9. The results, given in Figure 4.1.10, illustrate the variation of extent of polymerization with time for all the monomers studied at 40 °C. It is clearly seen that when monomers were exposed to the irradiation in the presence of CQ and DMpT initiator system, polymerization developed very rapidly and reached high conversions in a very short period of time (Monomers reached more than 65 % of their ultimate conversions in 2 min after the light was turned on.). PropBisAdm, as well as other experimental low viscosity monomers polymerized to considerably higher conversion than BisGMA. Initial slopes of the curves also indicate that monomers with lower viscosites and lower T_gs polymerize faster prior to autoacceleration than the control BisGMA.

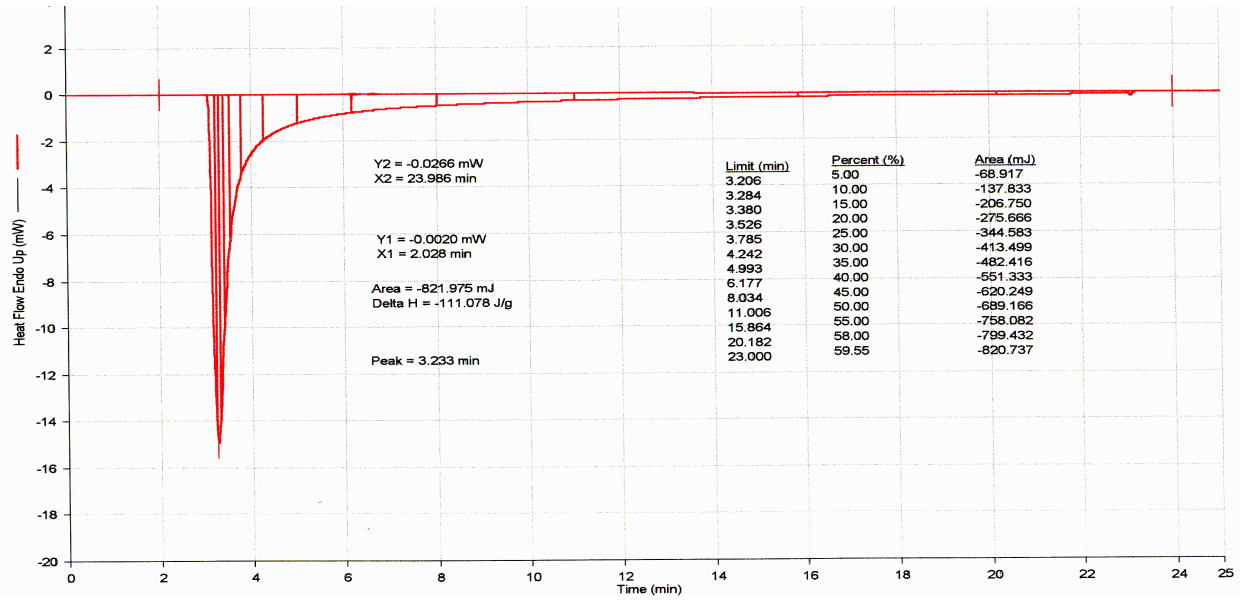

Figure 4.1.9 *Calculation of Ep (%) versus Time by DSC*

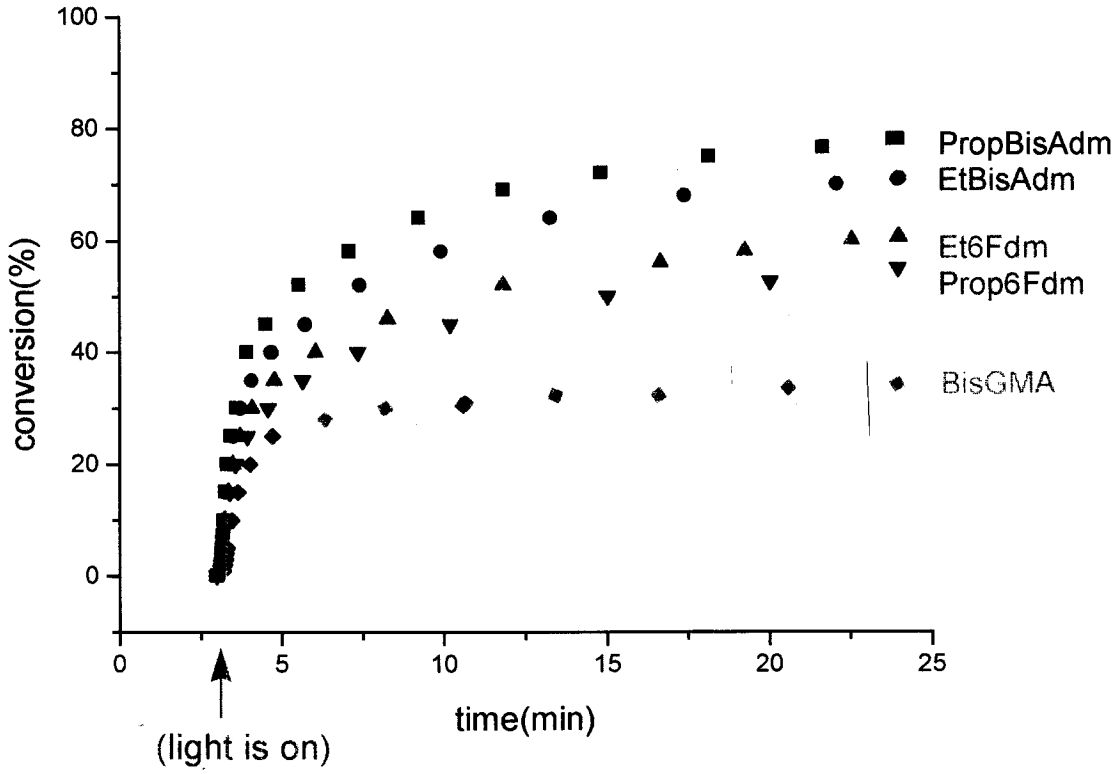

Figure 4.1.10 *E_p (%) versus Time for Several Monomers at 40 °C*

From the conversion versus time data, the rate of polymerization versus conversion was calculated. Figure 4.1.11 illustrates the rate of polymerization as a function of double bond conversion for the photopolymerization of PropBisAdm at 40 ^{0}C.

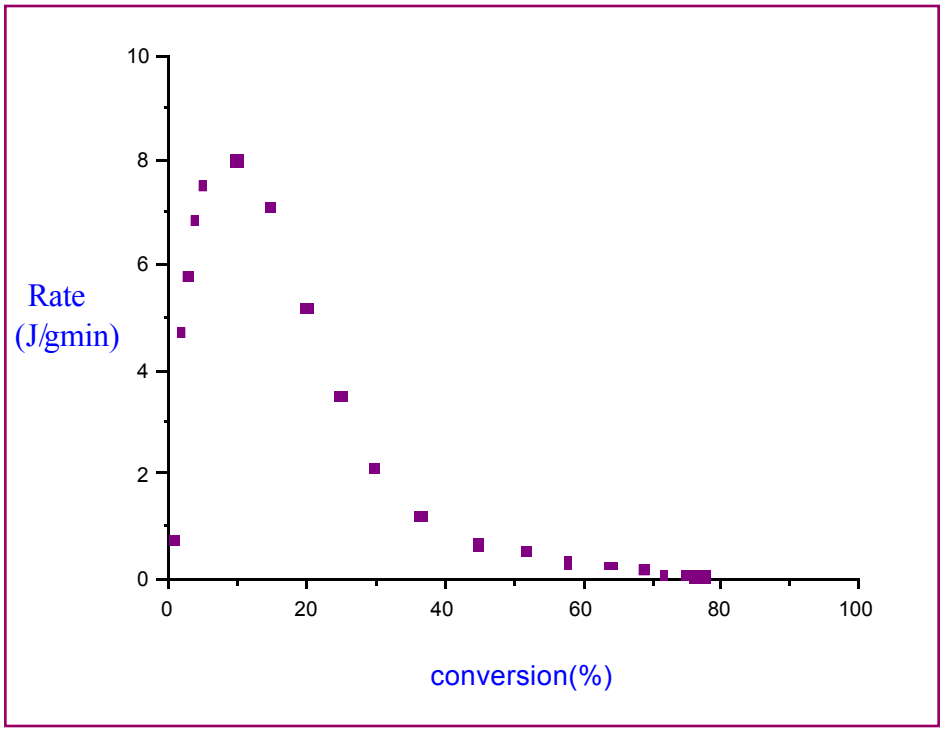

Figure 4.1.11 *Rate versus Conversion (%) for PropBisAdm at 40 °C*

In this figure, two more distinct features of polymerizations of multifunctional monomers are illustrated. The rate of polymerization of PropBisdm resin first increases very sharply at very low conversions and exhibits a maximum in the rate curve at around 10 % conversion. This increase and maximum in the rate curve, known as the Trommsdorff effect, is due to the reduction in radical mobility resulting in a decrease in the termination rate constant (k_t). As the polymerization proceeds, the rate of polymerization decreases from its maximum point to almost zero due to the considerable reduction in all the rate constants (k_t, k_p, k_i).

Maximum rate at the exotherm peak was calculated for each monomer at 40 °C and the results are given in Table 4.1.3. As the monomer viscosity decreases in the order

of BisGMA> Prop6Fdm>Et6Fdm>EtBisAdm>PropBisAdm, the rate at the exotherm peak increases in the same order:

BisGMA < Prop6Fdm < Et6Fdm < EtBisAdm < PropBisAdm.

Table 4.1.3 *Total Heat of Polymerization and Exotherm Peak Rate for Monomers at 40 °C*

Monomer	Total Heat -dH(J g^{-1})	Peak Rate (J g^{-1} min^{-1})
PropBisAdm	175.65	7.99
EtBisAdm	167.34	6.89
Et6Fdm	117.45	5.41
Prop6Fdm	100.58	4.52
BisGMA	68.7	3.13

Polymerization was performed at 40^{0}C and 4.51 mW/cm^2 light intensity

The maximum rates in the exotherm curves also give an approximately linear correlation with the ultimate extents of conversion (Figure 4.1.12). Mobility of the unreacted monomer and flexibility of the developing network structure are some of the important parameters in the extent of continued polymerization. Lower viscosity monomers with greater potential for diffusion exhibit higher rates of polymerization at the exotherm peak and higher ultimate conversions. They start to vitrify at later stages of the reaction and therefore reach higher conversion values.

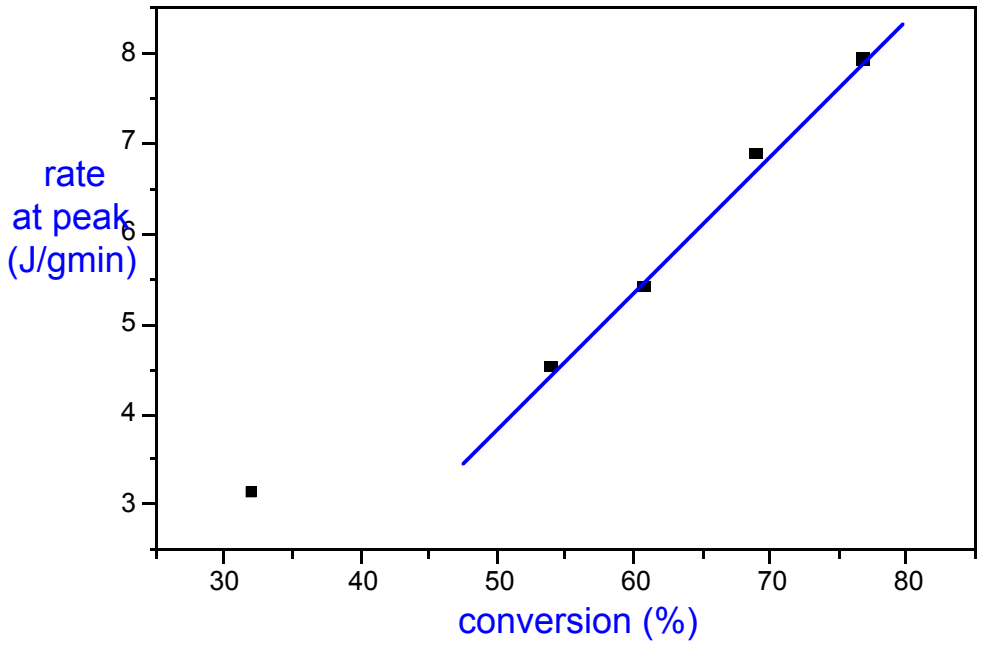

Figure 4.1.12 *Variation of Exotherm Peak Rate as a function of ultimate conversion for Monomers at 40 °C*

4.1.2.2 Effect of Temperature

Influence of the temperature on the photopolymerization reaction was studied with a photoinitiator concentration of 1.0 mol % CQ and 0.3 wt % DMpT. The light intensity was 4.51 mW/cm^2 from a 470 nm monochromatic source. The ultimate conversions were measured for temperatures in the range of 30-60 °C. Figure 4.1.13 shows the photopolymerization rate versus time for Et6Fdm at various polymerization temperatures. At low temperatures, the polymerization is very slow. As the temperature is raised the maximum in the rate is slightly shifted to shorter times and the rate increases markedly. Similar behavior has been observed for other monomers by Cook (79) with

dimethacrylates based on the bisphenol-A backbone, and Anseth et al. with multiethylene glycol dimethacrylates (107).

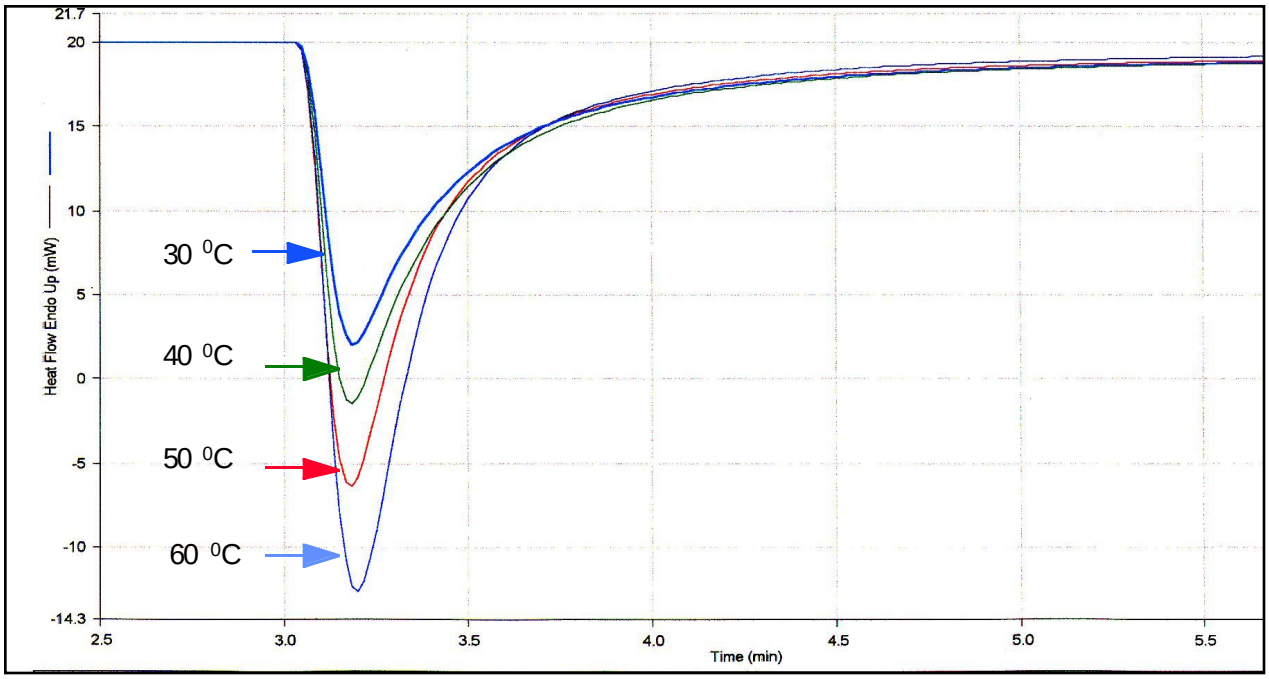

Et6Fdimet+1.0 mole% CQ + 1.0 mol% DMpT was run at 4.51 mW/cm^2 light intensity

Figure 4.1.13 *Effect of Temperature on Photopolymerization of EtBisAdm*

The maximum attainable conversions for the homopolymerization of these dimethacrylate monomers were calculated from the exotherm curves obtained at four different temperatures and the results are shown in the Table 4.1.4.

Table 4.1.4 *Variation of E_p (%) with Temperature(^0C)*

	EXTENT Of CONVERSION (Ep%)			
MONOMER	**30 °C**	**40 °C**	**50 °C**	**60 °C**
PrBisAdm	70	77	80	84
EtBisAdm	61	69	74	80
Et6Fdm	49	60	66	70
Prop6Fdm	40	54	57	64
BisGMA	25	32	39	43

Conversion versus time curves are plotted in Figure 4.1.14 for temperatures 30, 40, 50 and 60 °C. At the beginning of the reaction, the initial slopes of the conversion plots (R_{pi}) increase slightly with temperature.

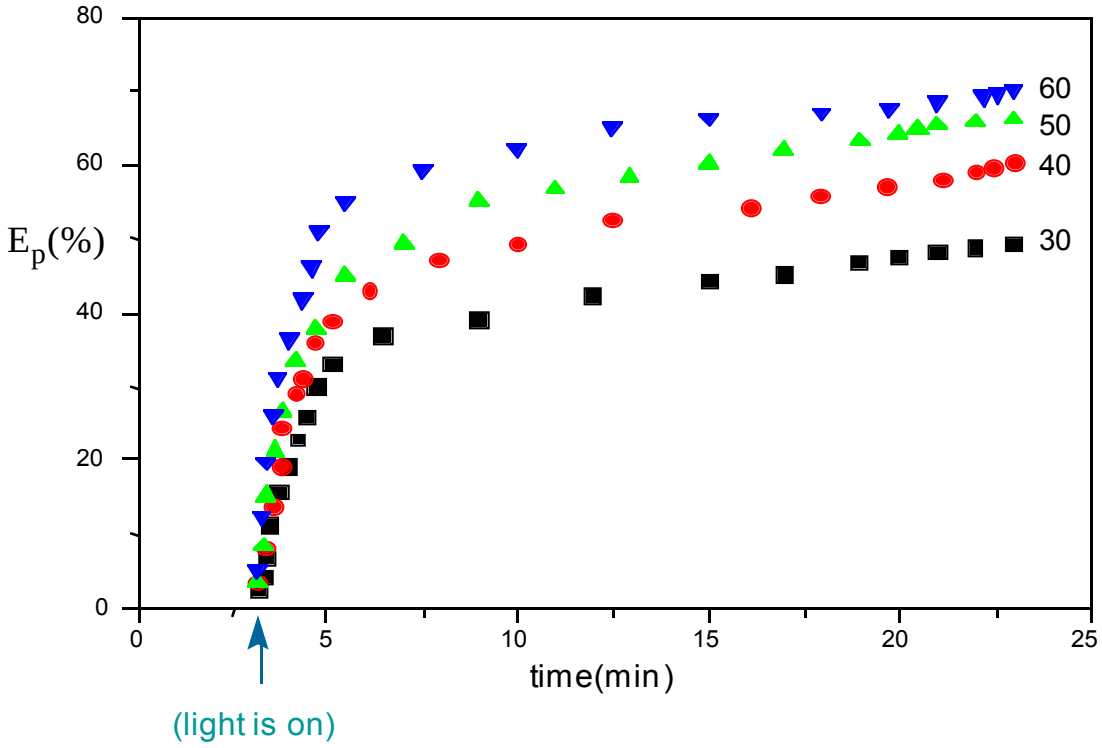

Figure 4.1.14 *Conversion (%) versus time for Et6Fdm at various temperatures, ^0C.*

We also notice in Table 4.1.4 and in Figure 4.1.14 that conversion increases with temperature. Although gelation decreases the mobility and the diffusion of the reactive species leading to a progressive rate deceleration, the reaction almost completely stops when the glass transition temperature of the crosslinked material is reached (glassy state).

At the very start of the reaction, an instantaneous rise in the rate and in the conversion can be seen in Figure 4.1.13 and Figure 4.1.14. In this early stage of the reaction the radical concentration rapidly rises, reaches its maximum value and then decreases. A number of studies (13, 20, 87) have suggested that during the formation of the dense network structure, radicals become trapped in the matrix. It has been considered that these trapped radicals are effectively inactive at the reaction temperature and incapable of propagation and termination reactions. However, they can be activated by increasing the reaction temperature. This behavior was explained by the assumption that the free volume

available in the system is not evenly distibuted to the radicals. As the temperature is raised, the free volume increases thus giving enough room and sufficient mobility to some of the trapped radicals to react.

Calculation of Apparent Activation Energies

The consideration of the temperature effect on the course of polymerization permits calculation of overall activation energies (E_a). The slopes of the Arrhenius plots depend not only on the temperature dependence of R_p but also on other processes influencing the polymerization rate and having their own activation energies, such as decomposition of polymer or initiator, chain transfer, oxygen consumption and diffusion etc.(109).

The usual expression for the activation energy is given by the relation 4.1:

$$E_a = E_{prop} + 0.5E_i - 0.5E_t \qquad \text{(Equation 4.1)}$$

where E_{prop} is activation energy of propagation, E_i is activation energy of initiation and E_t is activation energy of termination.

In the case of photochemical initiation in which a bimolecular termination takes place:

$$E_a = E_{prop} - 0.5E_t \qquad \text{(Equation 4.2)}$$

since activation energy for initiation (E_i) is assumed very small or zero. However, Equation 4.2 was derived for bimolecular termination when k in the Arrhenius equation:

$$k = A \exp(-E_a / RT) \qquad \text{(Equation 4.3)}$$

is determined by the relation:

$$R_p = k\,[M] \qquad \text{(Equation 4.4)}$$

with photochemical initiation and bimolecular termination:

$$k = k_p (\Phi I_a)^{0.5} / (2 k_t)^{0.5} \qquad \text{(Equation 4.5)}$$

where k_{prop} = propagation rate constant, k_t = bimolecular termination rate constant,

Φ = quantum yield of initiation, I_a= intensity of absorbed light and [M]= concentration of double bonds.

In order to calculate E_a, exotherms were recorded at four different temperatures and rate data were obtained for Arrhenius plots at five conversions. The slope of the plot of log rate against reciprocal temperature is proportional to the apparent activation energy, E_a, for the polymerization. Figure 4.1.15 presents Arrhenius plots for PropBisAdm at 20, 30, 40, 50 and 60 % conversions.

Table 4.1.5 summarizes the apparent activation energies, determined using a least-square calculation of slopes. As can be seen from the table, the overall apparent activation energy changes with conversion, first increasing with increase of conversion and then decreasing as the reaction proceeds. One possible explanation of the observed conversion-dependent behavior of the apparent activation energy can be differing diffusion-controlled mechanisms in the propagation and termination steps. The values of E_{prop} and E_t are both expected to increase with conversion. At the very beginning of the reaction the decrease in termination rate due to mobility decrease is greater than the decrease in propagation rate due to mobility decrease. In later stages the effect of mobility change on the two processes becomes more comparable.

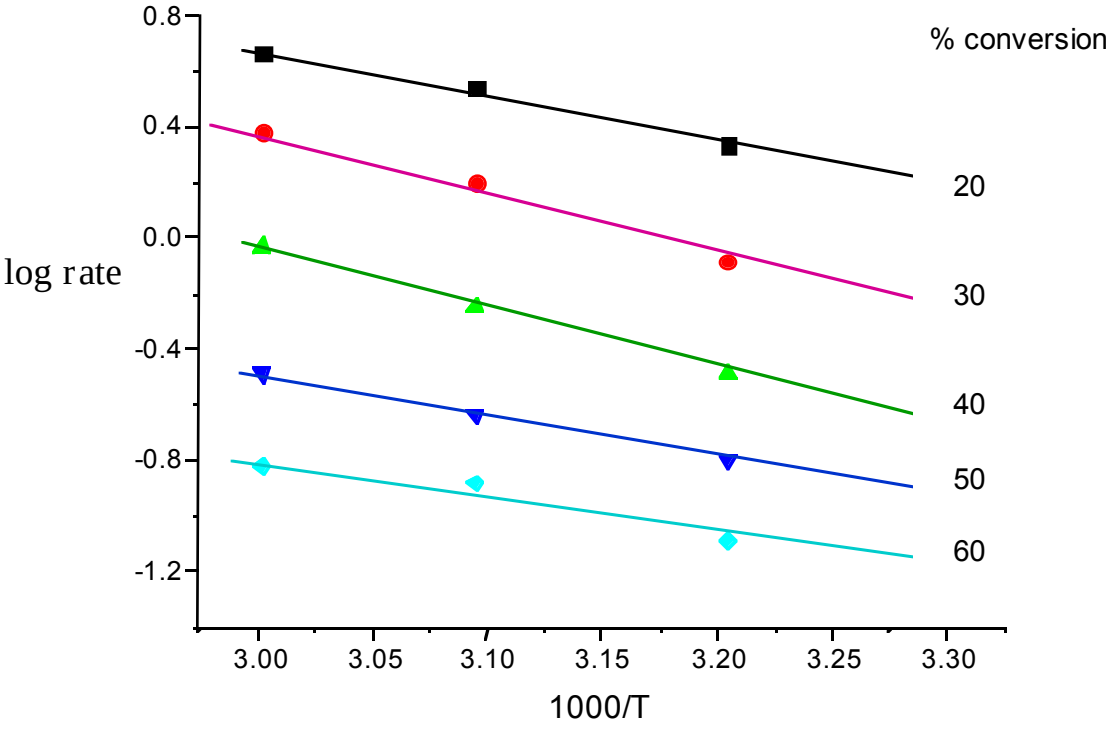

Figure 4.1.15 *Arrhenius plots for PropBisAdm at five chosen conversions*

Since the apparent activation energy (E_a) is the combination of the activation energy for propagation (E_p) and one half of the termination activation energy (E_t), the apparent activation energy increases until the reaction reaches its maximum rate due to the increase in the concentration of radicals. Somewhere between 30 % and 40 % conversion of PropBisAdm the propagation step also becomes more strongly diffusion controlled and the rate of polymerization slows down. In this region diffusion controlled termination predominates and the activation energy for termination increases more than the activation energy for propagation. Similar studies can be found in the literature. Tryson and Shultz's paper (73) was the first to demonstrate the kinetics of a crosslinkable system using a DSC-based photocalorimeter.

Table 4.1.5 *Apparent Activation Energy versus Conversion for PropBisAdm*

% Conversion (30-60 ^{0}C)	Ea (kcal/mole)
20	3.08
30	4.11
40	4.07
50	2.64
60	2.50

Monomers were mixed with 1 mol % CQ and 0.3 wt% DMpT
Polymerizations were performed at 4.51 mW/cm^2 light intensity

4.1.2.3 Effect of Light Intensity

To determine the dependency of rate on intensity, the reaction characteristics observed during the photopolymerization of each monomer were recorded at several different light intensities. The light intensity at 470 nm was adjusted using neutral density filters. Relative and incident intensities through the filters are given in Table 4.1.6.

Table 4.1.6 *Relative and Incident Light Intensities Through the Filters*

Serial #	Relative Intensity (I_{rel})	$I_{incident}$ (mW/cm^2)
000 (no filter)	1.0	4.51
112	0.316	1.43
907	0.0871	0.393
29	0.0288	0.13

4.51 mW/cm^2 was the highest intensity we obtained from the lamp assembly as measured by DSC. The measurement of intensity was discussed in detail in the experimental part, section 3.2.3. For such measurements, graphite discs were inserted into the measuring cells to absorb the incident light intensity. During the irradiation, sample cell and reference cell were covered alternately without touching the sample holder cover and the heat flow values were taken when the light is on and off. The data below indicate the heat flow values taken during a measurement of light intensity by DSC. The average of three heat flow readings when the sample side is opened (S opened) and both sides are closed (R/S closed) were taken and the difference in heat flow values was divided by the area of light at sample position using the equation (light intensity = [($mW_{(light\ on)}$ - $mW_{(light\ off)}$) / area of light (cm^2)]).

Cell (R = reference, S = sample)	Heat flow reading (mW)		
R/S closed	19.9972		
R/S closed	19.2260		
R/S closed	19.9961	1.7891	
S opened	18.2070		
R/S closed	19.9942	1.7867	1.7864
S opened	18.2075		
R/S closed	19.9906	1.7833	
S opened	18.2073		
R/S closed	19.9931		
R opened	21.0140		

Heat flow reading = 1.7864 mW

Area of light = 0.385 cm^2

Intensity of light = 1.7864 / 0.385

= 4.51 mW/cm^2

Using neutral density filters of differing attenuating efficiency as just described, polymerization exotherms were recorded for all the monomers, while maintaining an identical initiator concentration and temperature, only changing the light intensity. The light was switched on at the 3 min mark and maintained at the selected intensity for 20 min. DSC thermograms shown in the Figure 4.1.16 illustrate the effect of light intensity on the reaction rate. From the general shape of the curves, one observes the immediate onset of autoacceleration at highest intensity, 4.51 mW/cm^2, but a much broader exotherm at the lowest intensity, 0.13 mW/cm^2. As the light intensity increases, the rate curves shift to shorter times. This shifting is most easily observed in Prop6Fdm by determining the

conversion at which the rate reaches its maximum value (7 % to 21 %) and the maximum attainable conversion in 20 min (28 % to 54 %) at the intensities of 0.13 and 4.51 mW/cm^2 respectively.

Total extent of polymerization was calculated for each resin from the area under the exotherm curves at various intensities after the light is on for 20 min. The percent conversions, obtained by averaging the results of three replicates, are presented in Table 4.1.7.

Increase in light intensity caused an increase in the final conversion for all the monomers studied. Kloosterboer et al. (110) reported that this was due to the presence of a temporary excess volume in the reacting mass. This temporary free volume exists because the rate of volume shrinkage lags behind the reaction rate. As the light intensity was increased, the reaction rate also increased and more temporary excess free volume was available. This results in an increase in the final conversion. Such an increase in final conversion with an increase in light intensity has been also seen by others (5,14, 111).

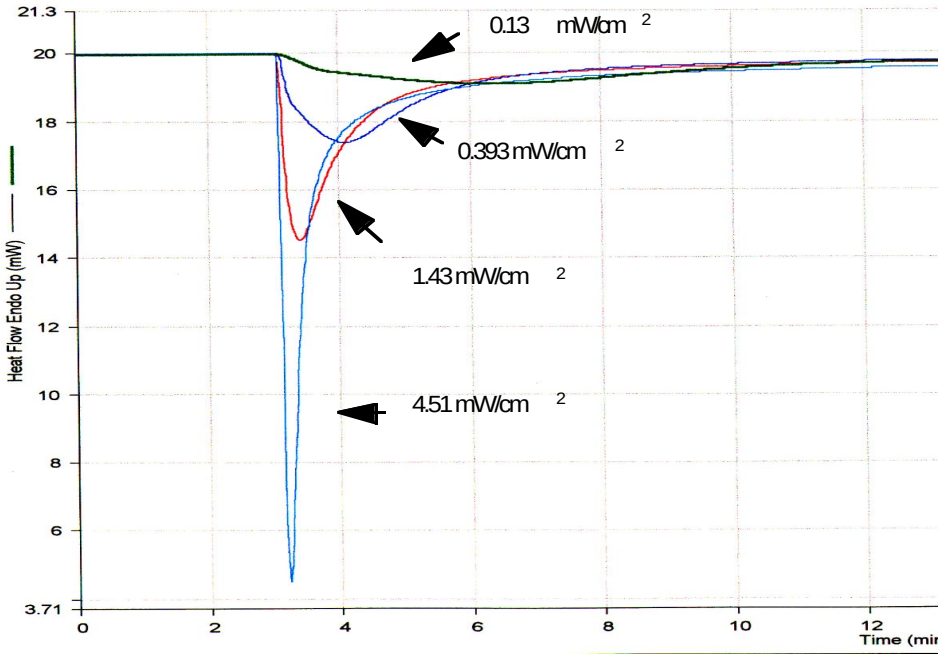

Prop6F+1.0 mole % CQ + 1.0 mole %DMpT
Polymerizations were performed at 40 ^0C

Figure 4.1.16 *PhotoDSC Thermograms at Various Light Intensities for Prop6Fdm.*

Kloosterboer reported (112) that a slow polymerization process occurs under low light illumination even after vitrification of the system. This is very important since it suggests that free radical polymerization in a cross-linked glassy matrix can proceed, although very slowly, to high conversions.

Table 4.1.7 *Extent of Polymerization (Ep %) at Four Different Incident Light Intensities*

MONOMER	EXTENT Of CONVERSION (Ep%)			
	0.13 mW/cm^2	0.39 mW/cm^2	1.43 mW/cm^2	4.51 mW/cm^2
PrBisAdm	49	56	68	77
EtBisAdm	41	50	62	69
Et6Fdm	34	41	50	60
Pr6Fdm	28	36	43	54
BisGMA	15	20	27	32

Monomers were mixed with 1.0 mol % CQ and1.0 mol% DMpT
Polymerizations were performed at 40C

Figure 4.1.17 illustrates the conversion versus time behavior for Prop6Fdm at 40 °C and various incident light intensities. Except for the curve at 0.13 mW/cm^2 light intensity, all other curves at higher intensities exhibit an inverse L-shaped behavior observed in most of the autoacceleration systems. However all the curves illustrate the attainment of a maximum conversion. At higher intensities, due to the generation of more radicals, a higher number of growing polymer chain radicals are formed in the system. This results in a rapid rise in the polymerization rate to a maximum. Thus, at a

higher intensity a higher conversion is obtained in a very short period of time. Once the reaction rate reaches its maximum value, the kinetics starts to become diffusion controlled and the rate begins to fall off as the monomer is consumed. After this time, the conversion increases slowly due to vitrification.

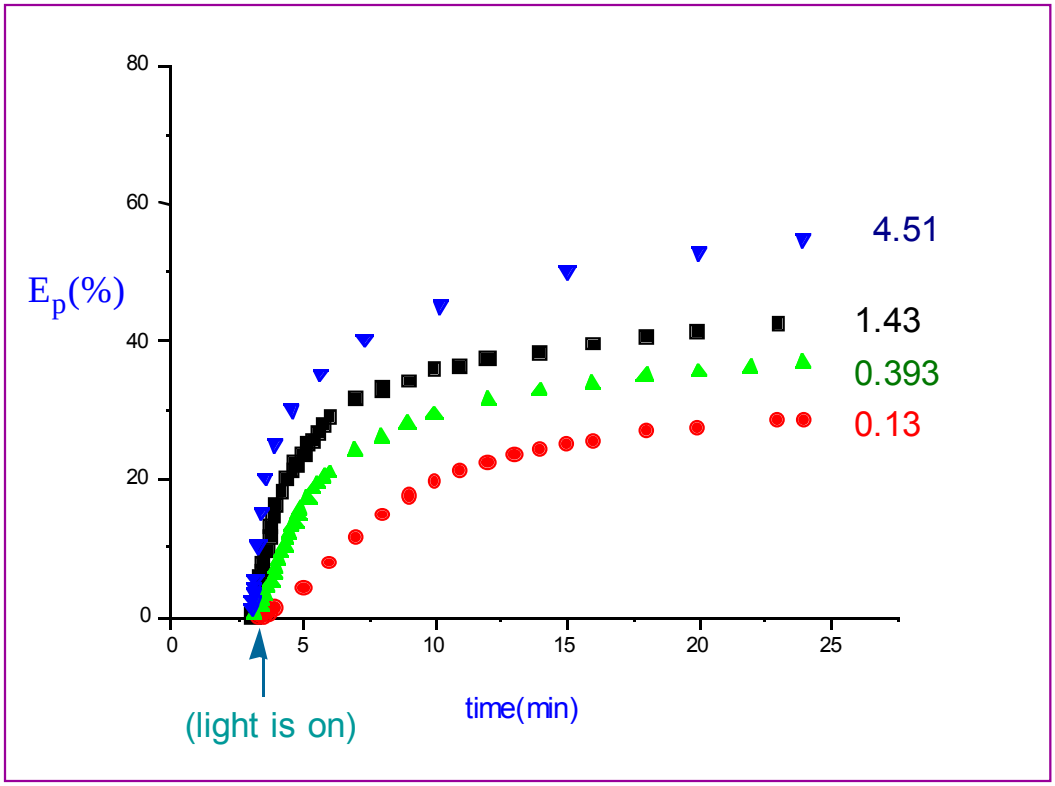

Figure 4.1.17*Conversion (%) versus Time at Four Light Intensities (mW/cm^2)for Prop6Fdm at 40 °C.*

Table 4.1.8 *Variation of Peak Rate with Light Intensity for Prop6Fdm at 40 °C.*

Light Intensity (mW cm $^{-2}$)	Total Heat - dH(J g $^{-1}$)	Rate at Peak (J g $^{-1}$ min $^{-1}$)
0.13	52.15	0.29
0.393	67.05	0.98
1.43	80.09	2.08
4.51	100.58	4.52

One can clearly see from Figure 4.1.17 and Table 4.1.8 that the maximum double bond conversion that is reached increases from 28 % for the polymerization initiated by 0.13 mW/cm^2 to 54 % for the polymerization initiated by 4.51 mW/cm^2. The increased double bond conversion is probably caused by a delay in the volume shrinkage rate (5, 95). The delay in volume shrinkage leads to an increased free volume and, therefore increased mobility in polymerizations that proceed at faster rates. This is also the reason in the case of polymerizations initiated by higher initiator concentrations.

From DSC data on the photopolymerization of the various dimethacrylate monomers it is possible to determine the dependence of reaction rate on incident light intensities. The slope of a log-log plot of exotherm rate (proportional to the reaction rate) versus light intensity gives the power dependence of the rate on the incident light intensity. Figure 4.1.18 shows the experimentally observed dependence of the peak exotherm rate on light intensity for Prop6Fdm at 40 °C.

From the theoretical considerations that have been discussed earlier in Equation 4.5, one can see that the rate depends on the square root of the light intensity. In this study, the

values of the exponent were found to be greater than 0.5 for all the five monomers. The intensity exponent for the photopolymerization exotherm rate at peak of PropBisAdm is 0.72 for EtBisAdm is 0.71, for Et6Fdm is 0.74, for Prop6Fdm is 0.73, and for the control BisGMA is 0.68. (With the possible exception of BisGMA, these exponents are essentially the same).

One explanation for an intensity exponent greater than 0.5 and less than unity is that, at high conversions, termination may occur by a unimolecular pathway as well as by the radical - radical reaction:

($RM_n^{\cdot} + RM_n^{\cdot} \xrightarrow{k_t}$ inactive species). Tryson and Shultz explained that if termination occurs by a unimolecular reaction with rate constants k_t and steady-state concentration of radicals is assumed and Equation 4.4 becomes:

$$R_p = k_p / (2\, k_t)\, (\Phi\, I_a)\ [M] \qquad \text{Equation 4.6}$$

for the polymerization rate. In this equation the rate depends on the first power of the photo absorption rate and therefore on the first power of incident light intensity. The Tryson/Shultz explanation of Rp depending on the exponent of I greater than 0.5 due to ‘monoradical termination” by isolation should be important only at higher conversion. it is most likely that the exponent of I at peak rate is mostly due to the delayed volume/shrinkage effect discussed earlier.

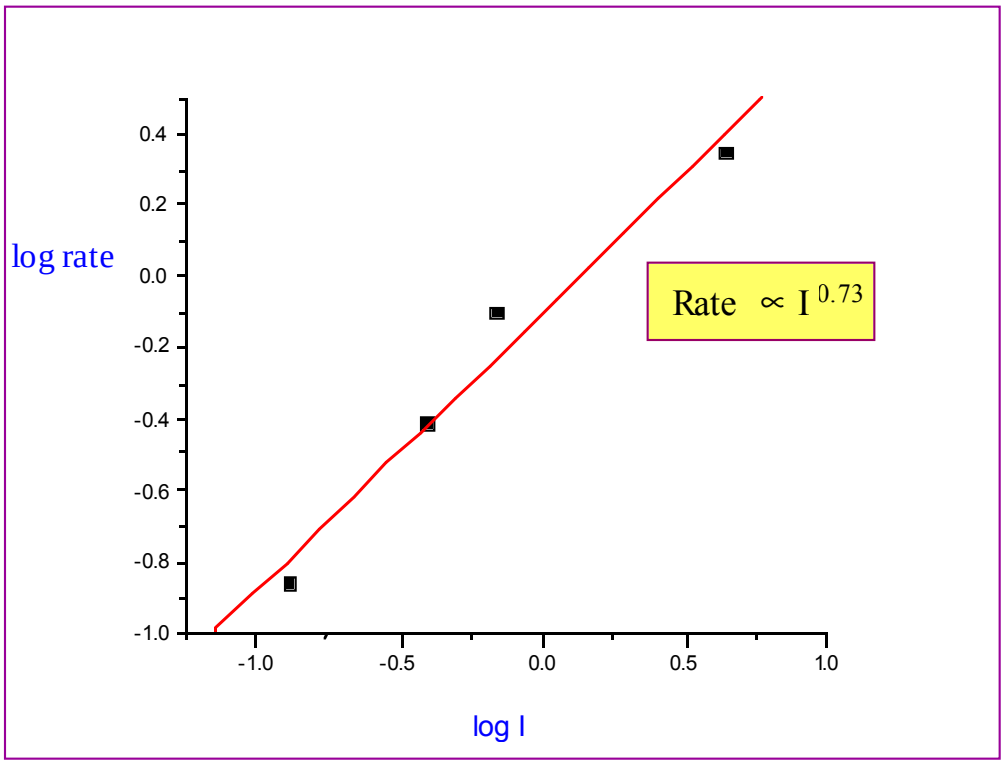

Figure 4.1.18 *Log-log plot of exotherm rate at peak against light intensity for Prop6fdm at 40 °C.*

4.1.2.4 Effect of Initiator Concentration

It is obvious that one of the key components in any photo-crosslinkable resin system is the amount of photoinitiator. Since the photoinitiator governs the number of radicals generated upon absorption of light, it is evident that the exotherm curve will reflect that the effect of photoinitiator concentration on the kinetics and rate of polymerization.

In order to study the effect of photoinititor (CQ) concentration on the photopolymerization rate of four experimental monomers as well as the control BisGMA, the monomers were mixed with various amounts of CQ, namely 0.25 mol %, 0.5 mol % and 1.0 mol %. In all these mixtures, the amount of DMpT used as a photoreducer kept

constant (1.0 mol %). Figure 4.1.19 shows the exotherm curves for the photopolymerization of EtBisAdm at these three initiator concentrations. Polymerizations were performed at a constant temperature and light intensity, 40 ^{o}C and 4.51 mW/cm^{2} respectively.

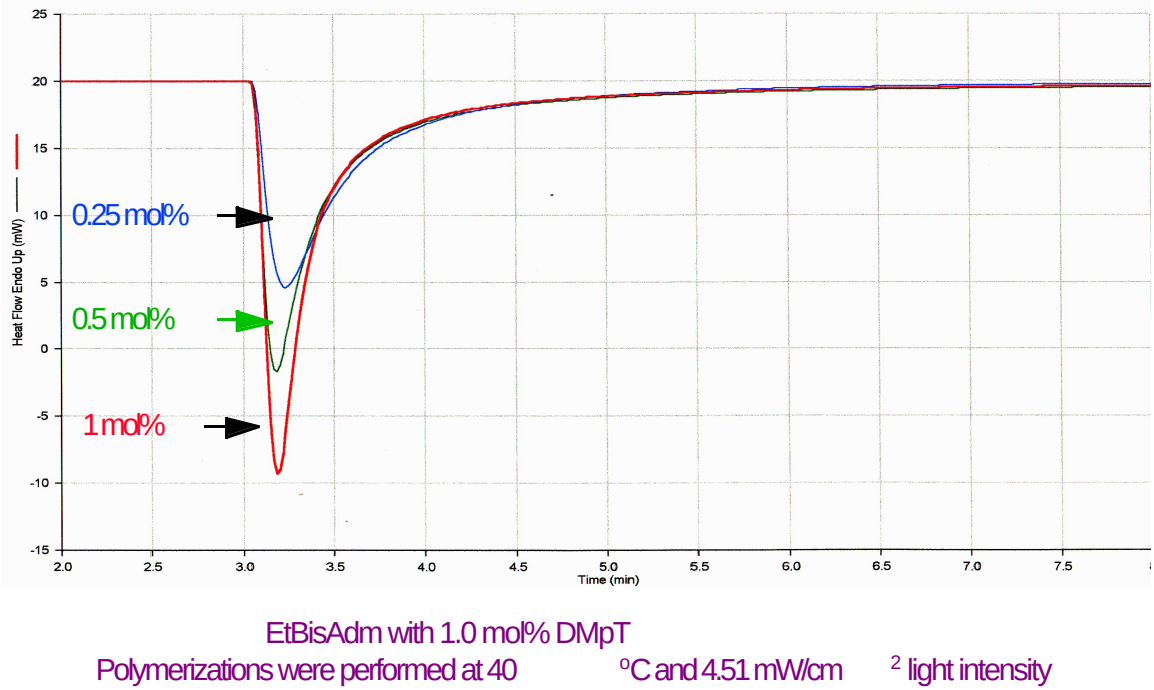

Figure 4.1.19 *Heat Flow (mW) versus time (min) for the photopolymerization of EtBisAdm containing 0.25, 0.50, and 1.00 mol % CQ.*

In this figure, it is obvious that very similar thermograms in which sharp increases in rate are seen. The difference in sharpness was obvious between the curves with 0.25 mol% and 0.5 mol%. However, practically there wasn't any difference in sharpness (initial slopes) between curves 0.5 and 1.0 mol% . The two distinct regions in the thermograms can be also identified easily. The first region involves a rapid increase in the rate reaching its maximum (in less than 15 sec for 0.5 and 1.0 mol % CQ amount and less than 20 sec

for 0.25 mol % CQ). The second region involves vitrification of the system resulting in a decrease in rate much more rapidly than can be accounted for by depletion of reactive groups. In general, similar results are found for the free radical polymerization of all mono- and multifunctional monomers, i.e., maximum in heat flow $((dH/dt)_{max}$ taken as polymerization rate) increases and then decreases at each photoinitiator concentration (67).

The ultimate conversions were calculated for each monomer with different initiator concentration. Table 4.1.9 shows E_p (%) data obtained from the exotherm curves after 20 min light exposure for the photopolymerization of all the monomers studied. Increase of initiator concentration by a factor of four (from 0.25 mol % to 1.0 mol %) results in a relative increase in extent of polymerization (Ep %) from 28 % (in PropBisAdm) to 54 % for Prop6Fdm.

Table 4.1.9 *Variation of Extent of Polymerization (Ep %) with Initiator Concentration*

Initiator (CQ)	Extent of polymerization(%)				
	PrBisAdm	EtBisAdm	Et6Fdm	Prop6Fdm	BisGMA
1 mol%	77	69	60	54	32
0.5 mol%	71	56	53	43	29
0.25 mol%	60	48	44	35	24

Polymerizations were performed at 40 °C and 4.51 mW/cm^2 light intensity
Monomers were mixed with 0.3 wt% DMpT

Maximum rate in the exotherm peak was calculated from conversion versus time data for EtBisAdm with various initiator concentrations at 40 °C and the results are given in Table 4.1.10. According to the equation (7), when the initiator concentration [*c*] increases, the polymerization rate constant (R_p) must increase as a result of an increase in I_{abs}. Furthermore, according to the theory of free volume, if R_p increases, the conversion must increase. It is discussed in literature (67) that the quantum yield ϕ connected to the photoinitiator efficiency can decrease when [*c*] increases. In steady-state assumption, ϕ correponds to the light dissociation efficiency of initiator as well as to competition between the reaction of the primary radical ($R^{\cdot}$) with a double bond during the initiation, whose rate is proportional to $[R^{\cdot}][M]_0$ and coupling of these two primary radicals which is proportional to $[R^{\cdot}]^2$. So the more $[R^{\cdot}]$ increases, the more ϕ decreases. Therefore, the increase of [*c*] and decrease of ϕ can be responsible for the maximum observed for R_p.

Table 4.1.10 *Variation of Exotherm Peak Rate with Initiator Concentration*

Initiator(CQ) Cont.	Total Heat - dH(J g $^{-1}$)	Peak Rate (J g $^{-1}$ min $^{-1}$)
1 mol%	175.65	6.89
0.5 mol%	161.92	5.37
0.25 mol%	136.83	3.8

Monomers were mixed with 1.0 mol % DMpT
Polymerizations were performed at 40 °C and 4.51 mW/cm ^{2} light intensity

The empirical dependence of reaction rate on initiator concentration was established from the slope the log-log plot of exotherm rate against initiator concentration (Figure 4.1.20). Slopes of the log-log plots were calculated using a least-squares approach. Dependence of rate at peak on camphorquinone (CQ) concentration for the monomers studied are as follows: 0.34 (for BisGMA), 0.38 (for Prop6Fdm), 0.41 (for Et6Fdm), 0.42 (for EtBisAdm), and 0.44 (for PropBisAdm). The rate depends on the concentration of CQ raised to a power less than 0.5 for all the monomers studied. This might be attributed to the somewhat complex photoinitiation mechanism in diketone/amine systems (34). However, an early photo DSC study (73) of 1,6-hexanedioldiacrylate polymerization using benzoin ethyl ether/UV light initiation found the rate proportional to $[BEE]^{0.31}$. A survey of the power dependence of rate on photoinitiator concentration in diacrylate and dimethacrylate polymerization is not in hand, but it is possible that an unexplained low power dependence is general (113).

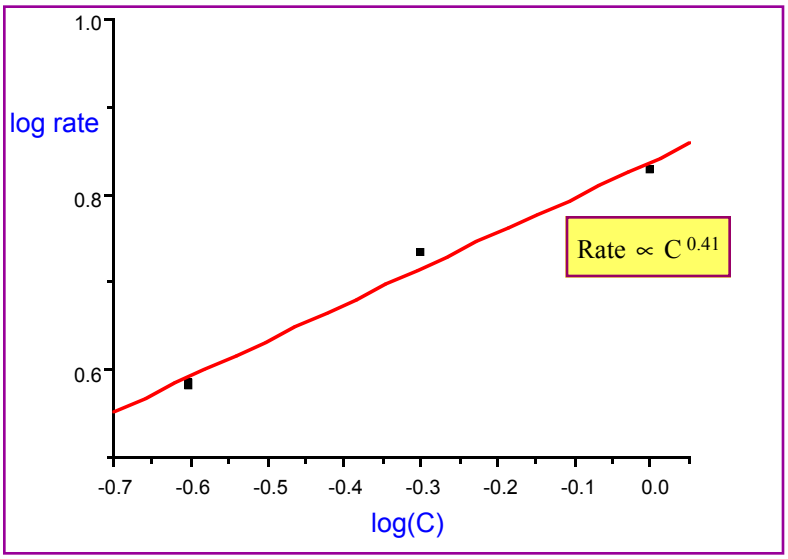

Figure 4.1.20 *Log-log Plot of Exotherm Rate at Peak against Initiator Concentration for EtBisAdm at 40 °C and 4.51 mW/cm² Light Intensity.*

4.1.2.5 **Calculation of Reaction Rate Constant Ratios**

In this part of the research, the polymerization exotherms were evaluated under both steady-state and nonsteady-state conditions. By switching off the light source at varying stages of the polymerization and recording heat release rate profiles as a function of time, dark reactions were carried out. Each sample was kept under nitrogen for 5 min. before the polymerization was started. The light was turned on at 3rd min and illumination

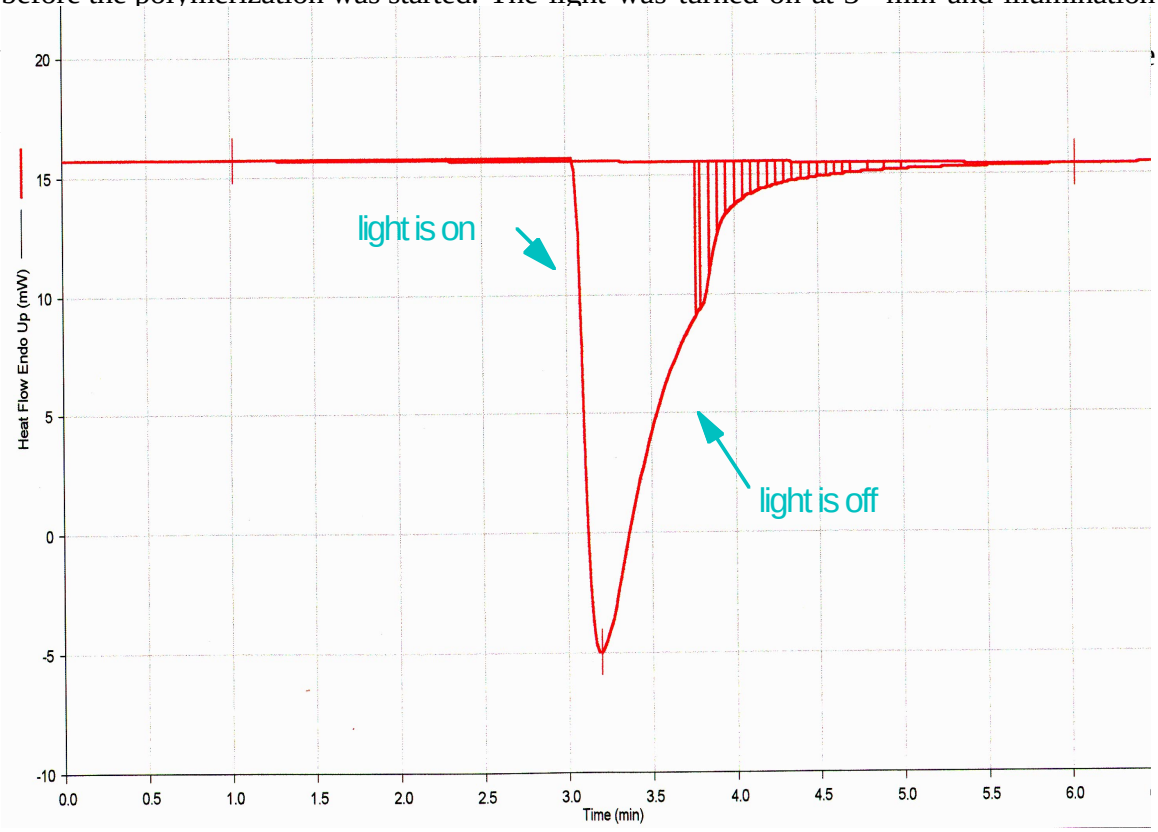

PropBisAdm with 1.0 mol% CQ and 1.0 mol % DMpT
Polymerization was performed at 40 °C and 4.51 mw/cm 2 light intensity

Figure 4.1.21 *DSC thermogram of a dark reaction for PropBisAdm*

The value $(\Phi I_{abs})^{0.5} k_p/(2k_t)^{0.5}$ was calculated from rate versus conversion data under constant illumination as the reaction proceeds. Analysis of rate versus time data under nonsteady-state conditions (light turned off) yields the ratio of k_t/k_p

In this set of experiments , at various stages of the reaction, the light delivered to the sample was abruptly terminated with a manual shutter placed between the lamp source and the DSC sample chamber. The percent conversion at the time of shuttering the lamp was defined as the monomer conversion $[M]_0$ at zero time. After terminating the exposure at a selected time, the decay of the rate of heat evolution was recorded as a function of time. The decay of the exotherm curve was then analyzed by Equation 4.7. in which termination is assumed by radical-radical interaction. In the equation $(-d[M]/dt)$ is related to the exotherm rate and [M] is determined from the monomer conversion. These quantities were determined to calculate $(\Phi I_{abs})^{0.5} k_p/(2k_t)^{0.5}$ under steady-state (actually continous illumination) conditions. Figure 4.1.22 show the resultant monomer disappearance rate $(-d[M]/dt)$ versus conversion plots for propBisAdm for several percent conversions at 40 ^{o}C. The numbers next to each curve represent the total conversions obtained from constant illumination for short periods of time illumination plus the subsequent dark reaction conversions.

continuous illumination :

$$\frac{-\,d[M]}{dt} = k_p \left(\phi I_{abs} / 2k_t\right)^{1/2} [M] \qquad \text{Equation 4.4.}$$

dark reaction :

$$\frac{[M]}{(-d[M]/dt)} = \frac{[M]_0}{(-d[M]/dt)_0} + \frac{2k_t}{k_p}\, t \qquad \text{Equation 4.7.}$$

where

$[M]_0$ = monomer concentration at time $t = 0$, when the light is terminated

$[d[M]/dt]_0$ = staedy-state polymerization rate at time $t = 0$, with $t = 0$ defined as time of shutter close

t = time after shutter close

k_p, k_t = polymerization and termination rate constants respectively as defined for Equation 4.5.

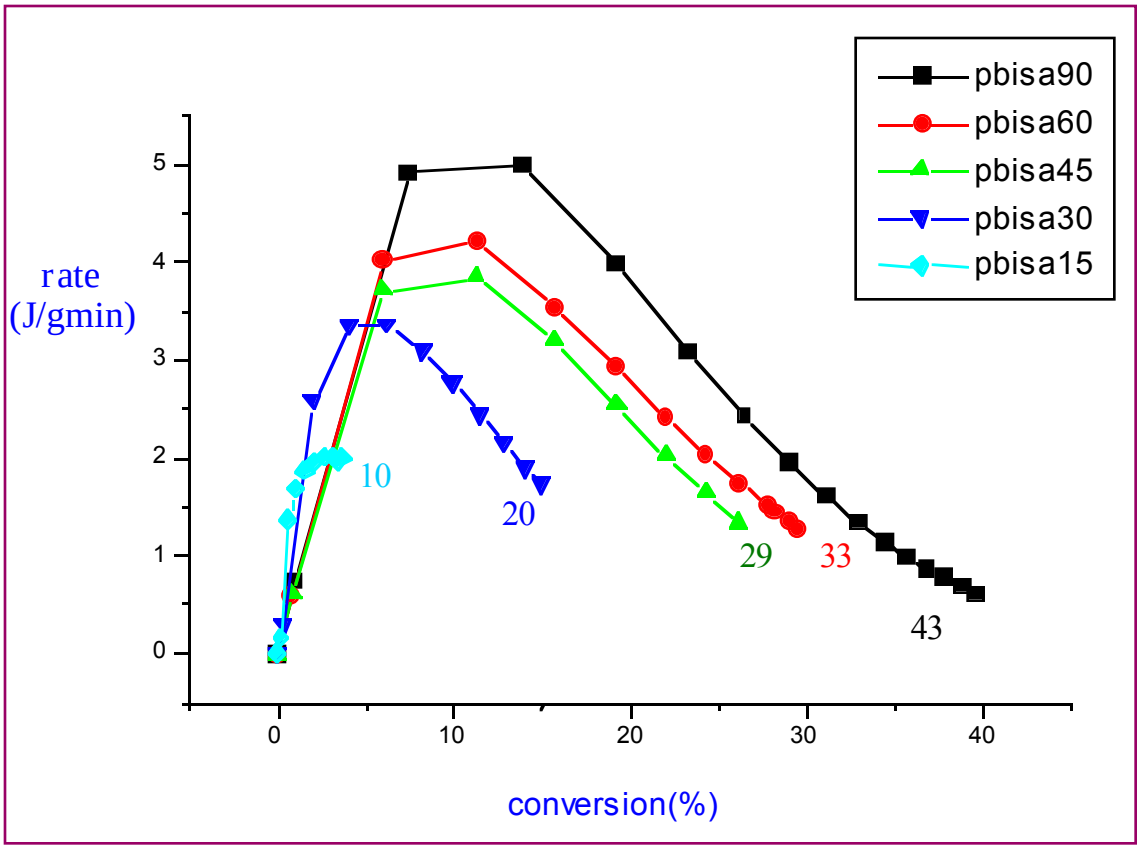

Figure 4.1.22 *Rate versus conversion (constant illumination) for PropBisAdm*

From the conversion of monomer, [M], the amount of remaining monomer was calculated. Figure 4.1.23 shows the effect of monomer concentration on rate for PropBisAdm. In both Figure 4.1.22 (rate dependence on conversion) and Figure 4.1.23 (rate dependence on monomer concentration) the complex DSC curve shape can be seen due to autoacceleration and autodeceleration. In Figure 4.1.22 for all the curves, rate increases sharply at the very beginning of the reaction and low conversion. After reaching its maximum value, polymerization rate decreases at a slower mode as the reaction proceeds. Numbers in the window (at the top right side) represent the times (seconds) of illumination. After the light was turned off at a selected time (namely 15 sec, 30 sec, 45 sec, 60 sec, 90 sec) conversions were calculated obtained only from constant illumination.

The small chart below (Table 4.1.11) gives the conversions at various times calculated from the DSC curves under constant illumination and dark reaction.

Table 4.1.11 *Total conversions obtained from DSC exotherms for PropBisAdm after constant illumination and after constant illumination + dark reaction.*

	conversion after constant illumination	conversion after constant illumination + dark reaction
pbisa15	4 %	10 %
pbisa30	15 %	20 %
pbisa45	26 %	29 %
pbisa60	29 %	33 %
pbisa90	40 %	43 %

The difference between first and second column values gives the conversion that occurred after the light was turned off. These data prove the continuation of the polymerization process even after the light is turned off.

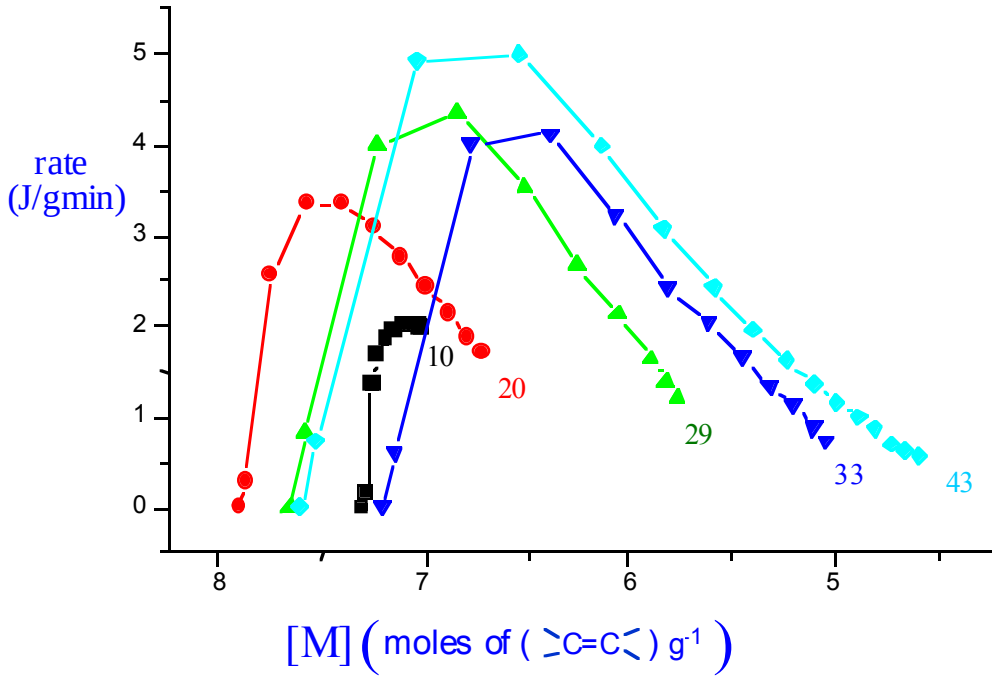

Figure 4.1.23 *Rate versus monomer concentration remaining (constant illumination) for PropBisAdm at 40 °C.*

The resultant [M]/ (–d[M]/d*t*) versus time plots for PropBisAdm according to the Equation 4.7 are shown in Figure 4.1.24 for several percent conversions at 40 °C.

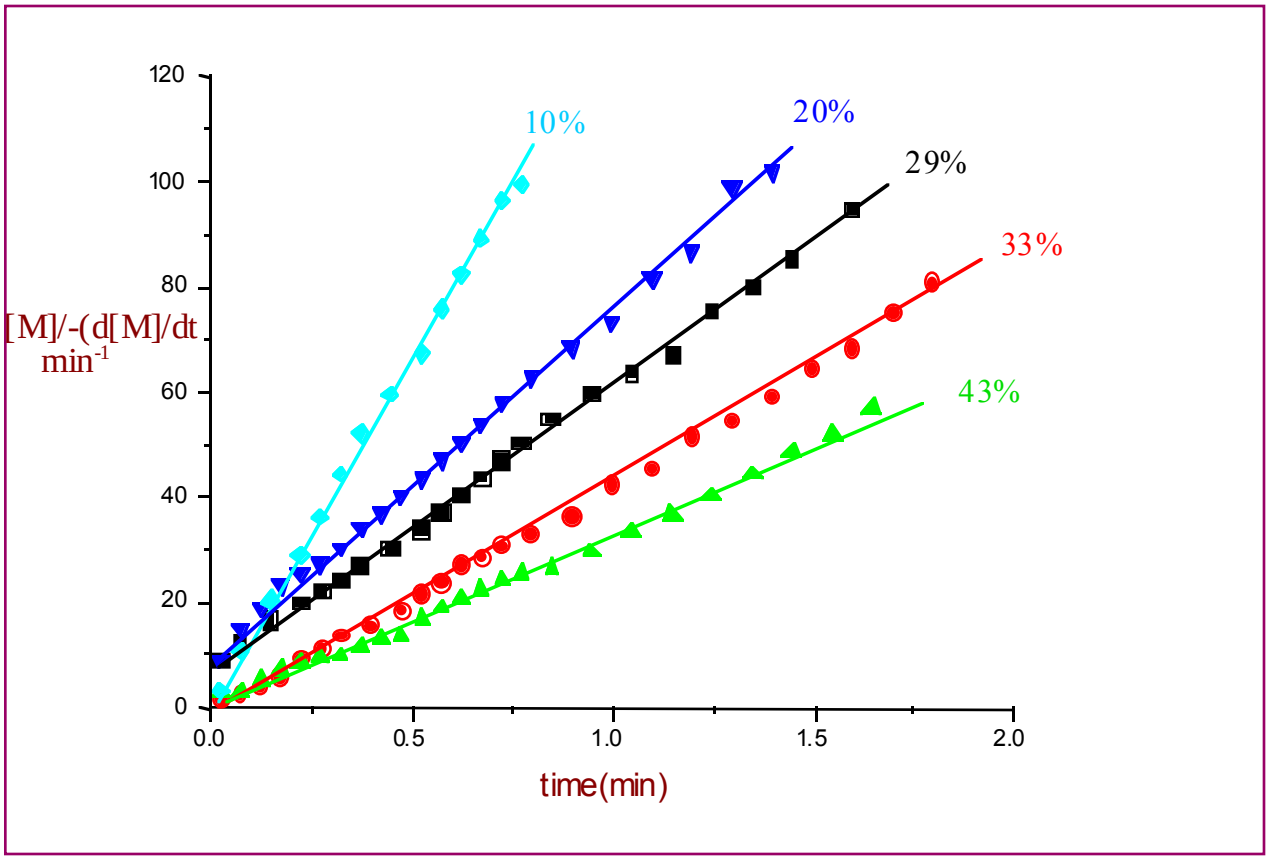

Figure 4.1.24 *Function of rate of monomer disappearance (dark reaction) versus time after the light is turned off at 40 °C. E_p shown for each line is the sum of the constant illumination and dark reaction conversions..*

At low conversions the slopes of the lines are grater than at higher conversions. This indicates that the rate of monomer disappearance is faster during the dark reaction when the illumination time is shorter. When the shutter is opened, radicals are generated right away by the absorption of the light. In the case of short illumination time, most of the radicals generated will continue the polymerization after the light is off. Therefore when the light is on only for 15 sec., more than half of the total conversion occurs after the light is off. However in the case of longer illumination periods, radicals generated under light will be reacting with double bonds during the

illumination. When the shutter is closed most of the available radicals have been already reacted, and the system has already started to vitrify. Only small amount of radicals will be able to reach to the monomers available in neighborhood. Thus, with longer illumination time, the rate of monomer disappearance will be slower after light is off.

From the slope of [M]/ (–d[M]/dt) vs. time curves in Figure 4.1.24, $2k_t$ / k_p values were calculated by a least-square method for several percent conversions according to Equation 4.7. The resultant $2k_t$ / k_p values under nonsteady-state conditions and $(\Phi I_{abs})^{0.5}$ $k_p/ (2k_t)^{0.5}$ values under steady-state conditions are reported in Table 4.1.12. After an initial increase in R_p/[M] = $(\Phi I_{abs})^{0.5}$ $k_p/ (2k_t)^{0.5}$ at lower conversions, there is a substantial decrease with increasing percent conversion. This result reflects the important effect of the crosslinked network in reducing all rate processes involved in the polymerization process. $2k_t$ / k_p decreases continously with increasing conversion. Similar behavior of the rate constants has been observed by Tryson and Shultz (73) for the polymerization of 1,6-hexanedioldiacrylate (HDDA) and pentaerythritolctetraacrylate (PET_4A). A further explanation for this behavior given by Tryson and Shultz is that as the reaction proceeds both k_t and k_p decrease, however k_t decreases more rapidly than k_p with conversion, suggesting that the termination rate decreases more than propagation reaction rate with conversion (Figure 4.1.25). As the reaction proceeds, an increasing number of radicals become trapped on the network. Due to the viscosity of the system and geometric restraint their diffusions together are increasingly prohibited. This results in a decrease in k_t. Increasing network formation further inhibits diffusion of monomer to the reactive radicals and results in a decrease in k_p as well. This explanation can be also supported by experimental evidence in which a sample of PropBisAdm which had been "completely reacted" at 50 ^oC by photoinitiation was thermally scanned. The thermal

scan of the "completely cured" sample from 30 °C to 200 °C (heating rate 10 °C min^{-1}) showed an exotherm above 50 °C which can be attributed to reaction of remaining monomer diffused to radicals isolated in the network.

% Conversion	$2k_t/k_p$	$(\Phi I_a)^{1/2} k_p/2k_t^{1/2}$ (min^{-1})
9.81	127	0.15
19.66	66	2.07
29.42	55	2.48
33.46	43	2.31
43.15	32	2.25

Table 4.1.12 *Ratio of Rate Constants for PropBisAdm at 40 °C.*

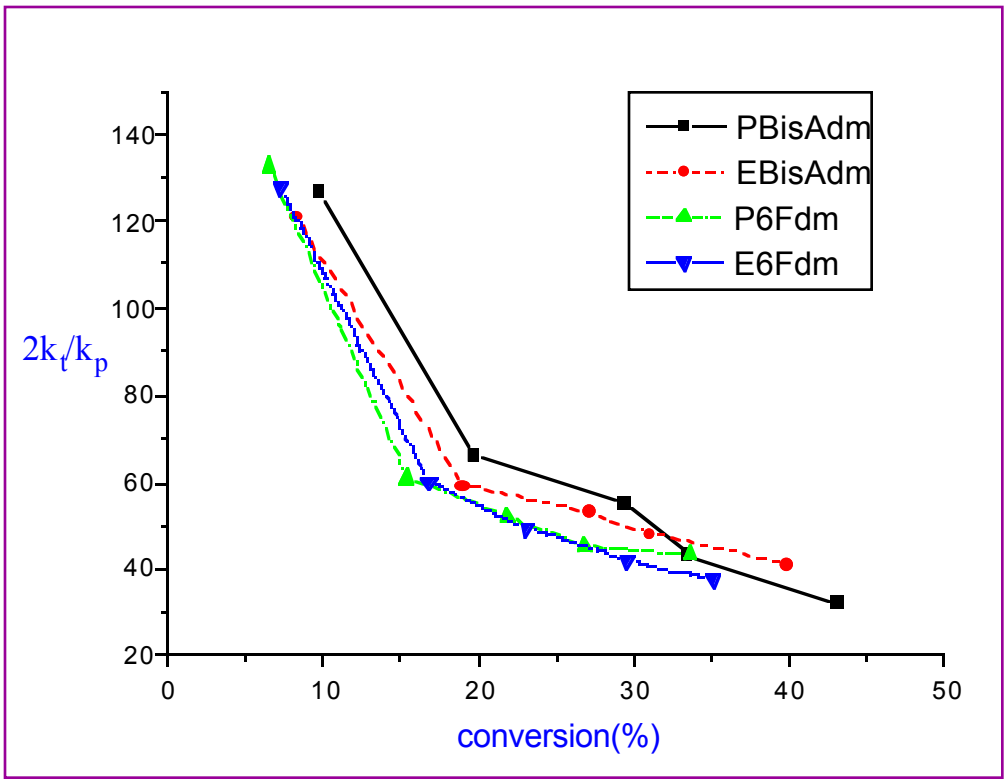

Polymerization was performed at 40⁰C and 4.51 mW/cm² light intensity

Figure 4.1.25 *Ratios of rate constants as functions of conversion*

Soh and Sunderberg have discussed in their paper (114) that the kinetic behavior of the linear free radical polymerization process can be divided into four regimes. At very low conversions (called phase I) the termination step is believed to be under diffusion controll. However, at higher conversions (phase II), the motion of the polymer chains which brings the radicals together is slowed down by chain entanglement., so that this step becomes the rate-determining step. Subsequent reaction further reduces the rate of diffusion resulting in a reduction of the termination rate constant and a rise in radical concentration. This produces a rapid increase in polymerization rate known as the gel or Trommsdorf effect which is mentioned earlier in various places of this thesis.

Continued polymerization in phase II results in raised molecular weight along with an increase in entanglement and thus reduction in k_t. As the reduction in k_t continues, radical concentration and polymerization reaction rate increases. This region of accelerating rate finishes when the rate of translational diffusion (114) so slow. In phase III, termination is dominated by the reaction diffusion mechanism in which two radicals are brought in contact so that combination or disproportionation may occur. Thus k_t becomes proportional to the propagation rate. Finally in phase IV, vitrification may occur leading to free volume control of propagation and a further reduction in the polymerization rate (114). It is expected that network forming systems should pass through similar stages (12).

4.2 Effect of Dilution on the Photopolymerization Kinetics of BisGMA-TEGDMA Mixtures

In this part of the thesis, a systematic study has been carried out to determine the effect of dilution of BisGMA (*2,2-bis(4-(2-hydroxy-3-methacryloxyprop-1-oxy) phenyl)propane*) with TEGDMA *(triethylene glycol dimethacrylate),* a low viscosity reactive diluent, on the extent of polymerization.

For this purpose, a series of monomer mixtures were prepared with various BisGMA and TEGDMA ratios. Table 4.2.1 shows the weight percent compositions of the monomer mixtures used for the photopolymerization. The glass transition temperatures (DSC) and viscosities (Cone and Plate Viscometer) of the monomers were previously measured by Shobha et al. (115) and bulk viscosities and T_g of the monomer mixtures are provided in Table 4.2.1. BisGMA exhibits very high viscosity. Dilution with TEGDMA significantly reduces the viscosity of the mixtures, e.g., a 50/50 mixture of BisGMA/TEGDMA gives a viscosity less than 1/10000 times lower than the viscosity of BisGMA itself. BisGMA exhibits a very high T_g value because intermolecular hydrogen bonding results in a rigid structure. As the amount of

TEGDMA is increased in the mixture. The T_g of the mixture is significantly decreased due to the increase of the flexibility in the system.

Table 4.2.1 *Variation of viscosity and T_g with the composition of the monomer mixtures*

Monomer Mixture	BisGMA (wt%)	TEGDMA (wt%)	Viscosity (cp)	T_g (%)
BisGMA	100	0	1.2×10^6	-6.6
BisGMA90	90.0	10.0	–	-20.7
BisGMA50	50.0	50.0	282	-61.0
BisGMA15	15.0	85.0	38	-76.7
TEGDMA	0	100	15	-81.7

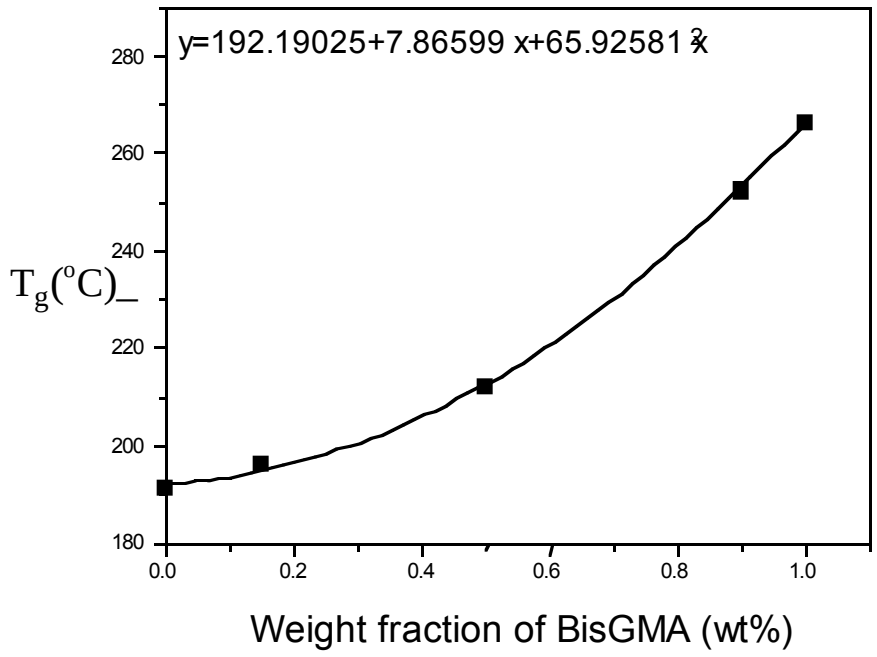

Figure 4.2.1 *Dependence of T_g on the composition of the monomer mixture*

Isothermal polymerizations of the mixtures were carried out using the DSC-DPA7. All the photopolymerizations were performed using 1.0 mol% CQ and 1.0 mol % DMpT at 1.43 mW/cm^2 light intensity from a 470 nm monochromatic source. Summary of the polymerization procedure is provided in Table 4.2.2.

Table 4.2.2 *Summary of the polymerization procedure for BisGMA/TEGDMA mixtures*

- Initiator System: 1.0 mole % CQ + 1.0 mole % DMpT
- Light Intensity : 1.43 mW/cm^2
- Wavelength : 470 nm
- 7-8 mg of sample
- Nitrogen was purged for 5 min. before exposing the samples to the curing light and purging was continued during the polymerization
- 20 min. irradiation at (40, 50, 60 ºC)
- Extent of polymerization (E_p %) was calculated from the area under the exotherm curve after the light is on for 20 min.

PhotoDSC thermograms of the mixtures polymerized at 40 ^{o}C and 1.43 mW/cm2 light intensity are shown in Figure 4.2.2.

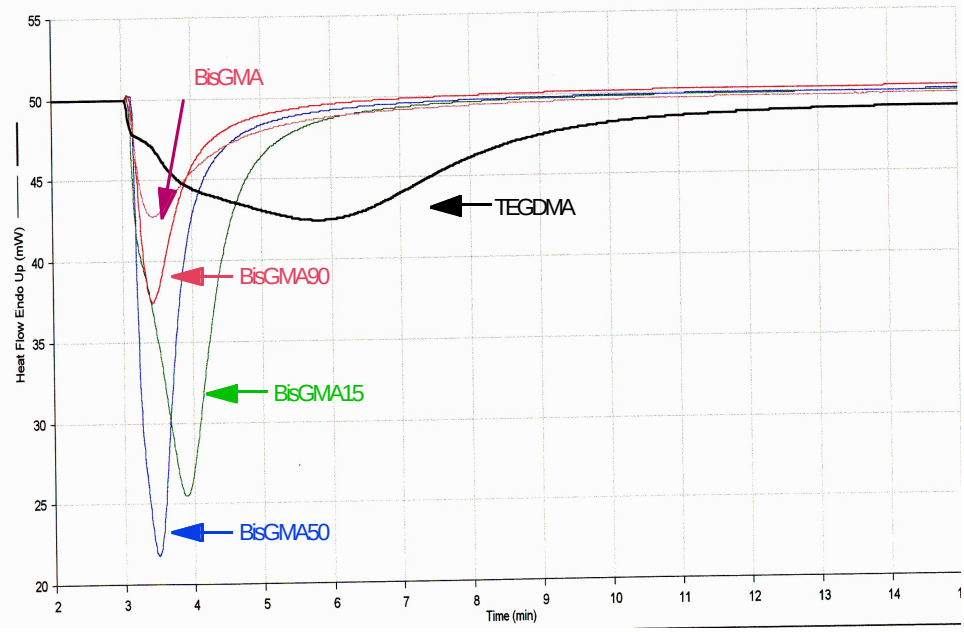

Figure 4.2.2 *PhotoDSC Thermograms of Various Compositions of BisGMA/TEGDMA Mixtures*

From the area under each exotherm peak, the extent of polymerization [E_p(%)] was calculated using Equation 6. This equation is a modified form of the relationship developed by Miyazaki and Horibe (115).

$$Ep\ (\%) = \frac{\Delta h}{H_m \left(\frac{X_1}{M_1} + \frac{X_2}{M_2} \right) x\ 2} \ x\ 100$$

where

Δh : Heat of Polymerization (J /g)

H_m : Heat of Polymerization of methyl methacrylate (-13.1 kcal/mol)

M_i : Molecular weight of the monomers (g/mol)

x_i : Weight fraction of the monomers

Equation 6. *Calculation of Extent of Polymerization [E_p(%)] for BisGMA/TEGDMA Mixtures*

Variation of the glass transition temperatures of the bulk mixtures with the ultimate conversions calculated for each monomer mixtures at 40 ^oC and 1.43 mW/cm^2 light intensity is given in Table 4.2.3.

Monomer Mixture	Tg (°C) [a] (DSC)	E_p (%)
BisGMA100	-6.6	27
BisGMA90	-20.7	35
BisGMA50	-61.0	44
BisGMA15	-76.7	53
TEGDMA	-81.7	65

Monomers were mixed with 1 mol % CQ and 1.0 mol % DMpT
Polymerizations were performed at 40 °C

Table 4.2.3 *Variation of extent of polymerizations [E_p(%)] with Glass Transition Temperatures (T_g) of the Monomer Mixtures*

This table indicates that the extent of polymerization increases with dilution and decreasing monomer mixture glass transition temperature. Pure BisGMA (BisGMA100) exhibits a high glass transition temperature (-6 ^{0}C) compared to the BisGMA/TEGDMA mixtures due to the strong intermolecular hydrogen bonding of the BisGMA molecules which requires greater thermal energy to disrupt the interchain forces. As the low viscosity comonomer is introduced to the system, intermolecular interactions are disrupted resulting in monomer mixtures with lower viscosities and glass transition temperatures. At a constant temperature, monomer mixtures with lower T_gs will polymerize to higher conversion values due to having a wider polymerization window between T_{cure} and T_g. However, polymerization will stop when the T_g of the network approaches the curing temperature due to the vitrification.

Figure 4.2.3 shows a monotonic decrease of E_p (%) with increase in T_g of the mixtures.

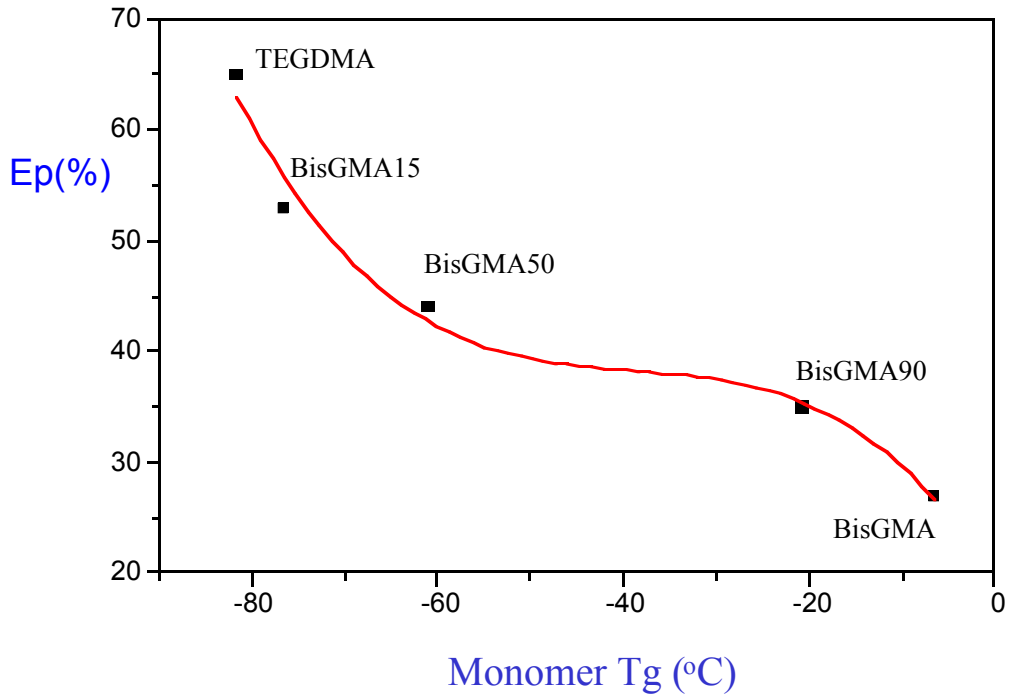

Figure 4.2.3 *Variation of Extent of Polymerizations [E_p(%)] with Glass Transition Temperature (T_g) of the Monomer Mixtures at 40 °C and 1.43 mW/cm^2 light intensity*

Variation of monomer conversions with polymerization time was calculated from the integrated exotherm curves and was plotted in Figure 4.2.4. The curves indicate that the addition of the reactive diluent, TEGDMA, influences the extent of the photopolymerization. As soon as the irradiation starts, due to the autoacceleration, the

reaction mixtures exhibit increasing rate of polymerization (initial slopes) and reach almost their maximum conversions in the first 2-3 min. of irradiation. It can be clearly seen from the conversion-time curves that although TEGDMA achieves considerably higher conversion than BisGMA, the onset of autoacceleration is delayed in the case of TEGDMA.

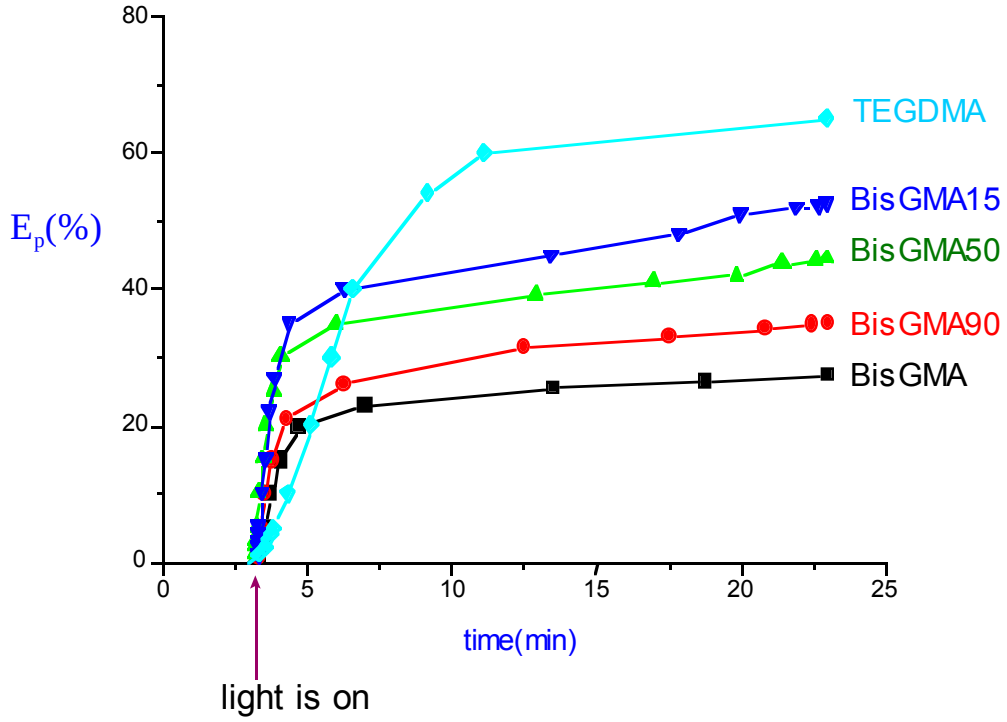

Figure 4.2.4 *Variation of Conversion (%) with Polymerization time (min) for the Monomer Mixtures at 40 °C and 1.43 mW/cm² light intensity*

The isothermal polymerizations were carried out for the mixtures at three different temperatures (40, 50, 60 °C) and E_p values were determined. The results are shown in Table 4.2.4. The E_p values are found to increase with increasing temperature and dilution.

As the temperature is increased and viscosity is reduced, the system exhibits more mobility which is responsible for the increased conversions. However, it is found that the viscosity of the mixture is more responsible for the increase in conversion than the polymerization temperature. The results indicate that at the same temperature, the limiting conversion increased (more than two times at 40 ^{0}C) as the viscosity decreased from BisGMA to TEGDMA. This is because a decrease in the viscosity increased the diffusivity of the unreacted pendant double bonds resulting in higher conversions.

Table 4.2.4 *Variation of E_p(%) on dilution at three different isothermal polymerization temperatures*

Temperature	Extent of Polymerization (%)				
(°C)	BisGMA	BisGMA90	BisGMA50	BisGMA15	TEGDMA
40	27	35	44	53	65
50	34	45	52	60	72
60	41	52	59	68	79

Monomers were mixed with 1.0 mol % CQ and 1.0 mol % DMpT
Polymerizations were performed at 1.43 mW/cm^2 light intensity

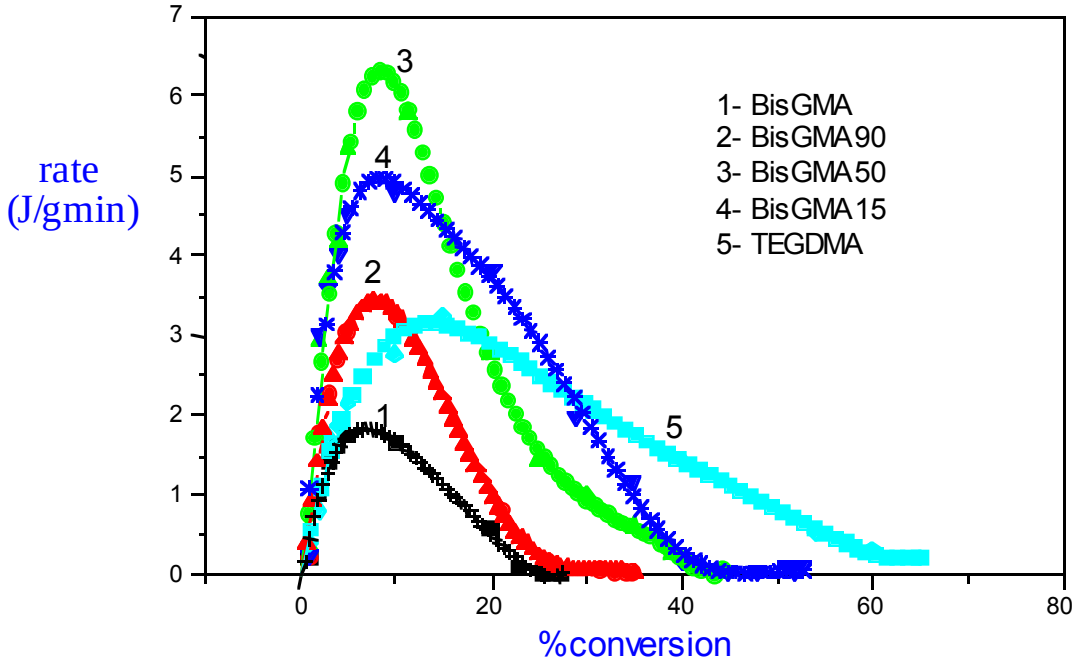

Figure 4.2.5 *Variation of Polymerization Reaction Rate with Conversion (%) for Various Combination of BisGMA/TEGDMA mixtures.*

The peak reaction rates were calculated from Figure 4.2.5 as the percent of initial monomeric units being reacted per unit time for all the mixtures at 40 °C and results are provided in Table 4.2.5. The peak reaction rates indicate the magnitude of the gel effect. One might expect that with a decrease in the viscosity, the mobility of the system increases causing an increase in the diffusivity of pendant double bonds. As a result of this, the propagation rate constant should increases. The results in Table 4.2.5

indicate that BisGMA50 exhibits the highest reaction rate at peak compared to the other mixtures. BisGMA, on the other hand exhibits the lowest rate at peak due the its very high viscosity. Although TEGDMA itself gives higher conversions than the any of the mixtures, the polymerization rate of this diluent monomer is lower than any of the BisGMA/TEGDMA mixtures. So, one can say that while TEGDMA is responsible for higher conversions, BisGMA is responsible for faster polymerization rates Similar results are also evidenced in the literature (117).

Table 4.2.5 *Variation of Exotherm Peak Rate for Various Combination of BisGMA/TEGDMA mixtures.*

Monomer Mixture	Total Heat -dH(J/g)	Rate at Peak (J/g.min)
BisGMA	58.6	1.74
BisGMA90	80.4	3.54
BisGMA50	131.4	6.48
BisGMA15	191.1	5.06
TEGDMA	248.9	3.23

Polymerization was performed at 40 ^{o}C and 1.43 mW/cm ^{2} light intensity

In order to determine the extent of residual polymerization in these systems, cured samples were kept under the illumination for 20 more min at the same isothermal temperature previously cured. The values for BisGMA15 and BisGMA90 are shown inTable 4.2.6.

Table 4.2.6 *Variation of Total Extent of Polymerization with the Isothermal Polymerization Temperatures*

Monomer Mixture	T(°C)	Extent of polymerization(%)		
		Isothermal E_p(%)	Residual E_p(%)	Total E_p(%)
BisGMA15	40	53	14	67
	50	60	9	69
	60	68	3	71
BisGMA90	40	35	18	53
	50	45	13	58
	60	52	8	60

Monomers were mixed with 1.0 mol % CQ and 1.0 mol % DMpT
Polymerizations were performed at 1.43 mW/cm² light intensity

The results indicate that the extent of polymerization (E_p) during the re-curing is influenced by the isothermal temperatures of the first scan. For instance, the residual E_p values were found to be higher for both BisGMA15 and BisGMA90 when they were polymerized isothermally at a low temperature (40 ^{0}C) in the previous scan. As the extent of unreacted double bonds was relatively higher in these systems, they exhibited an increased residual polymerization in the subsequent isothermal scan. The extent of residual polymerization is also affected by the dilution of the mixtures. For example, BisGMA90 exhibited higher residual E_p at all three isothermal polymerization temperatures than did the BisGMA15 mixture. Similar results were obtained by Shobha et al.(113) in the study of thermal polymerization of BisGMA/TEGDMA mixtures. It is explained that the high viscosity mixture of BisGMA shows reduced E_p values at these temperatures. That means

that they possess a higher concentration of unreacted double bonds which will be cured during the second illumination.

The total extent of polymerization (which is the sum of the E_p during the first isothermal illumination and the E_p during the subsequent illumination) are shown in Table 4.2.6. The total E_p results indicate that the final conversions of the double bonds in these highly crosslinked systems are much less than 100 %. The total E_p values are found to be slightly dependent on the isothermal polymerization temperatures. As the temperature is increased, total E_p is increased for both BisGMA15 (4 %) and BisGMA90 (7 %). However, the total E_p values are found to be strongly influenced by the dilution of the mixtures. For instance, BisGMA15 exhibited higher total value compared to BisGMA90. In the literature (113) it is explained that this is because the amount of residual double bonds in BisGMA90 is higher than that of the BisGMA15 mixture even after the second post-polymerization step. This may be due to the less rigid chains produced in the latter mixture. This less rigidity will give more mobility to the system and enhance the total curing.

Calculation of the ratio of rate constants

By switching off the light source at varying stages of the polymerization and recording heat release rate profiles as a function of time, the polymerization exotherms for BisGMA50 were evaluated under both steady-state and nonsteady-state conditions.

The light was turned on at 3rd min and illumination was continued for 15 sec, 30 sec, 45 sec 60 sec and 90 sec. The value $(\Phi I_{abs})^{0.5} k_p/(2k_t)^{0.5}$ was calculated from rate versus conversion data under constant illumination (Equation 4.4) at the time at which the light was turned off. Analysis of rate versus time data under nonsteady-state conditions (light turned off) yields the ratio of $2k_t/k_p$ (Equation 4.7). Figure 4.2.6 shows the resultant monomer disappearance rate ($-d[M]/dt$) versus conversion plots for BisGMA50 for

several percent conversions at 40 °C. The numbers next to each curve represent the total conversions obtained from constant illumination for various period of time plus dark reaction. In Figure 4.2.7 (rate dependence on conversion) for all the curves the complex DSC curve shape can be seen in which rate increases sharply at the very beginning of the reaction and low conversion due to autoacceleration. After reaching its maximum value, polymerization rate decreases at a slower mode as the reaction proceeds due to the vitrification of the system with increasing viscosity.

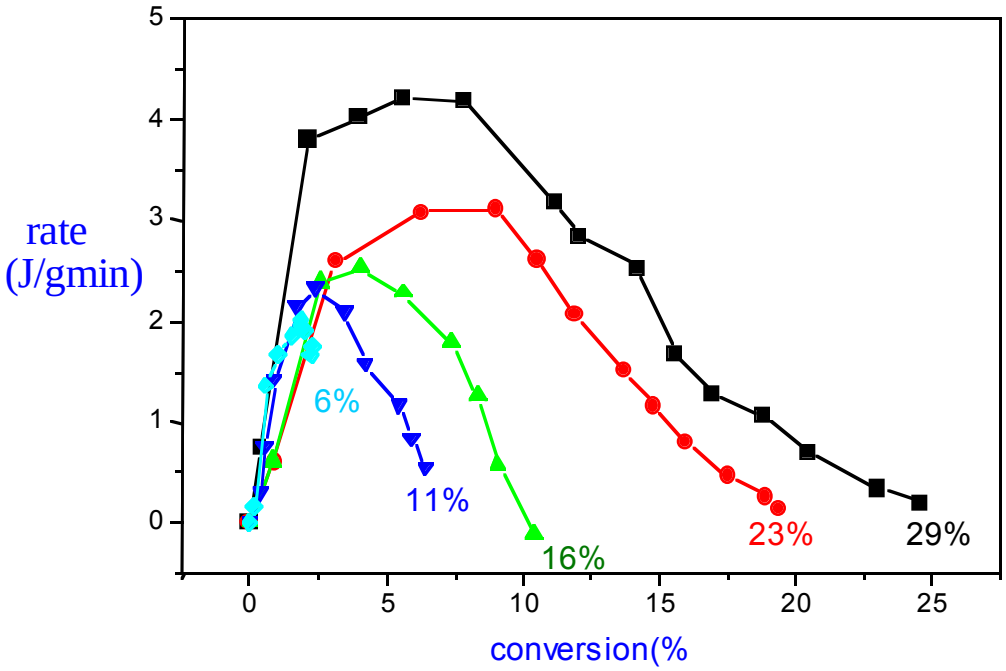

Figure 4.2.6 *Rate (J/g min) versus Conversion (%) at various stages of the polymerization(constant illumination) for BisGMA50.*

The resultant [M]/ (–d[M]/d*t*) versus time plots for BisGMA50 according to the Equation 4.7 are shown in Figure 4.2.7 for several percent conversions at 40 °C. The slopes of the straight lines decrease as the conversion increases at longer illumination

times. This explains that rate of monomer disappearance is slower under dark reaction when the illumination time is longer.

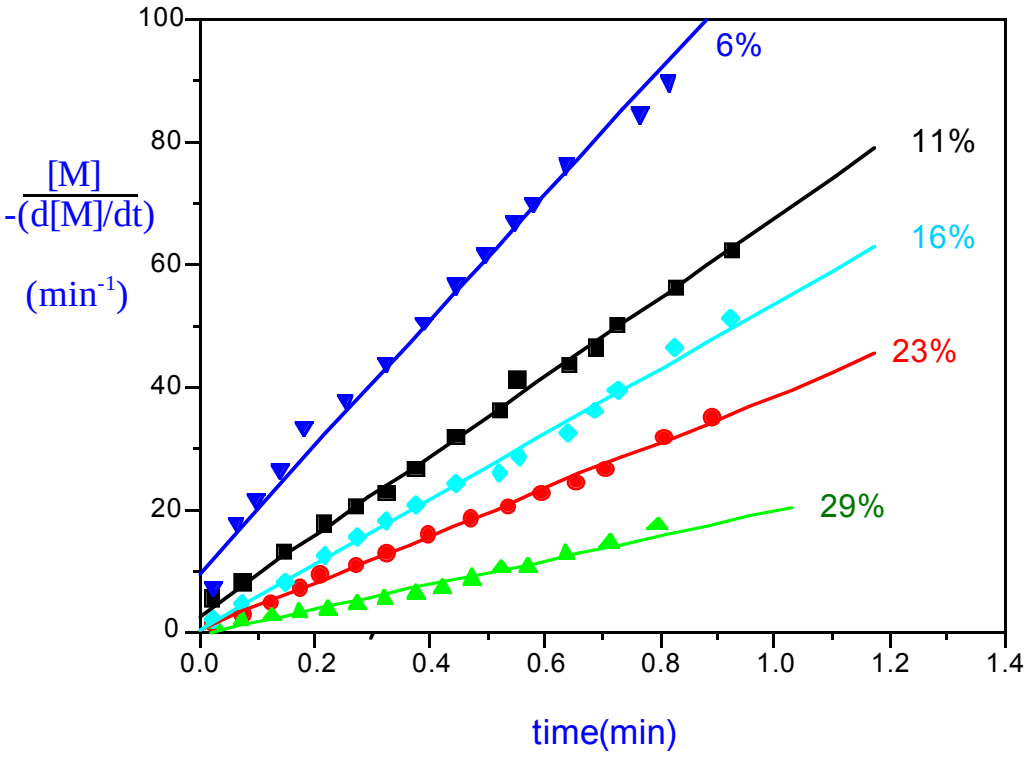

Figure 4.2.7 *[M]/ (- d[M]/dt) versus time (dark reaction) for BisGMA50 at 40 °C.*

From the slope of [M]/ (–d[M]/dt) vs. time curves in Figure 4.2.8, $2k_t$ / k_p values were calculated by a least-square method for several percent conversions. The resultant $2k_t$ / k_p values under nonsteady-state conditions and $(\Phi I_{abs})^{0.5}$ $k_p/ 2k_t^{0.5}$ values under steady-state conditions at the moment when the light is turned off for BisGMA50 are reported in Table 4.2.7. There is a continuous decrease in the ratio of the rate constants with increasing percent conversion. As the reaction proceeds, due to the viscosity of the system, increasing numbers of radicals are trapped in the network. Due to the lack of diffusivity of the radicals together, termination process is mostly prohibited resulting in

decrease k_t. At the later stages of the reaction inhibited diffusion of monomer to the reactive sites results in decrease in k_p as well.

Table 4.2.7 *Ratio of Rate Constants for BisGMA50 at 40 °C*

% Conversion	$2k_t / k_p$	$(\Phi I_a)^{1/2} k_p / 2k_t^{1/2}$ (min^{-1})
6	103.4	0.92
11	64.7	1.63
16	54.3	0.74
23	38.1	0.41
29	20.0	0.27

4.3. Effect of Temperature, Light Intensity and Initiator Concentration on the Photopolymerization Kinetics of BisGMA

This part of my thesis includes our early photocalorimetric studies of a commercially available monomer, BisGMA with the instrument DSC-DPA7. This study was conducted to investigate the effects of temperature, light intensity and initiator concentration on the extent of conversion of visible-light activated BisGMA monomer.

4.3.1 Effect of Temperature

For this study, about 7-8 mg monomer sample was activated with 0.5 mol % camphorquinone (CQ) and 1.0 mol % N, N-dimethyl-p-toluidine (DMpT). The light intensity was 1.43 mW/cm^2 obtained from 470 nm monochromatic light source with an filter (0.316 relative intensity). Each monomer resin was irradiated for 20 min under nitrogen. The ultimate conversions were calculated at four different isothermal polymerization temperatures (30, 40, 50 and 60 ^oC) and the results are shown in Table 4.3.1. The results indicate that E_p values increase with increasing temperature due to the increase of the free volume in the system. However, even if the curing temperature is increased from 30 ^oC to 60 ^oC, the limiting conversion doesn't increase more than 31 %.

Table 4.3.1 *Variation of E_p (%) with Temperature for BisGMA*

t (°C)	% Ep
30	17
40	24
50	27
60	31

BisGMA was mixed with 0.5 mol% CQ and 1 mol% DMpT
Polymerizations were performed at 1.43 mW/cm² light intensity

In order to consider the effect of temperature on photopolymerization, polymerization activation energies (E_a) were calculated from the Arrhenius relationship. Exotherms were recorded at four different temperatures and rate data was obtained from Arrhenius plots as a function of percent conversion. Figure 4.3.1 represents plots of log rate against reciprocal temperatures at various percent conversions. Table 4.3.2 summarizes the apparent activation energies determined using a least square calculation of slopes. One can say that the overall activation energy is increasing with conversion. One possible explanation of the observed behavior of the apparent activation energies is that again a diffusion-controlled mechanism in the propagation and/or termination steps. This behavior explained by Tryson and Shultz (73) is that when diffusion control mechanism predominates, the observed activation energy will be the activation energy for the diffusion of the reactants. Radical size, polymer concentration, and formation of network can be also

important factors when the free radicals reactions advances, causing a shift toward diffusion controlled in the propagation and termination steps.

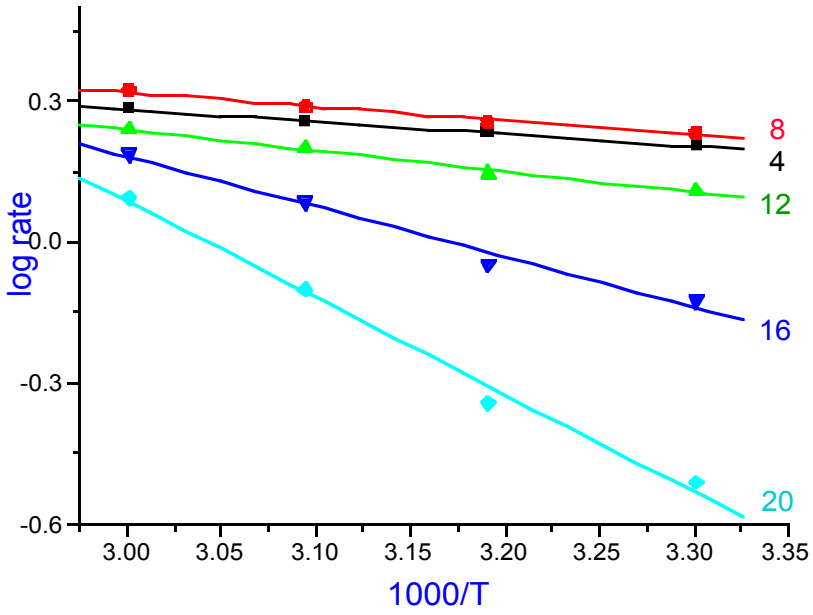

Figure 4.3.1 *Log rate versus 1000/T (K^{-1}) for temperatures 30 ^{0}C - 60 ^{0}C.*

Table 4.3.2 *Variation of Activation Energies (E_a) with Conversion*

% Conversion	E_a (kcal/mol)
4	0.53
8	0.64
12	0.89
16	2.15
20	4.07

BisGMA was mixed with 0.5 mol% CQ and 1.0 mol% DMpT
Polymerizations were performed at 1.43 mW/cm^2 light intensity

4.3.2 Effect of Light Intensity

Influence of light intensity was studied with a photoinitiator concentration of 0.5 mol % CQ and 1.0 mol % DMpT. Firstly, the study was carried out at 60 ^{o}C wih light intensity in the range of 0.13-4.51 mW/cm^2. We observe that ultimate conversion increase with light intensity (Table 4.3.3). Kloosterboer et al. (112) reported that this was due to the presence of a temporary excess volume in the reacting mass. This temporary free volume exists because the rate of volume shrinkage lags behind the reaction rate. As the light intensity was increased, the reaction rate also increased and more temporary excess free volume was available. This results in an increase in the final conversion. Such an increase in final conversion with an increase in light intensity has been also seen by others (32, 4, 115).

It is indicated in the literature (116) that a slow polymerization process occurs under low light illumination even after vitrification of the system. This is very important since it suggests that free radical polymerization in a cross-linked glassy matrix can proceed, although very slowly, to very high conversions.

Table 4.3.3 *Variation of Ep(%) with Light Intensity*

Intensity(mW/cm^2)	%Ep
0.13	13
0.393	20
1.43	31
4.51	41

BisGMA was mixed with 0.5 mol% CQ and 1 mol% DMpT
Polymerizations were performed at 60 °C

Using the DSC data on the photopolymerization of the BisGMA, the power dependence of the reaction rate on the incident light intensity was calculated from the slope of a log-log plot of exotherm rate (proportional to the reaction rate) versus light intensity. Experimental result of the power dependence of the reaction rate on the light intensity is shown in the Figure 4.3.2.

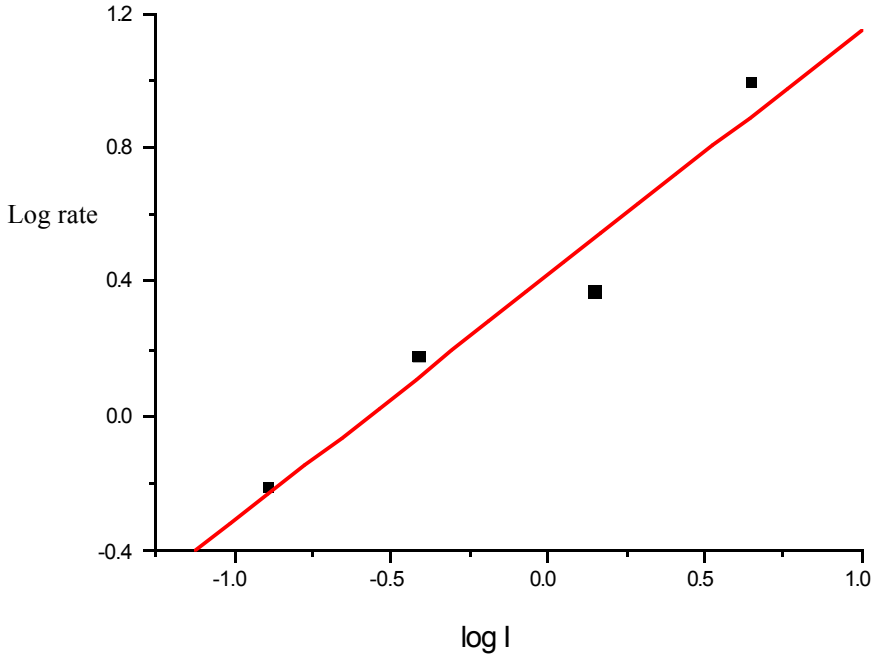

Figure 4.3.2 Log rate versus Log I for BisGMA at 60 ^{0}C.

From the figure above the radiation exponent was found to be 0.69 at 60 ^{o}C. This value is higher than the theoretical value of 0.5 It is reported that the deviation of the exponent toward unity is usually associated with a tendency for first-order termination kinetics caused by the reaction of the radicals with trace impurities or due to the immobilization of the radicals in the matrix (73). The former phenomenon should dominate at low conversions and radiation intensities, while both processes are likely to be important at higher conversions as the network structure develops. The increased temporary excess volume for reaction at higher light intensity is probably is the most important contributor to increasing the exponent from 0.5 to 0.69.

4.3.3 Effect of Initiator Concentration

In order to study the effect of camphorquinone (CQ) on the ultimate conversion of photopolymerization of BisGMA, CQ concentrations of 0.05, 0.5, and 1.0 mol % were mixed with the monomer and photopolymerizations were performed at 1.43 mW/cm2 light intensity and at 60 ^{0}C. The ultimate conversions were calculated from the curves obtained from the DSC (Table 4.3.3).

Table 4.3.4 *Variation of Ep (%) with Initiator Concentration*

Initiator Concentration (mol%)	Ep (%)
0.05	18
0.5	31
1.0	39

BisGMA was mixed with 1 mol% DMpT
Polymerizations were performed at 60C and 1.43 mW/cm^2 light intensity

Increasing CQ reveals the strong effect of increased ultimate conversion with increased polymerization rate. This effect again is most likely due to the delayed volume shrinkage. As noted in the Section 4.3.2, the rate of polymerization depends on the light intensity raised to a power greater than 0.5. However, the rate depends on the concentration of CQ raised to a power less than 0.5 (e.g. 0.35 for BisGMA) (Figure 4.3.3). This may be

attributed to the somewhat complex photoinitiation mechanism in diketone/amine systems (34). However, an early photo DSC study (74) of 1,6-hexanedioldiacrylate polymerization using benzoin ethyl ether/UV light initiation found the rate proportional to $[BEE]^{0.31}$. A survey of the power dependence of rate on photoinitiator concentration in diacrylate and dimethacrylate polymerization is not in hand, but it is possible that an unexplained low power dependence is general (119).

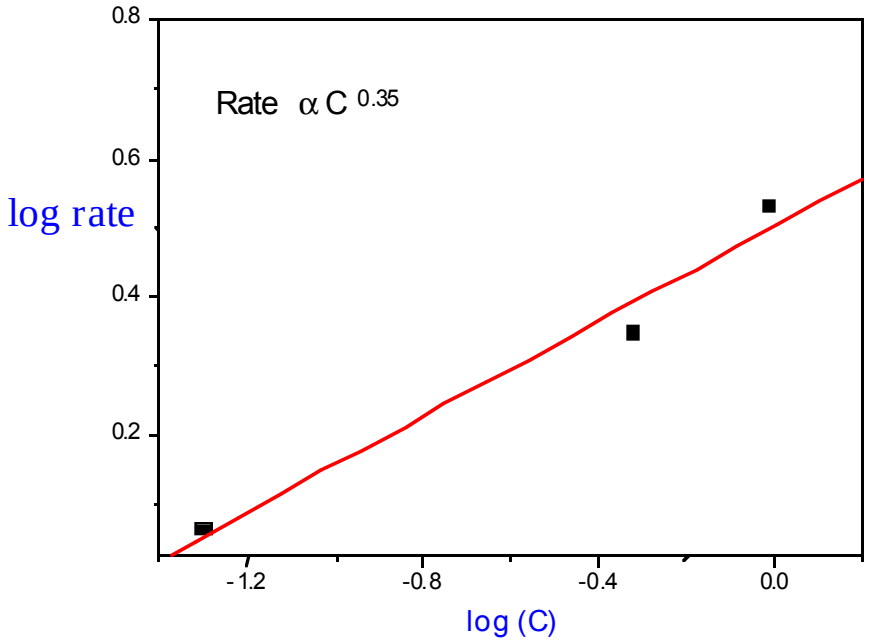

Figure 4.3.3 *Log rate versus Log (C) for BisGMA at 60 °C*

CHAPTER 5. CONCLUSIONS

Based on the studies of rapid exothermal photoinduced polymerizations by differential scanning calorimetry (Photo DSC), the following conclusions can be obtained.

1. In order to study the effect of monomer structure, polymerization temperature, initiator concentration, and light intensity on the kinetics of photopolymerization, four new difunctional methacrylate monomers, PropBisAdm, EtBisAdm, Prop6Fdm, Et6Fdm, which have some similarity to BisGMA were synthesized in a two-step reaction. Their structures were characterized by NMR and FTIR. The glass transition temperatures (Tg) and bulk viscosities of the neat monomers as well as the control BisGMA were previously measured by DSC and Cone and Plate Viscometer respectively (37). The preliminary studies on the structures and Tg and viscosity behavior showed that the experimentally prepared dimethacrylates have much lower viscosities and glass transition temperatures compared to that of BisGMA due to the absence of the hydrogen bonding in their structures. The photopolymerization rate and conversion data of the four new dimethacrylate monomers and BisGMA were examined in relation to monomer structure, temperature, incident light intensity, camphorquinone concentration and dark reaction rate. All the experimental monomers, which exhibit much lower viscosities than that of BisGMA, gave higher extents of polymerization exhibiting a remarkable linearity between ultimate conversion and monomer Tg. Although all the monomers studied show similar rate curves obtained from DSC-DPA7, the polymerization rate was faster with a lower viscosity monomer at a given temperature. Furthermore, ultimate conversions were increased with increasing temperature, initiator concentration, and light intensity for all the monomers studied. Observation of the polymerization rate behavior after closing the shutter on a photopolymerization run permitted us to determine the ratio of the termination rate constant to the propagation rate constant ($2k_t / k_p$). It was found that in the range of conversion examined the rate constant ratios continue to decrease with

conversion increase indicating that reaction diffusion control of both termination and propagation has not been reached.

2. In order to study the effect of dilution of BisGMA with a more flexible, lower viscosity comonomer, (TEGDMA), on the photopolymerization reactions, a series of monomer mixtures were prepared with various BisGMA / TEGDMA ratios. The glass transition temperatures and viscosities of the monomer mixtures were obtained (37). The results indicated that the extent of polymerization increased with decreasing glass transition temperature and dilution at a given temperature. The ultimate conversion was also increased with increasing isothermal temperature for all the monomer/comonomer mixtures. Although TEGDMA itself exhibited higher conversion than the any of the mixtures, the polymerization rate of this low viscosity monomer was slower than those of all the BisGMA/TEGDMA mixtures.

On the basis of this thesis, we suggest that further research work is needed. These efforts may include: (1) calculation of the propagation (k_p) and termination rate constants individually. To be able to find these constants the quantity (I_{abs}) must be evaluated and used in the equation : $k_p / k_t^{1/2} = (-d[M] / dt \quad (I_{abs})^{1/2} [M])$ (73). (2) In order to determine the percent of residual non-reacted monomer in a given sample, sol faction measurements by HPLC should be performed.

REFERENCES

1) A. R. Kannurpatti, K. J. Anderson, J. W. Anseth and C. N. Bowman, J. Polym. Science: Part B: Polym. Phys., 35, 2297 (1997).

2) R. L. Bowen, J. Dent. Res., 49, 810 (1970).

3) I. E. Ruyter and H. Oysaed, CRC Crit. Rev. Biocompat., *4*, 247 (1988).

4) L. T. Smith and J. M. Powers, Int. J. Prosthodont., *4*, 445 (1991).

5) J. G. Kloosterboer, Adv. Polym. Sci., 84, 1 (1988).

6) R. J. M. Zwiers and G. C. M. Dortont, Appl. Optics, 24, 4483 (1985).

7) J. P. Fouassier and J. F. Rabek, Radiation Curing in Polymer Science and Technology, Vol. IV: Practical Aspects and Applications, Elsevier Eds., New York, (1993).

8) H. J. Hageman, Prog. Org. Coat., 13, 123 (1985).

9) R. G. Gossink, Macromol. Chem., 145/146,365 (1986).

10) J. G. Kloosterboer, g.j.m. Lippits, J. Radiat. Curing 11 (1), 10 (1984).

11) K. S. Anseth, C. M. Wang, and C. N. Bowman, Polymer 35, 3243 (1994).

12) W. D. Cook, Polymer, 33, 10 2152 (1992).

13) J. G. Kloosterboer, Adv. Polym. Sci., 84, 1 (1988).

14) J. G. Kloosterboer, G. M. M. Van de Hei, and H. M. Boots, Polym. Commun., 25, 354 (1984).

15) J.G. Kloosterboer, C. Litjen, and H. M. Boots, Macromol. Chem., Macromol. Symp.,24, 223 (1989).

16) D. Bhattacharya and A. E. Hamielec, Polymer, 27, 905 (1986).

17) I. M. Yaraskavitch, J. L. Brash and A. E. Hamielec, Polymer, 28 489 (1987).

18) N. C. Bowman and A. N. Peppas, Macromolecules, 24, 1914 (1990).

19) J. Kopecek and D. Lim, Collect. Czech. Chem. Commun., 36, 3394 (1971).

20) S. Zhu, Y. Tian, A. E. Hamielec and D. R. Eaton, Polymer, 31,154 (1990).

21) R.L. Bowen, Synthesis of a silica-resin filling materials: progress report, J. Dent. Res., 37:90, (1958).

22) R.G. Craig, Restorative Dental Materials(8th ed.). St. Louis: Mosby, pp 255-262 (1989).

23) R.L. Bowen, J. Dent. Res. 35:360-369, (1956)

24) R. L. Bowen, J. Am. Dent. Assoc. 66:57-64, (1963).

25) K. S. Anseth, S. M. Newman, and C. N. Bowman, Adv. Polym. Sci. 122, 177 (1995).

26) D.C. Smith, Posterior Composite Dental Restorative Materials:Materials Development. In: G Vanherle and DC Smith (eds.). St. Paul, MN: Dental Products Division, 3M Co., pp 47-67 (1985).

27) Y. Liu, Master Thesis, *Studies of Unfilled, Dental Resins Based on Newly Synthesized Monomers with Improved Chemical and Mechanical Properties*, The Ohio State University (1995).

28) M. Braden, Oper. Dent. *3*, 97 (1978).

29) J.E. Ruyer and J.J. Sjovik, Acta Odontol Scand., 39:133-46,1981.

30) Y. Li, M.L. Swartz, R. W. Phillips, B.K. Moore and T. A. Roberts, J. Dent. Res., 64:1396-1401, (1985).

31) R. L. Bowen, US Patent 3,066, 112, (1962).

32) S. S. Starnatein and C.S. Van Buskirk, Poymer Creep, Encyclopedia of Polymer Science and Engineering, 12:470-486, (1984).

33) D. B. Mahler, J. VanEysden, and L.G. Terkal, IADR Program and Abstracts, No.245, (1977).

34) D. W. Cook and D. C. Watts, J. Dent. Res. 64:147-150, (1985).

35) M. L. Ferracane, Matsumoto and T. Okabe, J. Dent. Res. 64:1332-1336, (1985).

36) D. F. Taylor, S. Kalachandra, M. Sankarapandian, Q. Xu and J. E. McGrath, J. Adv. Mater., *28* (1996) 59.

37) H. K. Shobha, M Sankarapandian,. D. F. Taylor, S. Kalachandra and J. E. McGrath, J. Mater. Sci. Mat. Med. 1997, 8(6) 385.

38) M. W. Beatty, M. L. Swartz, B. K. Moore, R. W. Phillips and T. A. Roberts, J. Biomed. Mater. Res. 27, 403 (1993).

39) J. Tanaka, K.Inoue, H. Masamura, K. Masamura and H. Nakai, *ibid*. *12* 11 (1993).

40) I.E. Ruyter and H. Oysaed, Acta Odontol. Scand. 40:319-324, (1982).

41) Y. Papadogianis, D.B. Boyer, and R.S. Lakes, J. Biomed. Mater. Res. 18:15-24, (1984).

42) A. Oden, I.E. Ruyter, and H. Oysaed, Dent. Mater., 4:147-150, (1988).

43) M. Kawaguchi, T. Fukushima, K. Miyazaki, T. Horibe, T. Habe, N. Sawamaura, K. Nagaoka, J. Fukukoka Dent Coll., 10:453-60, 1983.

44) S. Hirano and T. Hirasawa, Dent. Mater. J. 8:93-99, (1989).

45) I.E. Ruyer and S. Espevik, Acta. Otontol. Scand., 38:169-77, (1980).

46) B.M. Culbertson, W.A. Brantley, E.C. Kao, and T. Grentzer, J. Dent. Res. 69:207,1990(Abstract 789).

47) B.M. Culbertson, W.A. Brantley, E.C. Kao, and M.L. Deviney, J. Dent. Res. 70:481,1981(Abstract 1718).

48) B.M. Culbertson, Biomedical applications of polymers and polymers as dental materials, Preprint of Guilin International Symposium on Biomedical and Fine Polymers. Oct. 3-7, 1991, Guilin, China pp.42-43.

49) H. K. Shobha, M. Sankarapandian, S. Kalachandra, D. F. Taylor and J. E. McGrath, J. Mater. Sci.: Mater. In Medicine, 8 385 (1997).

50) S. Kalachandra, D. F. Taylor, C. D. DePorter, H. J. Grubbs and J. E. McGrath, Polymer, 34, *4,* 778 (1993).

51) I.E. Ruyter, In: G. Vanherle and D.C. Smith, Eds., Op.cit., pp 130.

52) W. Schmitt, R. Purmann, P. Jochum, and W.D. Zahlr, US. Patent . 3,923,740, (1975).

53) G.F. Cowperthwa, J. J. Foy, M.A. Malloy, Polymer Sci. Tech., 14:379-85,1981.

54) J. P. Fouassier and J. F. Rabek, Radiation Curing in Polymer Science and Technology, Vol. 1: Fundamental and Methods, Ed. Elsevier, New York (1993).

55) S. P. Pappas, Radiation Curing, Science and Technology, Plenum Press, New York, 1992.

56) R. J. J. Williams, and C. I. Vallo, Macromolecules, 21, 2571 (1988).

57) K. K. Dietliker and J. V. Crivello, Chemistry and Technology of UV and EB Formulation for Coatings, Inks and Paints, P. K. I. Oldring, Ed., SITA Technology, London (1991).

58) F. S. Stone and R. Liberman, J. Rad. Curing, 14, 10 (1987).

59) H. C. Miller, Proc. Radiation Tech. Conf., Florence, (1989) p. 429.

60) N. S. Allen, M. A. Johnson and P. K. I. Oldring, UV and EB Formulation for Coatings, Inks and Paints, P. K. I. Oldring, Ed., SITA Technology, London (1991).

61) J. J. Wildi, Proc. Radiation Tech. Conf., Florence, (1989) p. 491.

62) C. Decker and K. Moussar, Eur. Polym. J., ***27***, 403 and 881 (1991).

63) J. P. Fouassier and J. F. Rabek, Radiation Curing in Polymer Science and Technology, Vol. 2,Photoinitiating Systems, Elsevier, New York, 188 (1993).

64) K. E. J. Barrett, J. Appl. Polym. Sci. 11, 1617 (1967).

65) H. E. Bair and L. L. Blyler, Proc. 14th NATAS, p.392 (1985).

66) M. J. M. Abadie and B. K. Appelt, Bull. Soc. Chim. Fr., 20 (1988).

67) D. D. Le, Conf. Proc., Radcure'84, pp.8-33, Soc. Manuf. Eng., Dearborn, Mich. (1984).

68) R.W. Bush, A.D. Ketley, C.R. Morgan, and D.G, Whitt, J. Radiat. Curing 7 (2), 20 (1980).

69) J. E. Moore, S. H. Schroeter, A. R. Shultz, and L. D. Stang, in: Ultraviolet Light Induced Reactions in Polymers, ACS Symp. Ser. 25 (S.S. Labana, ed.), p.90, Am. Chem. Soc., Washington, D.C. (1976).

70) J. E. Moore, Org. Coat. Plast. Prepr. 36 (2), 747 (1976).

71) W. I. Benough and H. W. Melville, Proc Roy. Soc. London Ser. A 225, 330 (1954).

72) W. I. Benough and H. W. Melville, Proc Roy. Soc. London Ser. A 260, 205 (1961).

73) G. R. Tryson and A. R. Shultz, J. Polym. Sci. Polym. Phys. Ed. 17, 2059 (1979).

74) G. Odian, Principals of Polymer Chemistry, Wiley-Interscience, New York (1981).

75) *A.* T. Doornkamp, and Y. Y. Tan, Polym. Commun., 31,362 (1990).

76) B. K. Appelt, and M. J. M. Abadie, Polym. Eng. Sci., 28, 367 (1988).

77) D. J. Broer, G. N. Mol, and G. Challa, Polymer, 32, 690 (1991)

78) R. Levin, A. Hale, A. L. Harris, N. J. Levinos, and F. C. Schilling

79) W. D. Cook, J. Polym. Sci.: Part A: Polym. Chem., 31, 1053 (1993).

80) B. Overton, C.R. Taylor, and A.J. Multer, Polym. Sci. Eng., (1989).

81) C. Decker, Macromolecules, 23, 5217 (1990).

82) C. Decker, J. Coatings Technol., 59, 97 (1987).

83) C. Decker and K. Moussa, Makromol. Chem., 189, 2381 (1988).

84) C. Decker and K. Moussa, J. Coatings Technol., 62, 55 (1990).

85) J. P. Fouassier and J. F. Rabek, Radiation Curing in Polymer Science and Technology, Vol. 3, Polymerization Mechanisms, Elsevier Sci. Pub. LTD, p.18 (1993).

86) C. Decker and A. D. Jeckins, Macromolecules, 18, 1241 (1985).

87) J. G. Kloosterboer, G. F.C.M. Lijten, and , F. J. A. M. Greidanus Polym. Commun., 27, 268 (1986).

88) J. G. Kloosterboer, G. F. C. M. Lijten, and F. J. A. M. Greidonus, Polym. Rep., 27, 269 (1986).

89) K. S. Anseth, K. J. Anderson, and C. N. Bowman, Macromol. Chem. Phys., 197, 833 (1996).

90) A. R. Kannurpatti, S. Lu, G. M. Bunker, and C. N. Bowman, Macromolecules, 29, 7310 (1996).

91) G. P. Simon, P. E. M. Allen and D. R. G. Williams, Polymer, 32, 2577 (1991).

92) T. W. Wilson, J. Appl. Polym. Sci., 40, 1195 (1990).

93) P. E. M. Allen, A. B. Clayton and D. R. G. Williams, Eur. Polym. J., 30, 427 (1994).

94) M. Kalnin and D. T. Turner, J. Mater. Sci. Lett., 4, 1476 (1985).

95) J. Bastide, L. Leibler, Macromolecules 21, 2649 (1988).

96) J. Bastide, L. Leibler and J. Prost, Macromolecules 23, 1821 (1990).

97) T. A. Vilgis, Macromolecules, 25, 399 (1992).

98) P. E. M. Allen, G. P. Simon, D. R. G. Williams, and E. H. Williams, Macromolecules, *22*, 809 (1989).

99) G. P. Simon, P. E. M. Allen, D. J. Bennett, D. R. G. Williams, and E. H. Williams, Macromolecules, *22*, 3555 (1989).

100) G. P. Simon, P. E. M. Allen, D. J. Bennett, D. R. G. Williams, Polym. Eng. Sci., ***31***, 1483 (1991).

101) K. S. Anseth, M. D. Rothenberg, and C. N. Bowman, Macromolecules, 27, 2890 (1994).

102) K. S. Anseth, T. A. Walker, and C. N. Bowman, ACS Symp. Ser., 598, 166 (1995).

103) K. S. Anseth and C. N. Bowman, J. Polym. Sci. Part B: Polym. Phys., 33, 1769 (1995).

104) G. M. Burnett and G. L. Duncan, Makromol. Chem., 51, 177 (1962).

105) N. Gunduz, A.R. Shultz, H.K. Shobha, M. Sankarapandian, and J.E. McGrath, Polymer Preprints, Vol. 32, 2, 1998.

106) H.K. Shobha, M. Sankarapandian, A.R. Shultz J. E. McGrath, S. Kalachandra, and D. F. Taylor, Makromol. Chem. Makromol. Symp., Recent Advences in Free Radical Polymerization, *11,* 73 (1996).

107) K.S. Anseth, M.D. Goodner, M.A. Reil, A.R.Kannurpatti, S.M. Newman, and C.N. Bowman, J. Dent. Res., 75 , *8* 1607 (1996).

108) K. Horie, A. Otagawa, M. Muraoka, and I. Mita, J. Polym. Sci., Polym. Chem. Ed., *13*, 690 (1975).

109) E. Andrzejewska, Polymer, 37, 6 1039 (1996).

110) J.G. Kloosterboer, G.M.M. Van de Hei, R.G. Gossink and G.C.M. Dortant, Polym. Commun., 25 322 (1984).

111) K. S. Anseth, L.M. Kline, T.A Walker, K. J. Anderson, and C. N. Bowman, Macromolecules, 28, **7** 2491 (1995).

112) J. G. Kloosterboer, , G. F.C.M. Lijten, Polymer 31, 95 (1990).

113) H. K. Shobha, M. Sankarapandian, Y. Sun S. Kalachandra, D. F. Taylor and J.E. McGrath, J. Mater. Sci.: Mater. In Medicine, 583, 8 (1997).

114) S.K. Soh, D.C. Sunderberg, J. Polym. Sci., Polym. Chem. Edn. 20 1315 (1982).

115) K. Miyazaki, M. Kawaguchi, T. Horibe, and Y. Mizukami, J. Dent. Mat., 504-510 (1985).

116) B.B. Reed, K. Choi, H. Dickens, and J.W. Stansbury, Polymer Priprints, 38, 2 (1997).

117) K. Horie, A. Otogawa, M. Muraoka, and D.G. Whitt, J. Radiat. Curing 7 (2), 20 (1980).

118) F. R. Wight, J. Polym. Sci. Polym. Lett. Ed. 16, 121 (1978).

119) C. R. Morgan, F. Magnotta, and A. D. Ketley, J. Polym. Sci. Polym. Chem. Ed. 15, 627 (1977).

120) C. Decker, J. Polym. Mater. Sci. Eng., 49, 32 (1983).

121) C. Decker, J. Coatings Technol., 56, 29 (1984).

122) K. Horie, A. Otogawa, M. Muraoka and D.G. Whitt, J. Radiat. Curing 7 (2), 20 (1980).

VITA

Nazan Gunduz, daughter of Huriye Kaptan and Kenan Kaptan, was born on January 1,1971 in Izmir, Turkey. She graduated from Suphi Koyuncuoglu High School in July of 1988, and began her undergraduate studies at Ege University in Izmir as a Chemistry major, receiving her B.Sc. degree in July of 1992. On May 19th, 1994 she married Irfan Gunduz in Antalya, Turkey. On May 18th, 1997 she gave a birth to her daughter, Erin Ilge Gunduz.

After starting the graduate program at EgeUniversity in the Chemistry Department, she entered the Chemistry Department and accepted a graduate teaching assistantship at Akdeniz University, Antalya in August of 1993. In February of 1994 she took a nationwide exam from the Turkish Educational Council to peruse her graduate studies in the USA and she joined the Chemistry graduate program at Virginia Polytechnic Institute and State University in September of 1995. Her M.S. research focused on the synthesis and photopolymerization of dimethacrylates. After receiving her Master of Science degree in June of 1998, she was accepted at Virginia Polytechnic Institute and State University in order to work towards her goal of obtaining a Ph.D.